TECHNISCHE UNIVERSITÄT MÜNCHEN

Integrative Research Institute Campus Straubing für Biotechnologie und Nachhaltigkeit

A Novel Perturbation Approach for the Thermodynamic Modeling of Poorly Specified Mixtures

Eva Maria Ursula Kirchinger

(geb. Baumeister)

Vollständiger Abdruck der von der promotionsführenden Einrichtung Campus Straubing für Biotechnologie und Nachhaltigkeit der Technischen Universität München zur Erlangung einer

Doktorin der Ingenieurwissenschaften (Dr.-Ing.)

genehmigten Dissertation.

Vorsitzender:	Prof. Dr.-Ing. Matthias Gaderer
Prüfer der Dissertation:	1. Prof. Dr.-Ing. Jakob Burger
	2. Prof. Dr.-Ing. Fabian Jirasek

Die Dissertation wurde am 11.03.2022 bei der Technischen Universität München eingereicht und von der promotionsführenden Einrichtung Campus Straubing für Biotechnologie und Nachhaltigkeit am 24.06.2022 angenommen.

Danksagung

Die vorliegende Arbeit entstand während meiner Tätigkeit als wissenschaftliche Mitarbeiterin der Professur für chemische und thermische Verfahrenstechnik am Campus Straubing für Biotechnologie und Nachhaltigkeit der Technischen Universität München.

An erster Stelle danke ich meinem Doktorvater Prof. Dr.-Ing. Jakob Burger für die Bereitstellung des interessanten Themas, für das entgegengebrachte Vertrauen und für die wertvollen Impulse in den fachlichen Diskussionen. Herzlichen Dank für die zielführende Betreuung meiner Doktorarbeit!

Prof. Dr.-Ing. Fabian Jirasek danke ich für die Begutachtung dieser Arbeit und Prof. Dr.-Ing. Mathias Gaderer für die Übernahme des Prüfungsvorsitzes.

Ein besonderer Dank geht an meinen Mentor JP Dr.-Ing. Maximilian Kohns für die Unterstützung bei fachlichen Fragen und Problemen und die zielführenden Diskussionen.

Vielen Dank auch an Marlit Köstler und Sabine Witzel für die unkomplizierte Unterstützung und Hilfe im Labor.

Ein herzlicher Dank geht an alle meine Kollegen der Professur für chemische und thermische Verfahrenstechnik für die angenehme und freundschaftliche Atmosphäre an der Uni und für die schöne Zeit auch darüber hinaus. Insbesondere danke ich Johannes Voggenreiter und Yannic Tönges für die zahllosen Diskussionen und angenehmen Gespräche. Herzlichen Dank auch an Christina Wolf für die Unterstützung bei Fragen und Problemen im Labor und an Birgit Aich-Bauer für die Hilfe bei administrativen Aufgaben und für die netten Gespräche.

Nicht zuletzt danke ich von Herzen meinen Eltern, meinen beiden Schwestern und Michi. Vielen Dank für euren Rückhalt, für eure Unterstützung in jeder Situation und dass ich immer auf euch zählen kann.

Straubing, im September 2022
Eva Kirchinger

Abstract

Liquid mixtures with a complex composition or liquid mixtures which cannot - or only with great effort - be fully analyzed appear regularly in many fields of process engineering. Thermodynamic modeling of such mixtures is challenging. Such models are needed in particular for process design and optimization. In the first part of the present work, a novel approach - a perturbation scheme - is presented to model poorly specified liquid mixtures comprised of specified and unknown components. Since the unknown components can have a crucial impact on the thermodynamic behavior of the specified components in the mixture, it is necessary to consider the impact of the unknown components in the thermodynamic model. The perturbation scheme models the effect of the unknown components on the activities of the specified components. As input, an activity model of the subsystem of the specified components and few experimental data on the property of interest in the poorly specified mixture are needed. The perturbation scheme is applied successfully to several example systems to model the thermodynamic behavior of the specified components. The example systems are based on pseudo experimental data or experimental data obtained from the literature. Additionally, the perturbation scheme is applied to different example processes based on experimental data from the literature. The last part of the present work reports experimental data of the solubility of α-lactose in solutions of water-ethanol-NaCl and water-ethanol-$CaCl_2$ at 298.15 K. The experimental solubility data are successfully modeled using two approaches, both of which are based on the UNIQUAC model. A modified UNIQUAC model extended by a Debye-Hückel term as well as a UNIQUAC model extended by the perturbation scheme introduced in the first part of the present work are used.

Kurzfassung

Flüssige Mischungen mit komplexer Zusammensetzung oder flüssige Mischungen, die nicht - oder nur mit sehr großem Aufwand - vollständig analysiert werden können, treten in vielen Bereichen der Verfahrenstechnik regelmäßig auf. Die thermodynamische Modellierung solcher Mischungen ist eine Herausforderung. Jedoch werden diese Modelle insbesondere für Prozessauslegung und -optimierung benötigt. Im ersten Teil der vorliegenden Arbeit wird ein neuer Ansatz - ein Störungs-Schema - zur Modellierung schlecht spezifizierter, flüssiger Mischungen, bestehend aus bekannten Komponenten und unbekannten Komponenten, vorgestellt. Da die unbekannten Komponenten einen entscheidenden Einfluss auf das thermodynamische Verhalten der bekannten Komponenten im Gemisch haben können, ist es notwendig, den Einfluss der unbekannten Komponenten im thermodynamischen Modell zu berücksichtigen. Das Störungs-Schema modelliert den Einfluss der unbekannten Komponenten auf die Aktivitäten der bekannten Komponenten. Das Störungs-Schema benötigt ein Aktivitätsmodell für das Teilsystem bestehend aus den bekannten Komponenten und einige wenige experimentelle Daten der schlecht spezifizierten Mischung zu der Größe, die von Interesse ist. Das Störungs-Schema wurde erfolgreich auf mehrere Beispielsysteme angewendet, um das thermodynamische Verhalten der bekannten Komponenten zu modellieren. Die Beispielsysteme basieren auf pseudo-experimentellen Daten oder experimentellen Daten aus der Literatur. Zusätzlich wurde das Störungs-Schema auf verschiedene Beispielprozesse angewandt, die ebenfalls auf experimentellen Daten aus der Literatur beruhen. Im letzten Teil der vorliegenden Arbeit werden experimentelle Daten zur Löslichkeit von α-Laktose in Lösungen bestehend aus Wasser-Ethanol-NaCl und Wasser-Ethanol-$CaCl_2$ bei 298,15 K präsentiert. Die experimentellen Löslichkeitsdaten wurden anschließend erfolgreich mit zwei verschiedenen Ansätzen modelliert. Beide Ansätze basieren auf dem UNIQUAC Modell. Zum einen wird ein modifiziertes UNIQUAC Modell mit einer Debye-Hückel-Term Erweiterung verwendet, zum anderen das UNIQUAC Modell kombiniert mit dem Störungs-Schema, das im ersten Teil der vorliegenden Arbeit vorgestellte wurde.

Declaration

This dissertation contains material that has been published previously, or that is included in submitted publications. In the following, these publications are listed together with a statement on the contributions of the author of the present dissertation.

- Baumeister, E., Burger, J.: General Perturbation Scheme to Model Activities in Poorly Specified Liquid Mixtures, Industrial & Engineering Chemistry Research 1 (2020) 413-422.

  The author developed, implemented, and tested the method, set up and performed the simulations, and evaluated the results. The author wrote the manuscript.

- Baumeister, E., Voggenreiter, J., Kohns, M., Burger, J.: Measurement and modeling of the solubility of α-lactose in water-ethanol electrolyte solutions at 298.15 K, Fluid Phase Equilibria 556 (2022), 113378.

  The author carried out the experiments, developed, implemented, and tested the method, set up and performed the simulations, and evaluated the results. The author wrote the manuscript.

Contents

List of Symbols

Latin Letters

A_{ij}	interaction parameter between component i and j / model parameter
$A_{k\mathrm{u}}$	interaction parameter between specified component k and the unknown part u / model parameter perturbation scheme
$A_{k\mathrm{e}}$	interaction parameter between specified component k and electrolyte part e / model parameter perturbation scheme
A_m	Debye-Hückel parameter
a_{ca}	Bromley parameter
a_k	activity of specified component k
$\tilde{a}_k$	activity of specified component k within the specified subsystem
a_{kl}	binary interaction parameter between component k and l of the NRTL model
B_{ca}	Bromley parameter
B_m	Debye-Hückel parameter
B_0	reference inverse molality
b_k	molality of specified component k
b_{kl}	binary interaction parameter between component k and l of the NRTL model
b_0	reference molality
$\bar{d}$	average absolute deviation (AAD)
f_k	fugacity of specified component k
$\tilde{f}_k$	fugacity of specified component k within the specified subsystem
G_{kl}	coefficient of the NRTL model
g^{E}	molar excess Gibbs free energy
Δh_k^{f}	enthalpy of fusion of specified component k
I_m	ionic strength
K	number of specified components
K_k	equilibrium constant of specified component k
K^{D}	equilibrium constant of dimerization

M_k	molar mass of specified component k
$\bar{M}_\mathrm{u}$	average molar mass of unknown part / model parameter perturbation scheme
m	mass
$\dot{m}_i$	mass flow of component i
n	mole number
N	number of all components in a mixture
P_k	vapor-liquid partition coefficient of specified component k
p	pressure
p_k^s	vapor pressure of component k
$p_k^{\mathrm{s}*}$	true vapor pressure of component k (chemical theory)
p^0	reference pressure
q_k	surface-area parameter of component k of the UNIQUAC model
Q	number of experimental data points
R	universal gas constant
r_k	volume parameter of component k of the UNIQUAC model
s	standard deviation
T	temperature
T_i^f	melting temperature of specified component k
u_{kl}	interaction parameter between component k and l of the UNIQUAC model
u_{im}^*	reference interaction parameter between ion i and solvent m of the
w_i	mass fraction of component i
w_u	mass fraction of the whole unknown part u
$\tilde{w}_k$	mass fraction of specified component k within specified subsystem
$\hat{w}_k$	mass fraction of specified component k in a reduced form (if all components but water are removed)
$\bar{w}_i$	mean mass fraction of component i
x_i	mole fraction of component i
x_e	cumulative mole fraction of all electrolytes
x_u	mole fraction of the whole unknown part u
$\tilde{x}_k$	mole fraction of specified component k within specified subsystem
x_k^p	colligative term of specified component k of the perturbation scheme
$\mathbf{x}$	vector of all mole fractions in the mixture
$\tilde{\mathbf{x}}$	vector of all mole fractions in the specified subsystem
$\mathbf{x}^*$	vector of all mole fractions in the reference mixture (Henry-like normalization)

y_i	mole fraction of component i in the vapor phase / overall mole fraction of component i in the vapor phase (chemical theory)
y_i^*	true mole fraction of component i in the vapor phase (chemical theory)
z	constant of the UNIQUAC model
z_i	charge number of ion i

Greek Letters

α_{kl}	NRTL nonrandomness parameter
γ_k	activity coefficient of specified component k normalized according to Raoult
$\tilde{\gamma}_k$	activity coefficient of specified component k normalized according to Raoult within specified subsystem
γ_k^*	activity coefficient of specified component k normalized according to Henry
$\tilde{\gamma}_k^*$	activity coefficient of specified component k normalized according to Henry within specified subsystem
γ_k^{p}	interaction term of specified component k in the perturbation scheme
$\delta_{ij,m}$	interaction parameter between ion i and j and solvent m of the UNIQUAC-DH model
Θ	experimental quantity
θ_k	surface-area fraction of component k
μ_k	chemical potential of specified component k
τ_{kl}	coefficient of the NRTL model
φ_k	fugacity coefficient of specified component k
$\tilde{\varphi}_k$	fugacity coefficient of specified component k
φ_k^{p}	interaction term of specified component k in the perturbation scheme
χ	evaporated mass fraction of initial mixture
χ_{a}	share of unknown part a within the combined unknown part
ϕ_k	volume fraction of component k
Ψ_{kl}	interaction parameter between component k and l of the UNIQUAC model

Subscripts

a	anion
c	cation
e	all electrolyte components summarized
i, j	general component
i,j	ions / electrolyte components
k, l, m, n	specified component
m	solvent
u	unknown part
$'$, $''$	liquid phase

Superscripts

C	combinatorial
DH	Debye-Hückel
excess	excess solid
exp	experimental
(i)	stream i
model	model
p	perturbation
R	residual

Abbreviations

AAD	average absolute derivation
DH	Debye-Hückel
LLE	liquid-liquid equilibrium
NRTL	non-random two-liquid
PS	perturbation scheme
SLE	solid-liquid equilibrium
UNIQUAC	universal quasichemical
VLE	vapor-liquid equilibrium

1 Introduction

Complex liquid mixtures of hundreds or thousands of components appear regularly in the process industry, e.g. in the petrochemistry [1, 2], wastewater treatment [3, 4], or biotechnology [5, 6]. Typically, these mixtures have one or a few specified components of main interest besides many unknown components that cannot - or only with great effort - be analyzed qualitatively and/or quantitatively. In many cases, it is not even known how many unknown components there are in the mixture. These poorly specified mixtures are challenging in thermodynamic modeling and process simulation since classical approaches [7, 8], e.g. g^{E}-models such as NRTL (non-random two-liquid) [9] or UNIQUAC (universal quasichemical) [10] or equations of state, require full specification of the mixture.

Although the chemical nature of the unknown components cannot be elucidated, they can have a crucial impact on the performance of many process units by affecting the properties and the behavior of the target components. Even though the impact of the unknown components is often not understood physically, it can be quantified in many cases. For example, the freezing point depression of water in aqueous electrolyte solutions can be measured [11–13]. To do so, it is not necessary to know the unknown components and the composition of the electrolyte solution besides the specified component water. This ability to measure the impact of the unknown on the specified part of the mixture opens the door for many approaches to model poorly specified mixtures.

The conceptually simplest form of modeling poorly specified mixtures is well-known under the term colligative properties [14, 15]. Thereby, the depression of a specified solvent's activity due to dilution by a specified or unknown solute, often an electrolyte, is considered. The activity of the specified solvent in the poorly specified mixture with specified or unknown solutes is modeled as the product of the pure solvent's activity with some constant smaller than one, which is dependent on the mole number but not on the chemical nature of the solute. In its core, a well-known property (the pure solvent's activity) is perturbed (by the multiplication with the constant) to model the same property in the complete (poorly specified) mixture. The concept of colligative properties is often applied to model freezing point depressions, melting point elevations, and osmotic pressures with acceptable accuracy for rather diluted solutions with single

solvents [14]. Thereby, it is conceptually no difference whether the solutes are specified or unknown.

If not a single solvent but rather a mixture consisting of several specified solvents and an additional unknown part is considered, alternative approaches are required. The most common approach to model such poorly specified mixtures is the pseudo component approach, mainly used in the field of petrochemical engineering [16–19]. Thereby, the subsystem of specified solvents is modeled with a standard thermodynamic model, e.g. a g^{E}-model [20–23] or an equation of state [24–30], and the unknown part is considered by adding one or more pseudo components to the model. The pseudo components' pure component properties and their interaction parameters are parameterized using assumptions or fits to experimental data. The exact procedure and effort for this parameterization depend strongly on the chosen thermodynamic model. The pseudo components approach can be also applied to process simulation [31]. However, usually no information of the molecular structure of the pseudo components is available [32]. A workaround to avoid this lack of information - in cases where necessary - the pseudo components or the complete mixture can be substituted by real components that behave similarly. This is done, for example, in process simulations in the fields of petrochemistry [32–34] or wastewater treatment [35, 36].

Although the pseudo-component approach is practically easy to implement, a challenge remains in selecting and parameterizing the pseudo components, as there remains some ambiguity in this step. Recently, the NEAT method (NMR spectroscopy for the estimation of the activity coefficients of target components in poorly specified mixtures) [6, 37–41] was introduced, which links the pseudo-component approach to experimental spectroscopic analysis. The specified components are modeled by the group contribution method UNIFAC (Dortmund) [42, 43] or the COSMO-RS model [44, 45], and the unknown pseudo components are selected automatically based on the unknown functional groups of the NMR spectrum of the complete mixture.

When using pseudo components, a discrete or fraction-wise characterization of the unknown part is applied. In contrast, continuous thermodynamics uses continuous functions to describe poorly specified mixtures. This approach is often applied to model polymer systems [46–53]. Also machine learning is used to optimize processes or predict process properties of poorly specified mixtures, in particular for petrochemistry, by using experimental or process data [54–60].

The present work provides an alternative and novel method to model the thermodynamic properties of poorly specified liquid mixtures. The starting point is a thermodynamic model of the subsystem consisting of all known and quantifiable components of the

mixture, typically a g^{E}-model or an equation of state of some sort. This subsystem and this model are called specified subsystem and base model, respectively, in the following. Since the mixture consists of additional unknown components, a perturbation term is added to the base model to consider the effect of the unknown components. This can be seen as an extension of the colligative properties approach. An extension in that sense that not only one specified solvent but a specified multicomponent subsystem serves as starting point, and that interactions with the unknown part are explicitly considered to overcome the limitation to highly diluted mixtures. The perturbation term that is derived in the present work is general, can be applied to any type of thermodynamic model, i.e. to g^{E}-models or to equations of state, and has only a small number of model parameters.

The idea to augment nominal thermodynamic models by perturbation terms in process modeling and simulation is already described in the context of considering model uncertainties of the base model [61–64]. Here we go one step further and capture even the impact of unknown components on the specified components.

The present work is structured as follows: In Chapter 2 the idea, the derivation, and the characteristics of the perturbation scheme are introduced. Chapter 3 presents several example systems to demonstrate the performance of the perturbation scheme. The data of the studied systems are obtained from fully specified thermodynamic models (pseudo experimental data) and from the literature (experimental data). The systems are comprised of organic and aqueous-organic mixtures as well as aqueous-electrolyte mixtures. Chapter 4 gives a workflow how to handle poorly specified mixtures in process simulation. Three different example processes with poorly specified mixtures are studied. In Chapter 5 experimental solubility data of α-lactose in aqueous-organic-electrolyte solvents are shown. Further, the solubility data are modeled using the UNIQUAC model extended with a Debye-Hückel term [65] and using the UNIQUAC model extended with the perturbation scheme of the present work. The final Chapter 6 summarizes the main findings.

2 Perturbation Scheme

2.1 Fundamentals

General

The perturbation scheme of the present work enables to model the thermodynamic properties of specified components in poorly specified mixtures. The poorly specified mixture, i.e. the complete mixture, with the known mass m and $i = 1 \dots N$ components, consists of two parts (cf. Figure 1): the specified subsystem comprised of $k = 1 \dots K$ ($K < N$) specified, i.e. known, components and the unknown part comprised of $v = 1 \dots (N - K)$ unknown components.

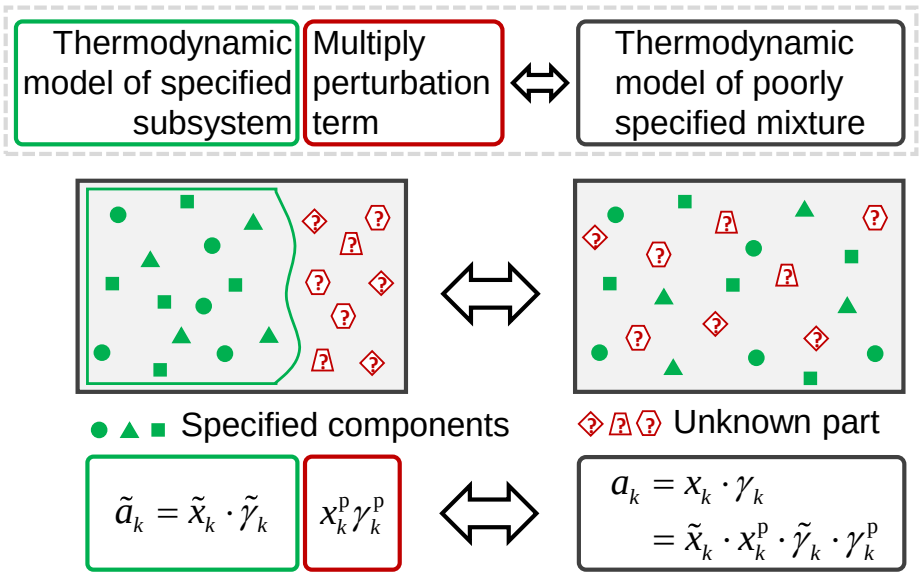

Figure 1: The proposed perturbation scheme of the present work. Top row: the thermodynamic model of the specified subsystem multiplied with the perturbation term gives the thermodynamic model of the complete poorly specified mixture. Middle row: hypothetical division of a poorly specified mixture into a specified subsystem and an unknown part. Bottom row: structure of the perturbation model.

It is required that the mass m_k or the molar amount n_k and the molar mass M_k of every component k in the specified subsystem are known. For the unknown part, almost no specific information is necessary. Neither the total number N of components in the mixture nor the chemical nature of the unknown components has to be known. There is one exception: the mass of the unknown part m_u must be known. This is no limitation since m_u can be calculated from

$$m_\mathrm{u} = m - \sum_{k=1}^{K} m_k = m - \sum_{k=1}^{K} n_k M_k. \tag{1}$$

In liquid mixtures, the activity a_k of a specified component k is a key property. If modeled accurately, the activity a_k leads beside other thermodynamic properties of the specified components to quantitative descriptions of many process-relevant phenomena, such as chemical equilibria or phase equilibria involving liquid phases. The activities of specified components in poorly specified mixtures can be measured. This becomes important later because the model parameters must be fitted to experimental data.

Here, the target is to model the activities a_k of the specified components in the complete mixture. The activity a_k and the activity coefficient γ_k can be defined in several ways, depending on the normalization of the chemical potential μ_k. Here, it is normalized with respect to the pure liquid at temperature T and pressure p of interest according to Raoult: [39]

$$\mu_k = \mu_k^{\mathrm{pure,liquid}}(T,p) + RT \ln\left(x_k \gamma_k\left(T,p,\mathbf{x}\right)\right), \tag{2}$$

where $\mu_k^{\mathrm{pure\,liq}}$ is the reference chemical potential, $\mathbf{x}$ is the vector of the mole fractions, and R is the universal gas constant. The corresponding activity a_k is expressed as the product of the mole fraction x_k and the activity coefficient γ_k of component k that depends on the temperature T, the pressure p, and the mole fractions of all components $\mathbf{x}$.

$$a_k = x_k \gamma_k(T,p,\mathbf{x}) \tag{3}$$

Let us, for now, focus on the conceptually isolated specified subsystem, i.e. as if the unknown part would be removed from the complete mixture. Additionally, we assume that it is comprised of only non-electrolyte components. All symbols which refer to properties of the conceptually isolated specified subsystem are denoted with a tilde (~). As all mole numbers of the specified subsystem are assumed to be known, the mole fractions of all specified components $\tilde{x}_k$ in the specified subsystem can be calculated.

$$\tilde{x}_k = \frac{n_k}{\sum_{k=1}^{K} n_k} \tag{4}$$

It is assumed that an activity coefficient model of the specified subsystem - called base model in the following - is given.

$$\tilde{\gamma}_k = \tilde{\gamma}_k(T, p, \tilde{\mathbf{x}}) \tag{5}$$

Thus, the activities of all specified components in the mixture comprised of only the specified subsystem are known.

$$\tilde{a}_k = \tilde{x}_k \tilde{\gamma}_k(T, p, \tilde{\mathbf{x}}) \tag{6}$$

If the complete mixture is considered, the right hand side of Eq. (6) would clearly not give the correct activity a_k of component k. Therefore we introduce a multiplicative perturbation on the right hand side of Eq. (6) to yield a_k in the complete mixture.

$$a_k = \underbrace{\tilde{x}_k x_k^{\mathrm{p}}}_{x_k} \cdot \underbrace{\tilde{\gamma}_k \gamma_k^{\mathrm{p}}}_{\gamma_k} \tag{7}$$

The perturbation has two terms: a colligative term x_k^{p} and an interaction term γ_k^{p}. The colligative term considers that the components' activities in the specified subsystem change due to dilution by adding the unknown part. The interaction term considers additional perturbations due to interactions between the specified components and the unknown part.

The colligative effects are considered by the term

$$x_k^{\mathrm{p}} = (1 - x_{\mathrm{u}}). \tag{8}$$

Therein, x_{u} is the mole fraction of the whole unknown part. Since only the total mass of the unknown part is known but not the mole number of unknown components, x_{u} is not known in most cases.

If the average molar mass $\bar{M}_{\mathrm{u}}$ [1] of the unknown part would be known, its mole fraction x_{u} could however be calculated from its mass m_{u}.

$$x_{\mathrm{u}} = \frac{n_{\mathrm{u}}}{n_{\mathrm{u}} + \sum_{k=1}^{K} n_k} = \frac{\frac{m_{\mathrm{u}}}{\bar{M}_{\mathrm{u}}}}{\frac{m_{\mathrm{u}}}{\bar{M}_{\mathrm{u}}} + \sum_{k=1}^{K} \frac{m_k}{M_k}} = \frac{\frac{w_{\mathrm{u}}}{\bar{M}_{\mathrm{u}}}}{\frac{w_{\mathrm{u}}}{\bar{M}_{\mathrm{u}}} + \sum_{k=1}^{K} \frac{w_k}{M_k}} \tag{9}$$

[1] In the present work, $\bar{M}_{\mathrm{u}}$ is considered as a model parameter of the perturbation, and it is fitted to experimental data with one exception: Jirasek et al. [39] found for a similar approach, that for **aqueous systems** the average molar mass of the unknown part $\bar{M}_{\mathrm{u}}$ has only a slight influence on the quality of the results as long as the value is large enough. In the present work, $M_{\mathrm{u}} = 50$ g/mol was found to be sufficiently large and gave very good results in all studied cases. Hence, for all aqueous specified subsystems, the model parameter of the average molar mass of the unknown part was set to that value and not fitted.

In the above equation, w_u and w_k are the mass fractions of the unknown part and the specified component k, respectively.

Inserting Eq. (8) into Eq. (7) leads to

$$a_k = \underbrace{\tilde{x}_k(1 - x_u)}_{x_k} \underbrace{\tilde{\gamma}_k \gamma_k^p}_{\gamma_k} . \tag{10}$$

One important aspect of the perturbation scheme is that the activities of only the specified components are modeled. The influence of the unknown part on the specified components is nevertheless considered. In many cases, this is sufficient to model or optimize processes. The perturbation scheme makes no predication about the activity of the unknown part or the activity of single unknown components in the complete mixture. This automatically leads to the thermodynamic consistency of the perturbation scheme regarding the Gibbs-Duhem equation. The reason for this is as follows: Since no information on the mole numbers and chemical potentials of the unknown components is available, the Gibbs-Duhem equation can not be checked. On the contrary, if one assumes that only one unknown component exists, one could gain information on its chemical potential from the Gibbs-Duhem equation.

Electrolyte Systems

In the derivation of the structure of the perturbation scheme before, the chemical potential μ_k of a specified electrolyte k was normalized according to Raoult. This normalization is used for non-electrolyte components. If the specified subsystem is contains electrolytes a different normalization of the chemical potential μ_k is used. For electrolytes, usually the chemical potential μ_k of a specified electrolyte k is normalized with respect to infinite dilution according to Henry:[66]

$$\mu_k = \mu_k^{\mathrm{ref,H}}(T, p, \mathbf{x}^*) + RT \ln\left(\frac{b_k}{b_0}\gamma_k^*(T, p, \mathbf{x})\right), \tag{11}$$

where $\mu_k^{\mathrm{ref,H}}$ is the reference chemical potential, $\mathbf{x}^*$ is the corresponding reference solution composition, b_k is the molality, i.e. the number of moles of the specified component k per kilogram of pure solvent (here: always water), and γ_k^* is the activity coefficient in the molality scale. The constant b_0 is defined as 1 mol kg^{-1} and used to get rid of the units. The corresponding activity is given as the product of the molality b_k and the

activity coefficient γ_k^*.

$$a_k = \frac{b_k}{b_0} \cdot \gamma_k^*(T, p, \mathbf{x}) \tag{12}$$

For an electrolyte component k, Eq. (10) would be as follows:

$$a_k = \frac{b_k}{b_0} \cdot \underbrace{\tilde{\gamma}_k^* \gamma_k^{\mathrm{p}}}_{\gamma_k^*} . \tag{13}$$

Figure 2 shows the schematic structure of the perturbation scheme for poorly specified electrolyte mixtures in analogy to Figure 1. In Figure 1, the specified subsystem is comprised of aqueous-organic components. In Figure 2, the specified subsystem is comprised of aqueous-electrolyte components. No details are given about the composition of the unknown part in either case.

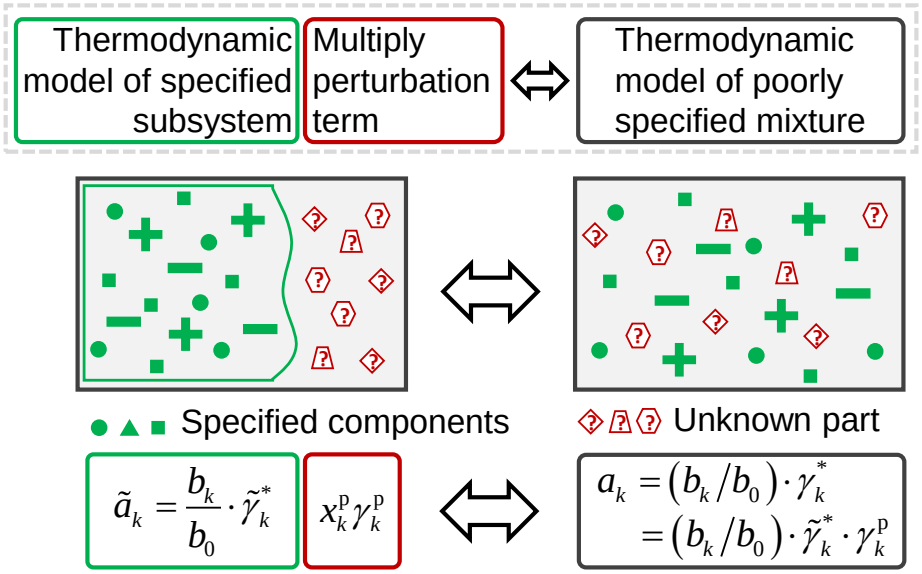

Figure 2: The proposed perturbation scheme of the present work for specified electrolyte subsystems. Top row: the thermodynamic model of the specified subsystem multiplied with the perturbation term gives the thermodynamic model of the complete poorly specified mixture. Middle row: hypothetical division of a poorly specified mixture into a specified subsystem and an unknown part. Bottom row: structure of the perturbation model for poorly specified electrolyte mixtures.

Equations of State

In cases where the base model is an equation of state, chemical equilibria, and phase equilibria are described rather with fugacities f_k than with activities a_k. The fugacity is the product of the mole fraction x_k and the fugacity coefficient φ_k.

$$f_k = x_k \varphi_k \tag{14}$$

It is assumed that the fugacity in the corresponding mixture consisting only of the specified components is known.

$$\tilde{f}_k = \tilde{x}_k \tilde{\varphi}_k \tag{15}$$

In full analogy to the activity, the perturbation is introduced as

$$f_k = \underbrace{\tilde{x}_k x_k^{\mathrm{p}}}_{x_k} \cdot \underbrace{\tilde{\varphi}_k \varphi_k^{\mathrm{p}}}_{\varphi_k} . \tag{16}$$

For the colligative term x_k^{p}, the same arguments hold as in the case of the activity, cf. Eq. (8) and Eq. (9). To derive an expression for the interaction term φ_k^{p} of the perturbation, we look at the chemical potential μ_k of component k in an arbitrary mixture, using one time the standard state of the pure ideal gas (resulting in the definition of φ_k) and the other time the standard state of the pure liquid (Raoult's standard state resulting in the definition of γ_k).

$$\mu_k(T, p, \mathbf{x}) = \mu_k^{\mathrm{pure,id.Gas}}(T, p) + RT \ln\left(x_k \varphi_k(T, p, \mathbf{x})\right) \tag{17}$$

$$\mu_k(T, p, \mathbf{x}) = \mu_k^{\mathrm{pure,liq.}}(T, p) + RT \ln\left(x_k \gamma_k(T, p, \mathbf{x})\right) \tag{18}$$

Applying Eq. (17) to the state of the pure liquid k yields

$$\mu_k^{\mathrm{pure,liq.}} = \mu_k^{\mathrm{pure,id.Gas}}(T, p) + RT \ln(\varphi_k^{\mathrm{pure,liq.}}(T, p)). \tag{19}$$

Inserting Eq. (19) into Eq. (18) and comparing with Eq. (17) yields

$$\varphi_k(T, p, \mathbf{x}) = \varphi_k^{\mathrm{pure,liq.}}(T, p) \gamma_k(T, p, \mathbf{x}). \tag{20}$$

Eq. (20) holds for the poorly specified mixture but also for the mixture consisting only of the components of the specified subsystem.

$$\tilde{\varphi}_k(T, p, \tilde{\mathbf{x}}) = \varphi_k^{\mathrm{pure,liq.}}(T, p) \tilde{\gamma}_k(T, p, \tilde{\mathbf{x}}) \tag{21}$$

Division of Eq. (20) by Eq. (21) yields

$$\underbrace{\frac{\varphi_k(T,p,\mathbf{x})}{\tilde{\varphi}_k(T,p,\tilde{\mathbf{x}})}}_{\varphi_k^{\mathrm{P}}} = \underbrace{\frac{\gamma_k(T,p,\mathbf{x})}{\tilde{\gamma}_k(T,p,\tilde{\mathbf{x}})}}_{\gamma_k^{\mathrm{P}}}. \tag{22}$$

The left-hand side of Eq. (22) is by definition equal to the interaction term φ_k^{P} in the perturbation scheme of the fugacity, the right hand side of Eq. (22) to the interaction term γ_k^{P} in the perturbation scheme of the activity. Thus, any perturbation term for γ_k^{P} can also be used straightforwardly for φ_k^{P}.

In full analogy to Eq. (10) one derives:

$$f_k = \tilde{x}_k(1-x_{\mathrm{u}})\tilde{\varphi}_k\gamma_k^{\mathrm{P}}. \tag{23}$$

2.2 Specification and Derivation of the Interaction Term

In principle, the functional of the perturbation term γ_k^{P} (cf. Eq. (7) and Eq. (13)) is almost arbitrary. One should however assure that the perturbation effect disappears when the unknown part of the mixture disappears (i.e. $\gamma_k^{\mathrm{P}} \to 1$ when $x_{\mathrm{u}} \to 0$). One could use for example the functional

$$\ln \gamma_k^{\mathrm{P}} = A_{k\mathrm{u}} x_{\mathrm{u}}^2 \tag{24}$$

with $A_{k\mathrm{u}}$ being an interaction parameter, which is fitted to experiments with the poorly specified mixture. We have tested the functional of Eq. (24) in several examples and found that it yields unsatisfactory results when more than one specified component is considered. In these cases, the simple Eq. (24) does not take into account how the presence of other specified components influences the interactions between the specified component k and the unknown part. To consider these interactions, we derived a more sophisticated interaction term γ_k^{P}.

The functional of the interaction term γ_k^{P} is based on the symmetric Margules-type model for the molar excess Gibbs free energy g^{E} [67]. For a binary mixture ($i = 1, 2$) the term for g^{E} in that case is

$$\frac{g^{\mathrm{E}}}{RT} = A_{12} x_1 x_2. \tag{25}$$

Therein, x_i is the mole fraction of the component i in the mixture, A_{ij} is the interaction

parameter between the component i and j, T is the temperature, and R the universal gas constant. From Eq. (25) the activity coefficients γ_i can be deduced. For component 1, the activity coefficient is

$$RT \ln \gamma_1 = A_{12} {x_2}^2. \tag{26}$$

For a ternary system ($i = 1, 2, 3$) the Margules-type equation for g^{E} is [67]

$$\frac{g^{\mathrm{E}}}{RT} = A_{12} x_1 x_2 + A_{13} x_1 x_3 + A_{23} x_2 x_3. \tag{27}$$

For component 1, the activity coefficient γ_1 results in

$$RT \ln \gamma_1 = A_{12} x_2 (1 - x_1) + A_{13} x_3 (1 - x_1) - A_{23} x_2 x_3. \tag{28}$$

To obtain the interaction term of the perturbation scheme, we assume for one moment that the specified subsystem consists of exactly two components ($K = 2$) and that the unknown part consists of one additional component (Index: u) similar to the pseudo-component approach. Analogous to Eq. (26), the activity coefficient $\tilde{\gamma}_1$ of component 1 in the mixture that consists of only the specified subsystem is

$$RT \ln \tilde{\gamma}_1 = A_{12} {\tilde{x}_2}^2. \tag{29}$$

Eq. (28) gives the activity coefficient γ_1 of component 1 in the complete mixture.

$$RT \ln \gamma_1 = A_{12} x_2 (1 - x_1) + A_{1\mathrm{u}} x_{\mathrm{u}} (1 - x_1) - A_{2\mathrm{u}} x_2 x_{\mathrm{u}} \tag{30}$$

From the definition of the perturbation scheme, cf. Eq. (7), we know that

$$\gamma_1 = \tilde{\gamma}_1 \gamma_1^{\mathrm{p}}, \tag{31}$$

or rearranged

$$RT \ln \gamma_1^{\mathrm{p}} = RT \ln \gamma_1 - RT \ln \tilde{\gamma}_1. \tag{32}$$

Inserting Eq. (30) in Eq. (32) and expanding the first term on the right hand side with $\frac{x_2}{x_2}$ leads to

$$RT \ln \gamma_1^{\mathrm{p}} = A_{12} x_2 (1 - x_1) \frac{x_2}{x_2} + A_{1\mathrm{u}} x_{\mathrm{u}} (1 - x_1) - A_{2\mathrm{u}} x_2 x_{\mathrm{u}} - RT \ln \tilde{\gamma}_1. \tag{33}$$

After replacing x_2 with $\tilde{x}_2 (1 - x_{\mathrm{u}})$, cf. definition of the colligative effect Eq. (8), we

obtain:

$$RT \ln \gamma_1^{\mathrm{p}} = \underbrace{A_{12} \tilde{x}_2^2}_{= RT \ln \tilde{\gamma}_1} \frac{(1 - x_{\mathrm{u}})^2 (1 - x_1)}{x_2} + A_{1\mathrm{u}} x_{\mathrm{u}} (1 - x_1) - A_{2\mathrm{u}} x_2 x_{\mathrm{u}} - RT \ln \tilde{\gamma}_1. \tag{34}$$

Inserting Eq. (29) and rearrangement leads to the expression of the interaction term of the perturbation.

$$\ln \gamma_1^{\mathrm{p}} = \ln \tilde{\gamma}_1 \left(\frac{(1 - x_{\mathrm{u}})^2 (1 - x_1)}{x_2} - 1 \right) + \frac{x_{\mathrm{u}}}{RT} \left(A_{1\mathrm{u}} (1 - x_1) - A_{2\mathrm{u}} x_2 \right) \tag{35}$$

We suggest some empirical modifications to Eq. (35) to also consider a specified subsystem with more than two components, which leads to the final interaction term:

$$\ln \gamma_k^{\mathrm{p}} = \ln \tilde{\gamma}_k \left(\frac{(1 - x_{\mathrm{u}})^2 (1 - x_k)}{1 - x_{\mathrm{u}} - x_k} - 1 \right) + \frac{x_{\mathrm{u}}}{RT} \left(A_{k\mathrm{u}} - \sum_{i=1}^{K} A_{i\mathrm{u}} x_i \right). \tag{36}$$

For subsystems comprised of electrolyte components the function for $\ln \gamma_k^{\mathrm{p}}$ is:

$$\ln \gamma_k^{\mathrm{p}} = \ln \tilde{\gamma}_k^{\star} \left(\frac{(1 - x_{\mathrm{u}})^2 (1 - x_k)}{1 - x_{\mathrm{u}} - x_k} - 1 \right) + \frac{x_{\mathrm{u}}}{RT} \left(A_{k\mathrm{u}} - \sum_{i=1}^{K} A_{i\mathrm{u}} x_i \right). \tag{37}$$

Despite the empirical modifications the interaction term has still the following characteristics: For one specified component ($K = 1$) the term γ_k^{p} simplifies to:

$$RT \ln \gamma_1^{\mathrm{p}} = A_{1\mathrm{u}} x_{\mathrm{u}}^2. \tag{38}$$

So, the unknown part is considered as a second component. For two specified components ($K = 2$) the term γ_1^{p} is equal to Eq. (35).

This interaction term (cf. Eq. (36) and Eq. (37)) overcomes the restrictions of the term in Eq. (24). For negligible fractions of the unknown part ($x_{\mathrm{u}} \to 0$, $\sum_{j=1}^{K} x_j \to 1$), it follows that $\gamma_k^{\mathrm{p}} \to 1$. There is one interaction parameter $A_{k\mathrm{u}}$ with the unknown part for every specified component. This parameter is a fitting parameter when applying the perturbation scheme. Thus, the perturbation approach has the following fitting parameters: One interaction parameter $A_{k\mathrm{u}}$ for each specified component and the average molar mass $\bar{M}_{\mathrm{u}}$ of the unknown part.

Obviously, other terms for the interactions of the specified components with the unknown part are possible. For example, in the derivation, one could use a g^{E}-model that is more sophisticated than the Margules-type equation. This would eventually lead to more parameters for the interactions with the unknown part. By studying examples, we

found that Eq. (36) and Eq. (37) yielded quite good results.

The focus of the following chapters is to explore both the practical applications and limitations of the presented perturbation scheme. Two aspects, however, shall be discussed here already. First, the perturbation scheme's applicability relies on the prerequisite that the composition and constitution (e.g. state of complexation, degree of dissociation) of the unknown part does not change during application. This prerequisite involves that the unknown part remains as a whole in the one liquid phase of interest. Most likely, this leads to significant limitations when liquid-liquid equilibria or vapor-liquid equilibria with volatile unknown components are studied. However, when studying solid-liquid equilibria, e.g. in crystallization or precipitation of a specified component, these constraints on the unknown part might be well met.

Second, we want to discuss the challenge of parameter estimation from experimental data. We assume that the poorly specified liquid mixture is given as a sample, and experiments such as solubility measurements can be done with it. If this is the case, one can determine the activities of specified components from the experiments. One could dilute the samples of the poorly specified mixture with known amounts of specified components and do additional experiments with the diluted samples to obtain experimental values for the specified components' activities at smaller mass fractions of the unknown part. We selected the experimental points used in the fit of the case studies in the following in this spirit.

2.3 Base Models

The perturbation scheme requires a base model to calculate the activity coefficient or the fugacity coefficient, respectively, of each specified component k in the specified subsystem. In the present work the g^{E}-models NRTL [9], UNIQUAC [10], and Bromley [68] are used as base models. In the following, the basics of these models are given.

NRTL Model

The g^{E}-model NRTL (non-random two-liquid) published by Renon and Prausnitz [9] gives a correlation between the activity coefficients and the mole fractions in a liquid aqueous-organic mixture. The equation for calculating the activity coefficient of a component k is:

$$\ln \gamma_k = \frac{\sum_{k=1}^{K} \tau_{kl} G_{kl} x_k}{\sum_{m=1}^{K} G_{mk} x_m} + \sum_{k=1}^{K} \frac{x_k G_{kl}}{\sum_{m=1}^{K} G_{mk} x_m} \left(\tau_{lk} - \frac{\sum_{n=1}^{K} x_n \tau_{nk} G_{nk}}{\sum_{m=1}^{K} G_{mk} x_m} \right). \tag{39}$$

The coefficient τ_{kl} is defined as:

$$\tau_{kl} = a_{kl} + \frac{b_{kl}}{T}, \tag{40}$$

where a_{kl} and b_{kl} are binary interaction parameters. The coefficient G_{kl} is defined as:

$$G_{kl} = \exp\left(-\alpha_{kl} \tau_{kl}\right), \tag{41}$$

where α_{kl} is a constant nonrandomness parameter for binary interactions.

UNIQUAC Model

Abrams and Prausnitz [10] proposed the g^{E}-model UNIQUAC (universal quasichemical) to calculate activity coefficients in aqueous-organic mixtures. There, the equation to calculate the activity coefficient γ_k of a component k consists of a combinatorial term γ_k^{C} and a residual term γ_k^{R}.

$$\ln \gamma_k = \ln \gamma_k^{\mathrm{C}} + \ln \gamma_k^{\mathrm{R}} \tag{42}$$

The combinatorial term γ_k^{C} is calculated as

$$\ln \gamma_k^{\mathrm{C}} = \ln \frac{\phi_k}{x_k} + 1 - \frac{\phi_k}{x_k} - \frac{z}{2} q_k \left(\ln \frac{\phi_k}{\theta_k} + 1 - \frac{\phi_k}{\theta_k} \right), \tag{43}$$

where q_k is the surface-area parameter of the component k, and z is a constant with the value 10. Moreover, θ_k is the surface-area fraction

$$\theta_k = \frac{x_k q_k}{\sum_l x_l q_l}, \tag{44}$$

and ϕ_k is the volume fraction

$$\phi_k = \frac{x_k r_k}{\sum_l x_l r_l}, \tag{45}$$

where r_k is the volume parameter of component k. The equation for the residual term γ_k^{R} is:

$$\ln \gamma_k^{\mathrm{R}} = q_k \left(1 - \ln \left(\sum_n \theta_n \Psi_{nk} \right) - \sum_l \frac{\theta_l \Psi_{kl}}{\sum_n \theta_n \Psi_{nl}} \right). \tag{46}$$

Therein, Ψ_{kl} is given by:

$$\Psi_{kl} = \exp\left(-\frac{u_{kl}}{T} \right). \tag{47}$$

u_{kl} is the interaction parameter between components k and l.

Bromley Model

The Bromley equation [68] is used here to calculate the activity coefficient of aqueous-electrolyte mixtures. The equation to calculate the activity coefficient $\gamma_{\pm}^{*}$ is: [68, 69]

$$\log_{10}\gamma_{\pm}^{*} = -A_m \mid z_c z_a \mid \frac{\sqrt{I_m}}{1 + a_{ca}\sqrt{I_m}} + \frac{\left(0.06 + 0.6\frac{B_{ca}}{B_0}\right) \mid z_c z_a \mid I_m}{\left(1 + \frac{1.5 I_m}{|z_c z_a|}\right)^2} + \frac{B_{ca}}{B_0} I_m \tag{48}$$

with

$$I_m = \frac{1}{2}\sum_i \frac{b_i}{b_0} z_i^2. \tag{49}$$

z_c, z_a, and z_i are the charge number of the cation, anion and any ion i, respectively, and b_i is the molality of the ion i. The constants b_0 and B_0 are defined as 1 mol kg^{-1} and 1 kg mol^{-1}, respectively. The parameter a_{ca} was set to the common value 1. In the present work, the temperature dependency of the parameter B_{ca} is neglected, so the parameter B_{ca} is considered constant. Furthermore, since all electrolyte systems of the present work are aqueous mixtures, the Debye-Hückel constant A_m was set to 0.5108 [69]. Further, in the considered temperature range, the temperature dependence of A_m is small and was hence neglected. Furthermore, this is consistent with neglecting the temperature dependency of the parameter B_{ca}.

3 Thermodynamic Modeling of Poorly Specified Mixtures

3.1 Introduction

The general perturbation scheme from Eq. (10) with Eq. (36) or Eq. (13) with Eq. (37) is applied to several example systems. Since experimental data of poorly specified mixtures are rarely published in the literature, experimental data of fully specified mixtures are used, and we pretend that at least one component is unknown. No information about these unknown components is used for the perturbation scheme, except for the cumulative mass fraction of all unknown components.

First, example systems that contain non-electrolyte components in the specified subsystem are studied. Secondly, example systems with aqueous-electrolyte specified subsystems are studied. Here, a system means a set of specific components, while a mixture is a set of components with a specific composition. A case study consists of several mixtures of one system. In this chapter, no experiments are done. Instead, two methods are applied to supply data. On the one hand, pseudo-experimental data are generated with fully specified NRTL models [9]. The NRTL model parameters for these calculations are given in Appendix A. On the other hand, experimental literature data are used. In both cases, the components in the systems are divided afterward into a specified subsystem and an unknown part. The data of the components in the specified subsystem are used in the fit and in the evaluation of the models created with the perturbation scheme. The information about the unknown part is discarded.

To create the perturbation models, a g^{E}-model of the subsystem of the specified components, i.e. the base model, is taken from the literature. Either the NRTL model or the UNIQUAC model [10] are used for the non-electrolyte subsystems, or the Bromley model [68] is used for the aqueous-electrolyte subsystems, cf. Chapter 2.3 for details about the models. The model parameters of the subsystems are given in Appendix A. At this point, it is important to note that the base model can be any type of g^{E}-model. The parameters of the perturbation scheme, i.e. one interaction parameter $A_{k\mathrm{u}}$ for every

specified component and for non-aqueous specified subsystems the average molar mass $\bar{M}_u$ of the unknown part (for aqueous specified subsystems the average molar mass was always set to the fix value 50 g/mol (cf. Chapter 2.1)), are fitted to parts of the pseudo experimental data or experimental literature data. The data points used for the fit were always equally weighted.

3.2 Non-Electrolytes Systems

3.2.1 Pseudo Experimental Data

3.2.1.1 Example Systems

Table 1 gives the components of the systems and the compositions of the respective specified subsystem and unknown part of the mixtures of non-electrolyte systems based on pseudo experimental data. In the case studies, the ratio of the specified part and the unknown part is varied, and thus this ratio is not given in Table 1. For all mixtures, it was ensured with the help of the simulation that a stable and homogeneous mixture is present, and no phase splitting occurs.

Table 1: Overview of the studied systems of non-electrolyte systems based on pseudo-experimental data in the present work and the composition of the studied mixtures. No information on the unknown part was used for the perturbation approach.

System	Specified subsystem		Unknown part		Base model
	Component k	Mass fraction	Component	Mass fraction	
I	methanol	1.00 g/g	water	0.80 g/g	-
			hexane	0.10 g/g	
			dodecanol	0.10 g/g	
II	methanol	0.40 g/g	hexane	0.50 g/g	UNIQUAC
	dodecanol	0.60 g/g	dodecane	0.50 g/g	
III	methanol	0.25 g/g	water	1.00 g/g	UNIQUAC
	ethanol	0.50 g/g			
	butanol	0.25 g/g			
IV	hexane	0.25 g/g	diethyl ether	0.80 g/g	NRTL
	cyclohexane	0.25 g/g	acetonitril	0.20 g/g	
	benzene	0.25 g/g			
	acetone	0.25 g/g			

3.2.1.2 Parameter Estimation

For the non-electrolyte example systems, always activities data, i.e. the activities of the specified components in some mixtures of each system, are used for fitting. The objective in the fit was to minimize the squared deviations in the activities between data and model. Finally, the activities and the activity coefficients of the specified components are calculated for all mixtures based on the pseudo experimental data using the parameterized perturbation scheme.

Here, the specified subsystems of all studied systems are non-aqueous systems. Hence, one interaction parameter $A_{k\mathrm{u}}$ for every specified component as well as the average molar mass $\bar{M}_{\mathrm{u}}$ of the unknown part must also be fitted to parts data points.

The quality of the predictions are judged using average absolute derivations (AAD) $\bar{d}_{\Theta}$ calculated for quantities Θ of interest, e.g. $\Theta = a_{\mathrm{methanol}}$. The deviation is the arithmetic mean of the absolute difference of the values of the experimental data points ${\Theta_q}^{\mathrm{exp}}$ and the value obtained from the perturbed model ${\Theta_q}^{\mathrm{model}}$ over all Q data points.

$$\bar{d}_{\Theta} = \frac{\sum_{q=1}^{Q} \mid {\Theta_q}^{\mathrm{exp}} - {\Theta_q}^{\mathrm{model}} \mid}{Q} \tag{50}$$

3.2.1.3 Results and Discussion

System I

Figure 3 shows the results for the case study of system I (cf. Table 1). The mixtures contain only methanol as a specified component and an unknown part, according to Table 1. In the top panel, the activity of methanol is plotted over the mass fraction w_{u} of the unknown part in the mixture. In this study, a maximal mass fraction of the unknown part of $w_{\mathrm{u}} = 0.45$ g/g was considered since the pseudo experiments showed a liquid-liquid phase split at higher mass fractions. The symbols denote the pseudo-experimental data. The perturbation scheme was fitted to the two data points indicated by filled squares and is shown as a solid line in the plot. In the fit, the interaction parameter of methanol and the unknown part resulted in $A_{\mathrm{methanol,u}} = 552.05$ J/mol, and the average molar mass of the unknown part resulted in $\bar{M}_{\mathrm{u}} = 21.75$ g/mol. The latter is very sensitive in the fit because the average molar mass of the unknown part scales the effect of dilution on the activity, which is dominating in this example. This becomes clear when the activity coefficient of methanol is considered in the bottom panel of Figure 3. The activity coefficient is quite close to 1, and the mixture is quite ideal.

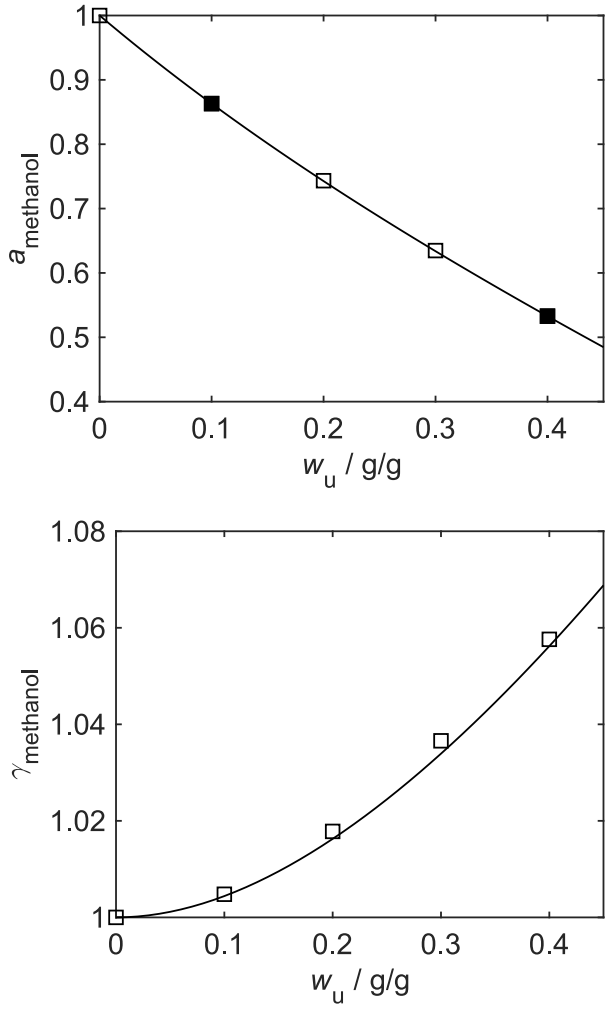

Figure 3: Activity a_{methanol} (top) and activity coefficient γ_{methanol} (bottom) of methanol (□, ■) in case study I (cf. Table 1) at 298.15 K. w_u is the mass fraction of the unknown part in the complete mixture. Open symbols: Pseudo experiments. Filled symbols: Pseudo experiments used for fit. Solid Line: Perturbation scheme with $A_{\text{methanol,u}} = 552.05$ J/mol and $\bar{M}_u = 21.75$ g/mol. AAD: Activity $\bar{d}_{a_{\text{methanol}}} = 3.13 \cdot 10^{-4}$, activity coefficient $\bar{d}_{\gamma_{\text{methanol}}} = 1.20 \cdot 10^{-3}$.

Considering the practical application of the perturbation scheme with real experimental data of activities from phase equilibrium measurements, one would typically only look at the plot of the activities (information on the mole fractions of the specified components and their activity coefficients would not be available due to the unknown nature of the unknown part). Thus we used only activity data in the fit. The results for activity coefficients are predictions. These predictions are expected to be the better, the closer $\bar{M}_u$ obtained in the fit is to the molar average of the molar mass of the unknown part. The perturbation scheme can reproduce the data points for the activity coefficient very well in this case study. Thus, the term of the perturbation scheme that considers the

interaction effects is reasonable. In the shown case, the perturbation scheme is able to describe mixtures with more than one component in the unknown part well. Since the perturbation scheme describes both the activity and the activity coefficient of methanol well, it is not surprising that the average molar mass of the unknown part found in the fit ($\bar{M}_\mathrm{u}$ = 21.75 g/mol) is very close to the one obtained as the molar average of the components of the unknown part in Table 1 ($\bar{M}^*_\mathrm{u}$ = 21.69 g/mol).

System II

Figure 4 shows the results for the case study of system II (cf. Table 1). In this case study, the specified subsystem comprises two components: methanol (Index: 1) and dodecanol (Index: 2). As stated before, the perturbation scheme, although derived with the Margules-type equation, can be combined with any g^E-model as the base model. Here, the UNIQUAC model is used as the base model. The presentation of Figure 4 is in full analogy to the one of Figure 3, with the only difference that two specified components are shown instead of one. The perturbation parameters were fitted to the activities of both specified components in the mixtures denoted with full symbols. The interaction parameters result in $A_{1\mathrm{u}}$ = 5.34 kJ/mol and $A_{2\mathrm{u}}$ = 2.07 kJ/mol. The average molar mass of the unknown part resulted in $\bar{M}_\mathrm{u}$ = 79.85 g/mol. This time, a strong influence of the molecular interaction with the unknown part becomes apparent: the activity of methanol remains almost constant, although the specified subsystem is diluted with unknown components. The perturbation scheme is again able to model the activity profiles well. Also, the activity coefficients (which were not used in the fit) are predicted quite well. The systematic deviations of the activity coefficients (the perturbed model yields always larger activity coefficients) can be explained by the deviation of the average molar mass of the unknown part in the perturbation model ($\bar{M}_\mathrm{u}$ = 79.85 g/mol) and the real one obtained from information about the unknown part in Table 1 ($\bar{M}^*_\mathrm{u}$ = 114.45 g/mol).

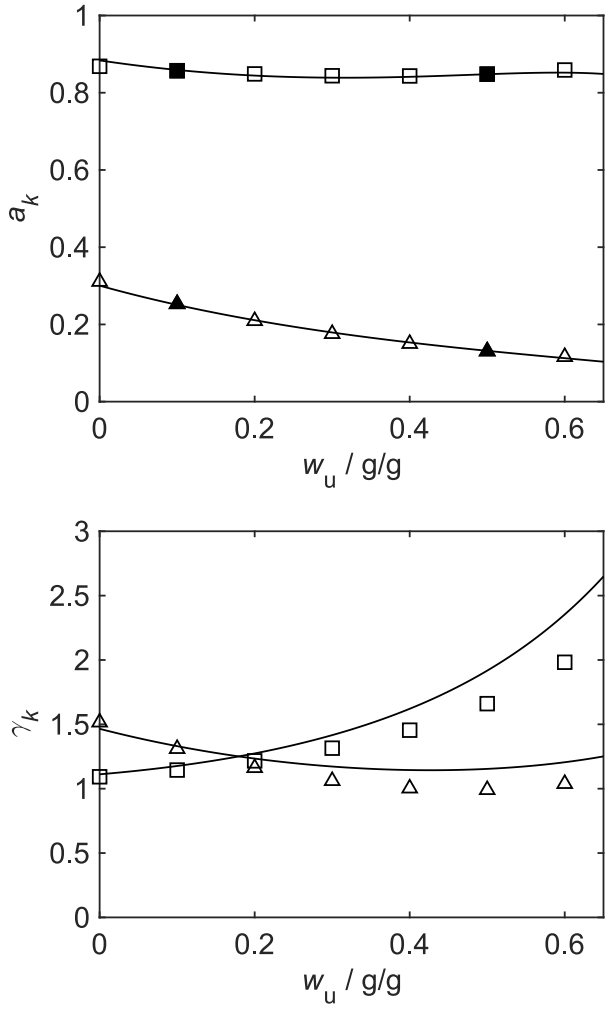

Figure 4: Activities a_k (top) and activity coefficients γ_k (bottom) of methanol (Index: 1; □, ■) and dodecanol (Index: 2; △, ▲) in case study II (cf. Table 1) at 298.15 K. w_u is the mass fraction of the unknown part in the complete mixture. Open symbols: Pseudo experiments. Filled symbols: Pseudo experiments used for fit. Solid Line: Perturbation scheme with A_{1u} = 5.34 kJ/mol, A_{2u} = 2.07 kJ/mol, and $\bar{M}_u$ = 79.85 g/mol. AAD: Activity $\bar{d}_{a_1} = 5.12 \cdot 10^{-3}$, $\bar{d}_{a_2} = 3.69 \cdot 10^{-3}$; activity coefficient $\bar{d}_{\gamma_1} = 1.44 \cdot 10^{-1}$, $\bar{d}_{\gamma_2} = 1.04 \cdot 10^{-1}$.

System III

Figure 5 shows the results in analogous fashion for the case study of system III (cf. Table 1). Here, the specified subsystem is comprised of three components: methanol (Index: 1), ethanol (Index: 2), and butanol (Index: 3). The specified subsystem is modeled with the UNIQUAC model. The four parameters of the perturbation scheme were fitted to the six marked data points (full symbols in Figure 5's top panel). The results are: A_{1u} = 1.40 kJ/mol, A_{2u} = 3.08 kJ/mol, A_{3u} = 4.84 kJ/mol, and $\bar{M}_u$ =

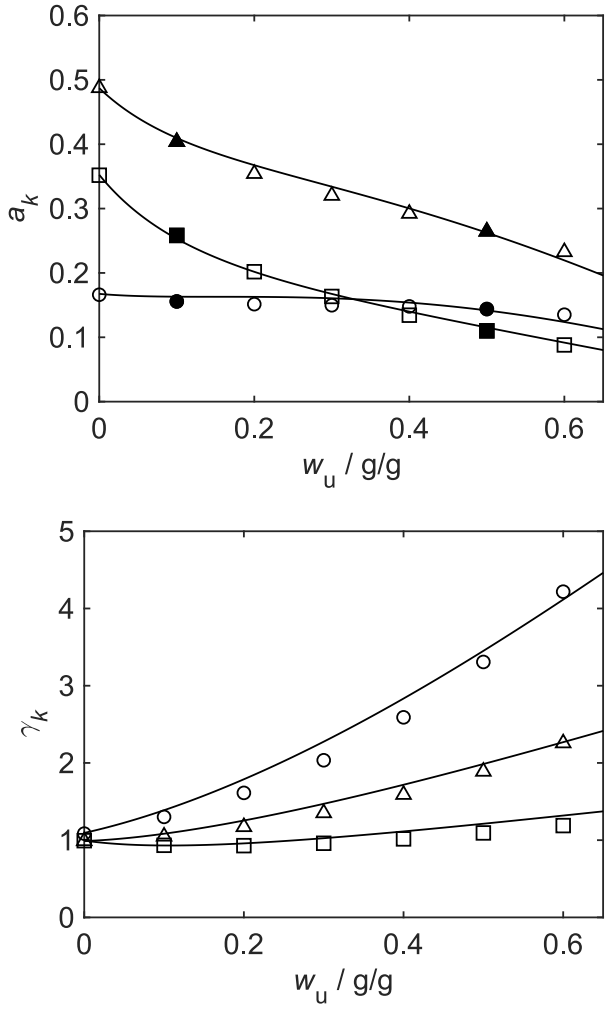

Figure 5: Activities a_k (top) and activity coefficients γ_k (bottom) of methanol (Index: 1; □, ■), ethanol (Index: 2; △, ▲), and butanol (Index: 3; ○, ●) in case study III (cf. Table 1) at 298.15 K. w_u is the mass fraction of the unknown part in the complete mixture. Open symbols: Pseudo experiments. Filled symbols: Pseudo experiments used for fit. Solid Line: Perturbation scheme with A_{1u} = 1.40 kJ/mol, A_{2u} = 3.08 kJ/mol, A_{3u} = 4.84 kJ/mol, $\bar{M}_u$ = 16.64 g/mol. AAD: Activity $\bar{d}_{a_1} = 3.46 \cdot 10^{-3}$, $\bar{d}_{a_2} = 8.07 \cdot 10^{-3}$, $\bar{d}_{a_3} = 7.20 \cdot 10^{-3}$; activity coefficient $\bar{d}_{\gamma_1} = 6.35 \cdot 10^{-2}$, $\bar{d}_{\gamma_2} = 6.79 \cdot 10^{-2}$, $\bar{d}_{\gamma_3} = 1.43 \cdot 10^{-1}$.

16.64 g/mol. As indicated by activity coefficients close to unity for w_u = 0 g/g, the specified subsystem is almost an ideal mixture. By adding the unknown part, the mixture deviates from ideal behavior. The model results for both the activities (used in the fit) and the activity coefficients (not used in the fit) agree very well with the pseudo-experimental data. On the one hand, this is not too surprising since the unknown part consists only of one component (water). On the other hand, this case study shows that the interaction term of the perturbation scheme works well for more than two

specified components. The average molar mass of the unknown part found in the fit ($\bar{M}_\mathrm{u}$ = 16.64 g/mol) is very similar to the one of pure water ($\bar{M}_\mathrm{u}^*$ = 18.01 g/mol), which is the unknown part in this case study.

System IV

Figure 6 shows the results for the case study of system IV (cf. Table 1) in full analogy to the studies before. The specified subsystem is comprised of four components: hexane (Index: 1), cyclohexane (Index: 2), benzene (Index: 3), and acetone (Index: 4). Here, the base model for the specified subsystem is the NRTL model. The parameters of the perturbation scheme were fitted to activities of all components of the specified subsystem denoted with full symbols (top panel of Figure 6). The results of the interaction parameters are: $A_{1\mathrm{u}}$ = 2.45 kJ/mol, $A_{2\mathrm{u}}$ = 1.92 kJ/mol, $A_{3\mathrm{u}}$ = 0.21 kJ/mol, $A_{4\mathrm{u}}$ = 0.29 kJ/mol. The average molar mass of the unknown part resulted in $\bar{M}_\mathrm{u}$ = 73.95 g/mol. Again the perturbation scheme is able to model the activity of all four components very well. Also, the activity coefficients are predicted acceptably. This case study shows that the perturbation term can capture different influences of the unknown part on the specified components. Here, benzene shows an almost ideal behavior for all mass fractions of the unknown part, whereas the unknown part has stronger interactions with the other specified components. In addition, this example confirms the previous findings that the perturbation scheme with the interaction term here works well for more than two specified components and for more than one component in the unknown part. The activity coefficients are throughout under-predicted in Figure 6 (bottom). Accordingly, the parameter $\bar{M}_\mathrm{u}$ (73.95 g/mol) is larger than the average molar mass of the unknown part ($\bar{M}_\mathrm{u}^*$ = 53.63 g/mol), just opposite compared to the situation in case study of system II and Figure 4.

In the results above, the interpolation abilities of the perturbation scheme are highlighted, i.e. the parameters are fitted to quite high fractions of the unknown part, and the scheme's performance is checked for intermediate fractions of the unknown part. Looking into possible practical applications, it is also crucial to look at the scheme's extrapolation capabilities. Regarding the extrapolation to other compositions of the specified part, the perturbation models obtained in case studies of the systems II and IV are taken, and the activities at different compositions of the specified components were predicted (since the previous study showed that the specified subsystem of system III is an almost ideal mixture, this case is not considered here). During the variations, the mass fraction of the unknown part is held constant at 0.5 g/g, and the composition of the unknown part remains constant as given in Table 1. The results for the mixtures

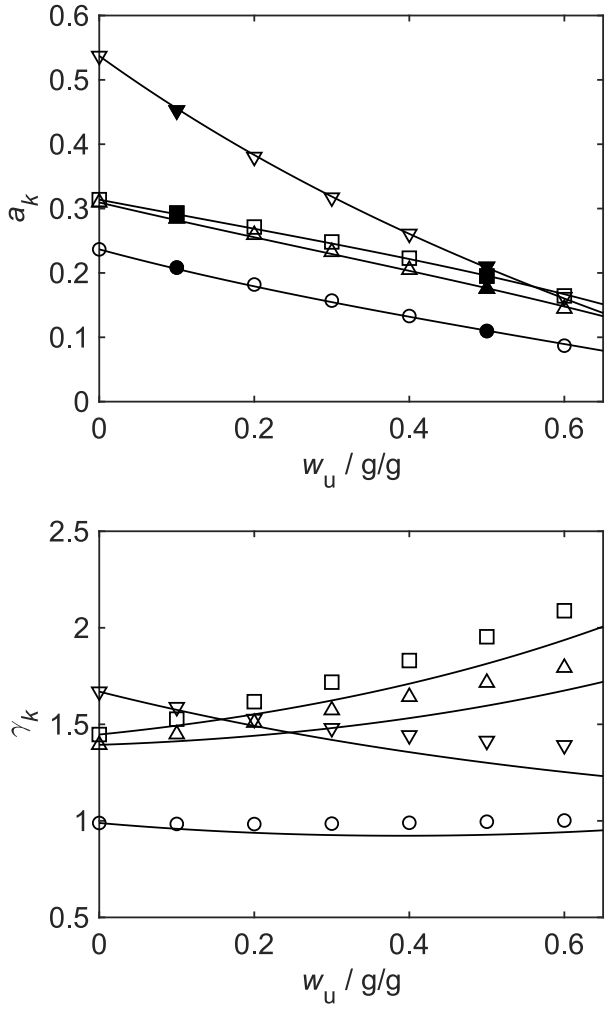

Figure 6: Activities a_k (left) and activity coefficients γ_k (right) of hexane (Index: 1; □, ■), cyclohexane (Index: 2; △, ▲), benzene (Index: 3; ○, ●), and acetone (Index: 4; ▽, ▼) in case study IV (cf. Table 1) at 298.15 K. w_u is the mass fraction of the unknown part in the complete mixture. Open symbols: Pseudo experiments. Filled symbols: Pseudo experiments used for fit. Solid Line: Perturbation scheme with A_{1u} = 2.45 kJ/mol, A_{2u} = 1.92 kJ/mol, A_{3u} = 0.21 kJ/mol, A_{4u} = 0.29 kJ/mol, $\bar{M}_u$ = 73.95 g/mol. AAD: Activity $\bar{d}_{a_1} = 1.63 \cdot 10^{-3}$, $\bar{d}_{a_2} = 2.20 \cdot 10^{-3}$, $\bar{d}_{a_3} = 1.66 \cdot 10^{-3}$, $\bar{d}_{a_4} = 1.63 \cdot 10^{-3}$; activity coefficient $\bar{d}_{\gamma_1} = 8.64 \cdot 10^{-2}$, $\bar{d}_{\gamma_2} = 7.78 \cdot 10^{-2}$, $\bar{d}_{\gamma_3} = 4.65 \cdot 10^{-2}$, $\bar{d}_{\gamma_4} = 6.42 \cdot 10^{-2}$.

corresponding to the case study of system II are shown in Figure 7. The composition of the specified part is varied between $\tilde{w}_{\text{methanol}} = 0$ g/g - 0.45 g/g and accordingly $\tilde{w}_{\text{dodecanol}} = 1$ g/g - 0.55 g/g (the pseudo experiments showed that a liquid-liquid phase split occurs at higher mass fractions of methanol). The perturbation scheme predicts the activities of the different compositions very well, even though only one composition of the specified subsystem was used in the fit.

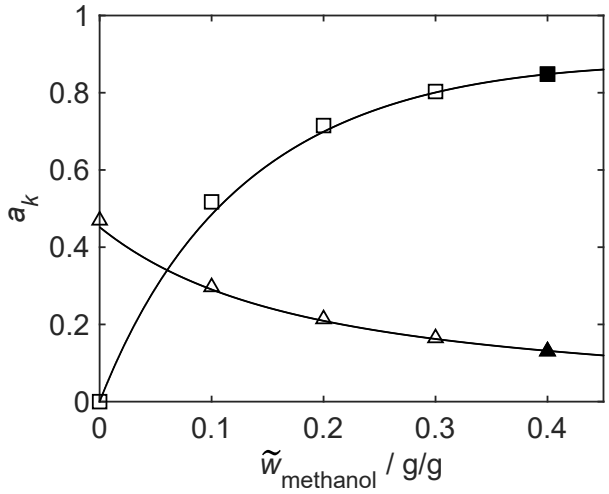

Figure 7: Activities a_k of methanol (Index: 1; □, ■) and dodecanol (Index: 2; △, ▲) at different compositions of the specified subsystem at 298.15 K (see caption of Figure 4 for more model details). $\tilde{w}_{\text{methanol}}$ is the mass fraction of methanol in the subsystem comprised of the specified components methanol and dodecanol. The composition of the unknown part is as given in Table 1 for system II and its mass fraction is $w_{\text{u}} = 0.5$ g/g. Open symbols: Pseudo experiments. Filled symbols: Pseudo experiments used for fit. Solid line: Perturbation scheme. AAD: $\bar{d}_{a_1} = 2.81 \cdot 10^{-2}$, $\bar{d}_{a_2} = 7.25 \cdot 10^{-3}$.

The results for the mixtures corresponding to the case study of system IV are shown in Figure 8. To vary the composition of the specified part, the specified subsystem was arbitrarily divided into two sub-subsystems: (1) hexane and cyclohexane, (2) benzene and acetone. The mass fraction ratio of the two sub-subsystems was varied over the complete range. However, the mass fraction ratio of the components within the sub-subsystems remained constant at 1:1 for all mixtures. Again, the activities of all components are predicted very well, even though the model parameters were obtained by fitting only to one composition of the specified subsystem. The results of both studies (cf. Figure 7 and 8) suggest that the perturbation scheme is able to describe the mixtures well even when the composition of the specified subsystem changes. However, it is crucial that the composition of the unknown part must stay the same.

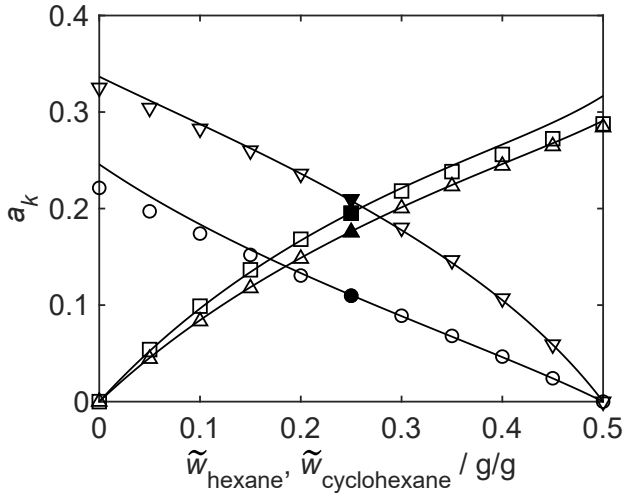

Figure 8: Activities a_k of hexane (Index: 1; □, ■), cyclohexane (Index: 2; △, ▲), benzene (Index: 3; ○, ●), and acetone (Index: 4; ▽, ▼) at different compositions of the specified subsystem at 298.15 K (see caption of Figure 6 for more model details). $\tilde{w}_{\text{hexane}}$, $\tilde{w}_{\text{cyclohexane}}$ are the mass fractions of hexane and cyclohexane, respectively, in the subsystem comprised of the specified components hexane, cyclohexane, benzene, and acetone. The mass fraction ratios of (hexane : cyclohexane) and (benzene : acetone), respectively, are (1 : 1). The composition of the unknown part is as given in Table 1 for system IV and its mass fraction is w_{u} = 0.5 g/g. Open symbols: Pseudo experiments. Filled symbols: Pseudo experiments used for fit. Solid line: Perturbation scheme. AAD: $\bar{d}_{a_1} = 6.68 \cdot 10^{-3}$, $\bar{d}_{a_2} = 1.66 \cdot 10^{-3}$, $\bar{d}_{a_3} = 5.45 \cdot 10^{-3}$, $\bar{d}_{a_4} = 3.20 \cdot 10^{-3}$.

3.2.2 Experimental Data

3.2.2.1 Example Systems

In addition to the previously studied systems based on pseudo experimental data, two systems based on real experimental data obtained from the literature are studied. Table 2 gives an overview of the two systems. System V comprises the components water, α-lactose (lactose) (assumed to be known), and ethanol (assumed to be unknown). System VI comprises the components acetone, methanol (assumed to be known), and the ionic liquid [AMIM]Cl (assumed to be unknown).

Table 2: Overview of the studied systems based on experimental data from the literature. No information on the unknown part was used for the perturbation approach.

System	Specified subsystem	Unknown part	Base model	Ref.
V	water α-lactose	ethanol	UNIQUAC	[70]
VI	acetone methanol	[AMIM]Cl	NRTL	[71]

3.2.2.2 Parameter Estimation

Here, the specified subsystem of system V is an aqueous system. Hence, for the average molar mass $\bar{M}_\mathrm{u}$ of the unknown part the constant value 50 g/mol is chosen (cf. Chapter 2.1). The interaction parameters $A_{k\mathrm{u}}$ are fitted to parts of the experimental literature data. The parameters of the perturbation scheme for system VI, i.e. both the average molar mass $\bar{M}_\mathrm{u}$ of the unknown part and the interaction parameters $A_{k\mathrm{u}}$, are fitted to parts of the experimental literature data.

Analog to the systems based on pseudo experimental data activities, data of the specified components in complete mixtures are used for fitting. The objective in the fit was to minimize the squared deviations in the activities between data and model. Finally, the solubility (system V) or the activities (system VI) of the specified components are calculated for all mixtures using the parameterized perturbation scheme. The quality of the predictions are judged analog to the systems before using the average absolute derivations (AAD) $\bar{d}_\Theta$ for quantities Θ of interest (cf. Eq. (50)).

3.2.2.3 Results and Discussion

System V - Experimental Solid-Liquid Equilibrium

Experimental data of the solid-liquid equilibrium (SLE) of mixtures of system V (cf. Table 2), in which only lactose is present in the solid phase, are taken from Machado et al. [70]. The UNIQUAC model (cf. Chapter 2.3) is used as the base model for the specified subsystem lactose and water. The required UNIQUAC model parameters for the base model are given in Appendix A. The composition of the unknown part must remain the same during the application of the perturbation scheme. This prerequisite applies here since the unknown part (ethanol) remains in the liquid phase. The procedure for applying the perturbation scheme on the SLE of lactose in the poorly specified aqueous

mixture is as follows. To calculate the solubility of lactose, i.e. the solid-liquid phase equilibrium, we assumed that the solid in the solid-liquid equilibrium is pure lactose. The difference of the heat capacities of lactose in the solid and liquid state is neglected, leading to the following phase equilibrium condition [72].

$$a_{\text{lactose}} = x_{\text{lactose}}\gamma_{\text{lactose}} = \exp\left[\frac{-\Delta h^{\text{f}}_{\text{lactose}}}{RT^{\text{f}}_{\text{lactose}}}\left(\frac{T^{\text{f}}_{\text{lactose}}}{T} - 1\right)\right] \tag{51}$$

Therein, the enthalpy of fusion $\Delta h^{\text{f}}_{\text{lactose}} = 66416.39$ J mol^{-1} and the melting temperature $T^{\text{f}}_{\text{lactose}} = 498.027$ K are adopted from Held et al. [73]. Using Eq. (51), the activity of lactose a_{lactose} is determined for every mixture. The perturbation scheme is used to predict the mass fraction of lactose in equilibrium at other mass fractions of unknown part and other temperatures.

The experimental data for the solubility of lactose at 298.15 K, 313.15 K, and 333.15 K are shown in Figure 9.

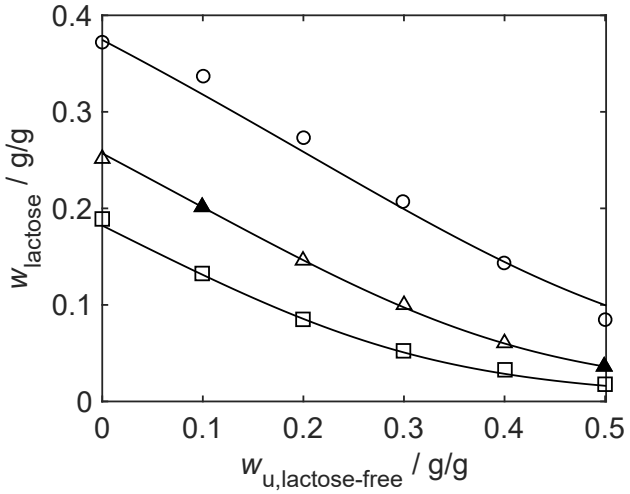

Figure 9: Experimental data for the solubility of lactose in the poorly specified aqueous mixture at 298.15 K (□), 313.15 K (△, ▲), and 333.15 K (○) [70]. w_{lactose} is the mass fraction of lactose in the saturated liquid phase. $w_{\text{u,lactose–free}}$ is the mass fraction of the unknown part (here: ethanol) in the liquid phase on a lactose-free basis. The perturbation scheme (solid lines) is only fitted to the data points at 313.15 K marked with the filled symbols. The perturbation parameters are: $A_{\text{lactose,u}} = -14.44$ kJ/mol, $A_{\text{water,u}} = -26.71$ kJ/mol, $\bar{M}_{\text{u}} = 50$ g/mol. The AAD for the different temperatures, respectively, are: $\bar{d}_{w_{\text{lactose}},298.15\,\text{K}} = 4.97 \cdot 10^{-3}$, $\bar{d}_{w_{\text{lactose}},313.15\,\text{K}} = 2.56 \cdot 10^{-3}$, $\bar{d}_{w_{\text{lactose}},333.15\,\text{K}} = 1.04 \cdot 10^{-2}$

It is obvious that the unknown part strongly influences the solubility of lactose: the solubility of lactose is high for pure water as solvent (left edge of the plot) and is

reduced by the addition of the unknown part. The two data points at 313.15 K marked with filled symbols were used to fit the model parameters of the perturbation scheme. The resulting parameters are: $A_{\mathrm{lactose,u}} = -14.44$ kJ/mol, $A_{\mathrm{water,u}} = -26.71$ kJ/mol. The average molar mass of the unknown part was set to the constant value $\bar{M}_{\mathrm{u}} = 50$ g/mol since the studied system is an aqueous system. The model parameters were also used to predict the solubility of lactose at 298.15 K and 333.15 K. The perturbation scheme predicts the experimental data well. The model parameters of the perturbation scheme are not temperature-dependent. The temperature dependency results solely from the base model comprised of the specified components. In cases where the data indicate a strong temperature dependency of the interactions of the specified components with the unknown part, temperature-dependent parameters in the perturbation scheme could be used, i.e. $A_{k\mathrm{u}}$ could be expressed e.g. as a simple polynomial: $A_{k\mathrm{u}} = a_{k\mathrm{u}} + b_{k\mathrm{u}}T$.

System VI - Experimental Vapor-Liquid Equilibrium

Experimental data of the vapor-liquid equilibrium (VLE) for mixtures of system VI (cf. Table 2) are taken from Li et al. [71] and are shown in a McCabe-Thiele plot in Figure 10.

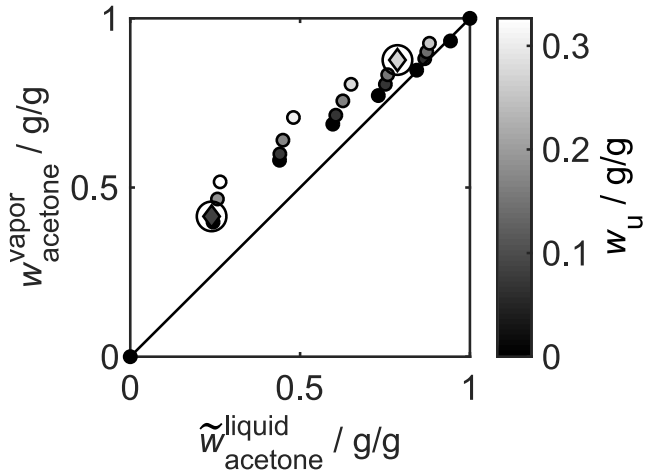

Figure 10: Experimental VLE data in the system (acetone + methanol + unknown part) at 101.3 kPa [71]. $w^{\mathrm{vapor}}_{\mathrm{acetone}}$ is the vapor mass fraction of acetone. $\tilde{w}^{\mathrm{liquid}}_{\mathrm{acetone}}$ is the liquid mass fraction of acetone on an unknown-free basis within the specified subsystem. The color code indicates the mass fraction of the unknown part in the liquid phase data points. The marked data points with the diamond symbol are used to fit the perturbation scheme.

The mass fractions of acetone in the specified subsystem (acetone + methanol) are shown. The color code gives the mass fraction of the unknown part in the liquid phase.

The binary system (acetone + methanol) is azeotropic. The unknown part (the ionic liquid [AMIM]Cl) clearly influences the VLE of the specified subsystem. The composition of the azeotrope is shifted towards pure acetone by adding the unknown part. In their original work, Li et al. even suggest that the azeotrope disappears if only enough unknown component (ionic liquid) is added [71].

Extended Raoult's law is used as phase equilibrium condition for the specified components methanol and acetone (Assumption: Poynting correction is negligible).

$$a_k = x_k \gamma_k = \frac{p y_k}{p_k^{\mathrm{s}}} \qquad k = \{\text{methanol, acetone}\} \tag{52}$$

Where x_k is the mole fraction of the liquid phase, y_k is the mole fraction of the vapor, p is the pressure, and p_k^{s} the vapor pressure. The pressure p is here 101.3 kPa. The vapor pressure p_k^{s} is calculated with the Antoine equation and the corresponding parameters from Botía et al. [74] as also used from Li et al. [71]. The Antonie equation and the respective numerical values are given in Appendix A. Using Eq. (52), the liquid activities of methanol and acetone are calculated for all experimental data points. The perturbation scheme is used to predict the VLE for the experimental data points shown in Figure 10. Here, the NRTL model is used as the base model for the specified subsystem (acetone + methanol). The model parameters are given in Appendix A.

The results are shown in Figure 11. The activity data of methanol and acetone of the two experimental points marked with diamond symbols and circles in Figure 11 are used for fitting the model parameters of the perturbation scheme. The values of the model parameters obtained from the fit are: $A_{\mathrm{acetone,u}} = 3.45\ \mathrm{kJ/mol}$, $A_{\mathrm{methanol,u}} = -7.03\ \mathrm{kJ/mol}$, $\bar{M}_{\mathrm{u}} = 115.7\ \mathrm{g/mol}$. The parity plots in the top and bottom panels of Figure 11 show that the activities calculated by the perturbation scheme match very well with the ones obtained from the experimental data. The dashed lines indicate a deviation of ± 5 %. The perturbation scheme is able to describe the VLE data very well.

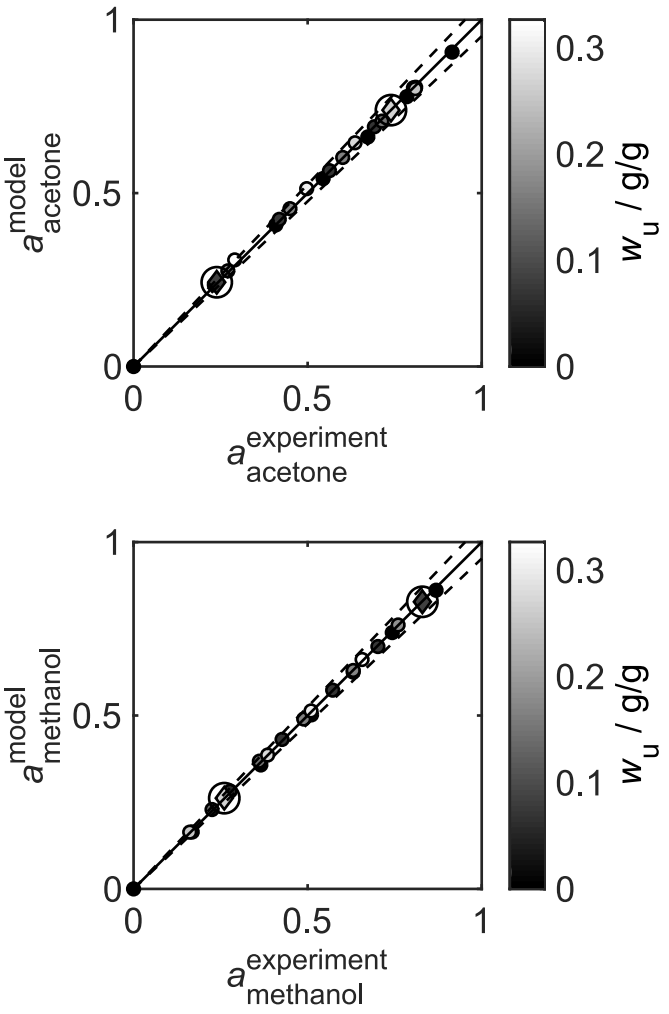

Figure 11: Parity plots for the activities of acetone (top) and methanol (bottom) calculated with the perturbation scheme and the activity obtained from the experimental data points. The dashed lines indicate a deviation of ± 5 %. The model parameters of the perturbation scheme are: $A_{\text{acetone,u}} = 3.45$ kJ/mol, $A_{\text{methanol,u}} = -7.03$ kJ/mol, $\bar{M}_{\text{u}} = 115.7$ g/mol. The color code indicates the mass fraction of the unknown part in the liquid phase data points. The marked data points with the diamond symbol are used to fit the perturbation scheme. The AAD for acetone and methanol are: $\bar{d}_{a_{\text{acetone}}} = 5.75 \cdot 10^{-3}$, $\bar{d}_{a_{\text{methanol}}} = 2.76 \cdot 10^{-3}$.

3.3 Electrolyte Systems

3.3.1 Example Systems

In the following, the systems comprised of specified aqueous-electrolyte subsystems are studied. For the electrolyte example systems, only experimental solubility data obtained from the literature are used. The different example systems are listed in Table 3.

Table 3: Overview of the studied electrolyte systems based on experimental literature data. No information on the unknown part was used for the perturbation approach.

System	Specified subsystem	Unknown part	Base model	Ref.
E-I.a	sodium chloride water	methanol	Bromley	[75]
E-I.b	sodium chloride water	ethanol	Bromley	[75]
E-II.a	potassium chloride water	methanol	Bromley	[75]
E-II.b	potassium chloride water	ethanol	Bromley	[76]
E-III.a	sodium bromide water	methanol	Bromley	[76]
E-III.b	sodium bromide water	ethanol	Bromley	[76]
E-IV.a	sodium chloride water	potassium chloride	Bromley	[76, 77]
E-IV.b	sodium chloride water	calcium chloride	Bromley	[76, 77]
E-IV.a+b	sodium chloride water	potassium chloride calcium chloride	Bromley	[76, 77]

The systems of type E-I, E-II, and E-III are solutions of a salt in water with an unknown alcohol. The systems of type E-IV are solutions of sodium chloride in water and one or two unknown salts. Along the systems of type E-IV the question is discussed, whether the perturbation schemes of two poorly specified systems can be combined to predict the solubility in mixtures comprised of these two poorly specified systems.

The Bromley electrolyte model [68] (systems E-I - E-IV) is used as the base model for the specified subsystems (cf. Chapter 2.3). The respective model parameters are given

in Appendix A.

3.3.2 Parameter Estimation

For determining the model parameters of the perturbation scheme, a few experimental data points of the solubility of sodium chloride (NaCl), potassium chloride (KCl), and sodium bromide (NaBr) are used. The solubilities are modeled using activity-based equilibrium constants K_k as follows:

$$K_{\mathrm{NaCl}}(T) = \frac{b_{\mathrm{Na^+}} \cdot b_{\mathrm{Cl^-}}}{b_0^2} \cdot \gamma^*_{\mathrm{Na^+}}(T) \cdot \gamma^*_{\mathrm{Cl^-}}(T), \tag{53}$$

$$K_{\mathrm{KCl}}(T) = \frac{b_{\mathrm{K^+}} \cdot b_{\mathrm{Cl^-}}}{b_0^2} \cdot \gamma^*_{\mathrm{K^+}}(T) \cdot \gamma^*_{\mathrm{Cl^-}}(T), \tag{54}$$

and

$$K_{\mathrm{NaBr}}(T) = \frac{b_{\mathrm{Na^+}} \cdot b_{\mathrm{Br^-}}}{b_0^2} \cdot \gamma^*_{\mathrm{Na^+}}(T) \cdot \gamma^*_{\mathrm{Br^-}}(T). \tag{55}$$

The values of the K_k are chosen carefully in accordance with the respective activity model of the specified subsystem, cf. Appendix A for details. The values of the K_k used in the present work are given in Table 4.

Table 4: Natural logarithm of the equilibrium constants used in the SLE model of the specified subsystems.

Constant	Value	Ref.
$\ln K_{\mathrm{NaCl}}(T)$	$4.629 - (303.474/(T/K))$	cf. Appendix A and [76]
$\ln K_{\mathrm{KCl}}(298.15\ \mathrm{K})$	2.0585	cf. Appendix A and [75]
$\ln K_{\mathrm{NaBr}}(298.15\ \mathrm{K})$	5.8614	cf. Appendix A and [76]

In the experimental SLE data, the mass fractions of all specified components in the liquid phase are known (including the single component present as solid, i.e. the solubility). To determine the parameters of the perturbation scheme, the deviation between the respective K_k values given in Table 4 and the one obtained from the perturbation scheme with the experimental data is minimized using a nonlinear least-squares solver. The number of experimental data points used for the fit was always equal to the number of model parameters that were determined. The number of model parameters depends on the number of specified components. There is one binary interaction model parameter $A_{k\mathrm{u}}$ for each specified component. Since only aqueous electrolyte systems (cf. Table 3) are studied here, the average molar mass $\bar{M}_{\mathrm{u}}$ of the unknown part is not fitted to the

experimental data but set to the constant value 50 g/mol (cf. Chapter 2.1). The resulting model parameters are used to predict the solubility of the respective solute in various mixtures with different compositions and conditions.

3.3.3 Results and Discussion

The interaction parameters of the perturbation scheme for all electrolyte example systems of Table 3 are given in Table 5.

Table 5: Interaction parameters $A_{k\mathrm{u}}$ of the perturbation scheme for the systems E-I.a - E-IV.b. The model parameter for the average molar mass of the unknown part $\bar{M}_{\mathrm{u}}$ is always set to 50 g/mol.

System	Component k	$A_{k\mathrm{u}}$ / kJ mol^{-1}
E-I.a, E-II.a, E-III.a	NaCl	0.85
	KCl	4.05
	NaBr	–4.44
	water	–5.59
E-I.b, E-II.b, E-III.b	NaCl	3.53
	KCl	6.21
	NaBr	0.70
	water	–3.61
E-IV.a	NaCl	33.01
	water	22.69
E-IV.b	NaCl	111.96
	water	87.81

Systems E-I - E-III

The solubility of NaCl (systems E-I), KCl (systems E-II), and NaBr (systems E-III) in water under the presence of two different unknown parts (a = methanol, b = ethanol) are considered. The results in Figure 12 indicate that the influence of the same unknown part on the solubility of different salts is different. The top panel shows that the influence of the unknown part a on the solubility of NaCl and KCl is very similar. In both cases, the solubility decreases with an increasing mass fraction of the unknown part, while the solubility of NaBr increases with higher mass fractions of the unknown part. In the bottom panel, the presence of the unknown part b decreases the solubility of all three salts, albeit to different extents.

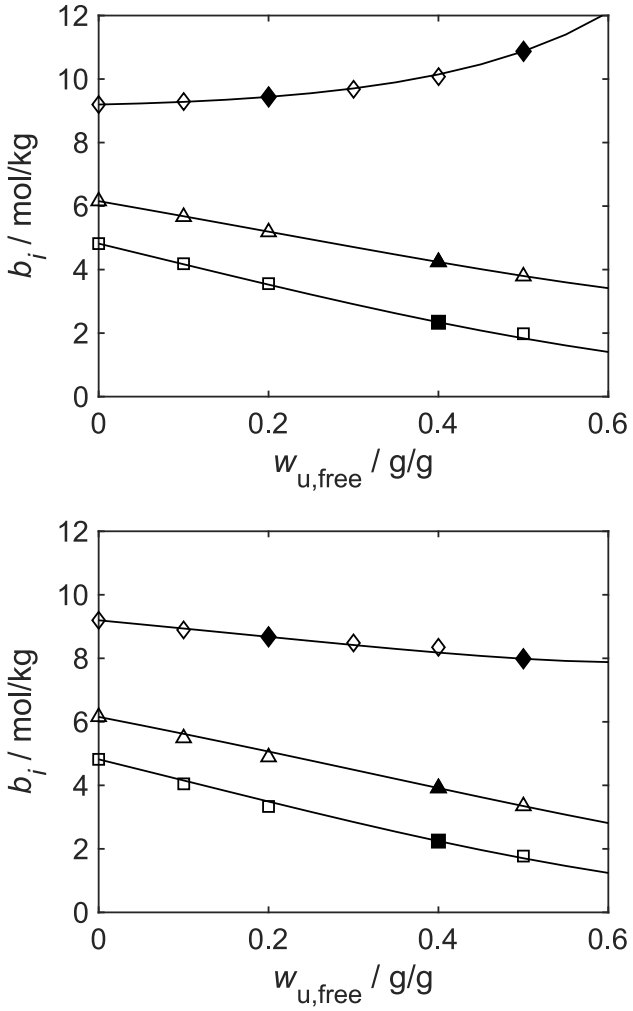

Figure 12: Experimental solubility data [75, 76] (symbols) and results of the perturbation model (lines) for i = NaCl (△,▲), KCl (□,■), or NaBr (◊,⧫) in poorly specified mixtures at 298.15 K plotted over the mass fraction of the unknown part on a salt-free basis $w_{u,free}$ (top panel: unknown part = methanol, systems E-I.a, E-II.a, E-III.a; bottom panel: unknown part = ethanol, systems E-I.b, E-II.b, E-III.b). The filled symbols mark the data points used to fit the interaction parameters of the perturbation scheme. The interaction parameters are given in Table 5.

Each system has two interaction parameters for the interaction of the specified components with the unknown part: salt-unknown and water-unknown. The latter one is assumed to be identical for the systems E-I.a, E-II.a and E-III.a and for the systems E-I.b, E-II.b and E-III.b, respectively. Therefore, the four interaction parameters ($A_{\mathrm{water,u}}$, $A_{\mathrm{NaCl,u}}$, $A_{\mathrm{KCl,u}}$, and $A_{\mathrm{NaBr,u}}$) for all systems with unknown part a were received in a simultaneous fit to the four data points indicated by filled symbols in the top panel of Figure 12. The same holds for the unknown part b and the bottom panel of Figure 12.

The results of the interaction parameters are given in Table 5. The Bromley electrolyte model agrees perfectly with the experimental data of the mixtures of the specified subsystems. Also, the perturbation model and the experimental data agree very well. When inspecting the numerical values of the interaction parameters of the salts with the unknown part, it can be seen that the interaction parameters for all salts have a positive sign when the solubility decreases with an increase of the unknown part and a negative sign when the solubility increases. Furthermore, it can be seen that the stronger the influence on the solubility, the larger the values of the interaction parameters.

Systems E-IV

The solubility of NaCl in different poorly specified aqueous mixtures in the temperature range between 290 - 340 K is modeled using the perturbation model. The experimental data for these systems are taken from the literature, cf. Table 3. Figure 13 shows the experimental data and the results of the perturbation model for the systems E-IV.a (top panel, unknown part = KCl) and E-IV.b (bottom panel, unknown part = $CaCl_2$). The solubility of NaCl slightly increases with increasing temperature. Figure 13 shows that both unknown parts clearly influence the solubility of NaCl. The solubility decreases with increasing mass fractions of the respective unknown part. This trend is stronger in the system with unknown part b (bottom panel) than in the system with unknown part a (top panel).

The systems E-IV.a and E-IV.b have two interaction parameters for the perturbation term, respectively, one for NaCl and one for water. The interaction parameters for system E-IV.a were obtained from a fit to the two data points indicated by the filled symbols in the top panel of Figure 13. The interaction parameters for system E-IV.b were obtained analogously. The results for the model parameters are given in Table 5. It can be seen in Figure 13 that the agreement of the experimental data of the specified subsystem (denoted with crosses) with the Bromley electrolyte model as well as the agreement of all further experimental data with the results from the perturbation model are very good. Hence, a small extrapolation to higher mass fractions of the unknown part is possible in both systems. Furthermore, a small extrapolation to higher or lower temperatures works very well, even though the interaction parameters do not depend on the temperature. This is not surprising since the temperature trend is already present in the specified subsystem and remains unchanged in the presence of unknowns. When inspecting the values of the interaction parameters, it can be seen that - as expected - the absolute values of the parameters of system E-IV.a are smaller than the values of system E-IV.b.

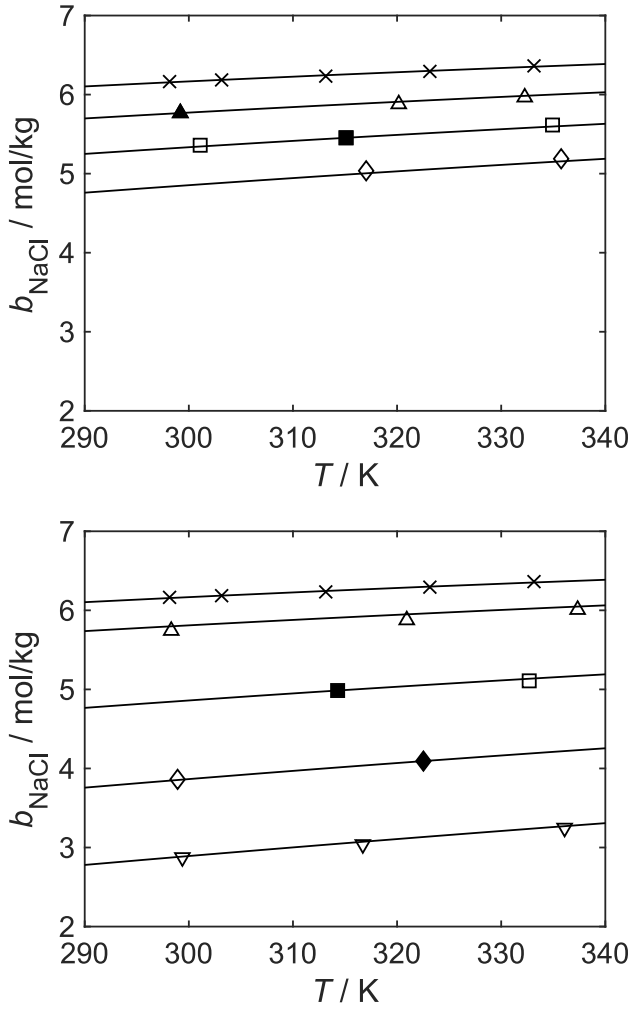

Figure 13: Experimental solubility data [76, 77] (symbols) and results of the perturbation model (lines) for NaCl in two different poorly specified mixtures plotted over the temperature (top panel: system E-IV.a, unknown part = KCl; bottom panel: system E-IV.b, unknown part = $CaCl_2$). The different types of symbols indicate different mass fractions of the unknown part on a salt free basis (top panel: $w_{u,free}$ = 0.00 g/g (×), $w_{u,free}$ = 0.05 g/g (△), $w_{u,free}$ = 0.10 g/g (□,■), $w_{u,free}$ = 0.15 g/g (◇,◆); bottom panel: $w_{u,free}$ = 0.00 g/g (×), $w_{u,free}$ = 0.20 g/g (△,▲), $w_{u,free}$ = 0.70 g/g (□,■), $w_{u,free}$ = 0.12 g/g (◇), $w_{u,free}$ = 0.17 g/g (▽)). The filled symbols mark the data points used to fit the model parameters of the perturbation scheme. The interaction parameters are given in Table 5.

The final example, system E-IV.a+b, also consists of the specified components NaCl and water. The unknown part is a mixture of the unknown parts of systems E-IV.a and E-IV.b. Poorly specified mixtures in the system E-IV.a+b can thus be obtained by mixing a poorly specified mixture of system E-IV.a and a poorly specified mixture of system E-IV.b. Let us assume that perturbed models for system E-IV.a and E-IV.b are

available (cf. Figure 13). The question arises whether those models can be combined to yield a perturbed model for system E-IV.a+b. It is assumed that the mass fractions $w_{\mathrm{u,a}}$ and $w_{\mathrm{u,b}}$ of both unknown parts a and b, respectively, in the combined mixture are known. Let

$$\chi_{\mathrm{a}} = \frac{w_{\mathrm{u,a}}}{w_{\mathrm{u,a}} + w_{\mathrm{u,b}}} \tag{56}$$

be the share of unknown part a in the combined unknown part. Then, the model parameters of the system V.a+b can be estimated by

$$A_{ku}^{\mathrm{a+b}} = \chi_{\mathrm{a}} A_{ku}^{\mathrm{a}} + (1 - \chi_{\mathrm{a}}) A_{ku}^{\mathrm{b}}. \tag{57}$$

The results of these predictions compared to the respective experimental data are shown in Figure 14 for four combinations of χ_{a} and $w_{\mathrm{u,free}}$ that are specified in Table 6 along with the perturbation parameters obtained with the coming rule in Eq. (57).

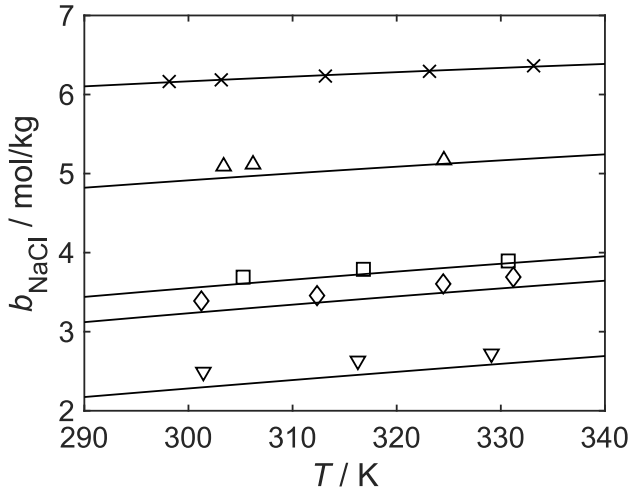

Figure 14: Experimental solubility data [76, 77] (symbols) and results of the perturbation model (lines) for NaCl in different poorly specified mixtures plotted over the temperature (system E-IV.a+b). The unknown parts of all measurement series are composed of the unknown parts of the systems E-IV.a (KCl) and E-IV.b ($CaCl_2$). The results of the perturbation model are a prediction solely based on the results of the systems E-IV.a and E-IV.b. The different types of symbols indicate the different measurement series, cf. Table 6 ($w_{\mathrm{u}} = 0.00$ g/g (×), No. 1 (△), No. 2 (□), No. 3 (◊), No. 4 (▽)). The values for χ_{a}, $w_{\mathrm{u,free}}$, and the resulting interaction parameters of the perturbation model are given in Table 6.

The perturbation model with the predicted interaction parameters yields a very good agreement with the experimental data. This finding is of general value whenever mixtures are considered that are combinations of several poorly specified mixtures.

Table 6: The values for χ_a, $w_{u,free}$ and the resulting interaction parameters of the mixing study.

No.	χ_a / g g^{-1}	$w_{u,free}$ / g g^{-1}	$A^{a+b}_{NaCl,u}$ / kJ mol^{-1}	$A^{a+b}_{water,u}$ / kJ mol^{-1}	$\bar{M}_u$ / g mol^{-1}
1	0.83	0.12	46.17	33.55	50
2	0.20	0.15	96.17	74.79	50
3	0.33	0.18	85.65	66.11	50
4	0.26	0.23	91.37	70.82	50

3.4 Conclusion

Poorly specified liquid mixtures, which contain one or more specified components besides many unknown components, regularly appear in the process industry. Modeling and predicting the thermodynamic properties of such poorly specified liquid mixtures play an important role in process design or optimization. A novel approach to model the activities, and thus phase equilibria, of the specified components in such poorly specified mixtures based on a perturbation scheme is applied to several example systems. The scheme takes good thermodynamic models of the subsystem of specified components, which are often available, and applies a flexible perturbation term to consider the impact of the unknown part of the mixture on the specified components.

The perturbation scheme has one interaction parameter for each specified component and one parameter for the average molar mass of the unknown part. The results of the present chapter show that the average molar mass of the unknown part is not system specific for aqueous mixtures. The value 50 g/mol showed promising results for all considered aqueous example systems. For non-aqueous example systems, the average molar mass is handled as a model parameter that is fitted to experimental data. The interaction parameters must always be fitted to a few experimental data of the poorly specified mixture. Only information about the specified components and a few experimental data points for the specified components' activities in the poorly specified mixture are needed to regress and use the perturbation scheme. No analysis of the unknown part is necessary.

The perturbation scheme can be combined with different thermodynamic models; thus, it is highly flexible. This flexibility was shown by combining it with different g^E-models for non-electrolyte and electrolyte systems. It has been shown that the perturbation scheme works well for many mixtures using several example systems based on pseudo-experimental or real experimental data. Organic or aqueous-organic mixtures, as well

as aqueous-electrolyte example systems, were studied. When using the perturbation scheme, one obtains a model of the activities of all specified components within a poorly specified mixture. As long as the composition and constitution of the unknown part remain unchanged, this model can predict the activities well, even if the composition of the specified components changes. The results further indicate that the approach can predict the behavior of poorly specified mixtures that result from mixing two different poorly specified mixtures for which perturbation models are available.

4 Process Simulation of Poorly Specified Mixtures

4.1 Introduction

In the previous chapter, thermodynamic calculations of poorly specified mixtures were considered. However, if one goes one step further, the question arises, how to handle these poorly specified mixtures in process simulation for process design or optimization. In this chapter, a general workflow is presented to set up a process simulation for a poorly specified mixture. Here, this workflow is combined with the perturbation scheme of the present work.

The workflow is applied to three different example processes. The first two processes are based on systems of the previous chapter (Chapter 3). In the first process, the crystallization of α-lactose is studied, which is based on the SLE of lactose in a poorly specified mixture (cf. Table 2 system V). In the second process, the evaporation of ethanol and methanol in an open still is studied, which is based on the VLE of ethanol and methanol (cf. Table 2 system VI). The system of the last example process is introduced here and deals with wood hydrolysate. As already mentioned in the chapter before, experimental data of poorly specified mixtures are rarely published in the literature. The studied processes here are also based on fully specified systems. However, no information of the as unknown defined components are used for the process simulation.

4.2 Workflow

The proposed workflow to handle poorly specified mixtures in process simulation is shown in Figure 15. The starting point is a poorly specified liquid mixture that is part of a process. First (step I), a thermodynamic model must be chosen that describes the thermodynamic behavior of poorly specified mixtures. Here, we always use the perturbation scheme of the present work. Next (step II), the chosen thermodynamic model is

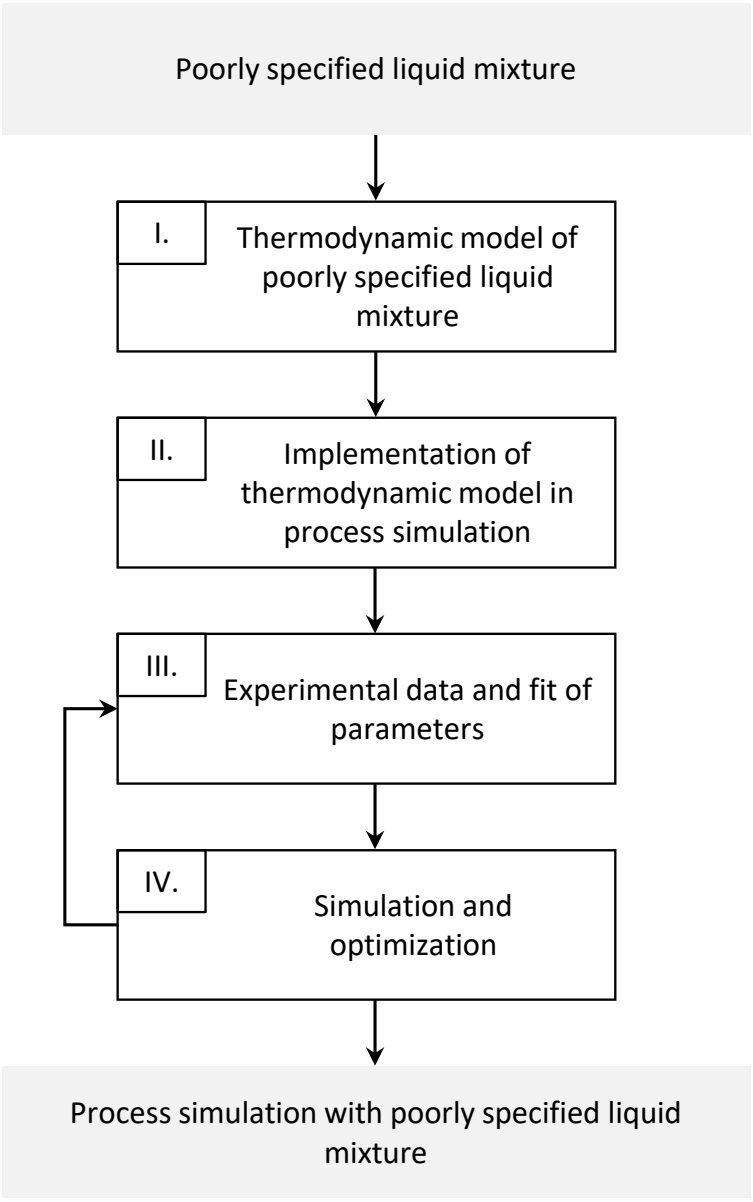

Figure 15: Workflow to handle poorly specified mixtures in process simulation.

implemented in the process simulation. Usually, not all required model parameters are known for poorly specified mixtures in advance. Therefore, experimental data of the poorly specified mixture are required to fit the remaining parameters (step III). The type and number of experimental data depend on the specific studied problem. Afterward (step IV), simulation and optimization of the process are possible. If necessary, further experimental data at other conditions can be used to adjust the parameters accordingly. Finally, the process simulation that is able to handle a poorly specified liquid mixture is obtained.

4.3 Example Processes

4.3.1 Crystallization of α-Lactose

The first studied process is the crystallization of α-lactose (lactose) in a poorly specified mixture. The process scheme for the crystallization is shown in Figure 16.

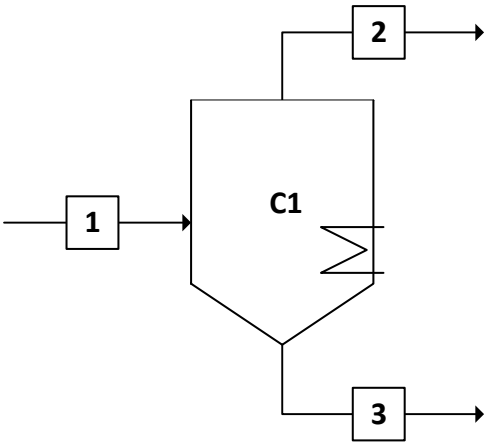

Figure 16: Process scheme for lactose crystallization.

The feed (stream 1) is a poorly specified mixture comprised of the specified components water and lactose, and the remaining unknown part u of the mixture (cf. Chapter 3.2.2, Table 2, system V). It is assumed that the mixture in the feed is oversaturated with lactose, and pure, solid lactose precipitates in the crystallizer (C1). Furthermore, the assumption is made that the crystallizer is ideal and reaches equilibrium at the given temperature. The pure, solid lactose in the crystallizer is separated by stream 3. Stream 2 is comprised of the remaining poorly specified liquid mixture.

To set up a process simulation for this crystallization process, the proposed workflow described before is used (cf. Figure 15):

Step I.
The perturbation scheme is used to model the thermodynamic properties of the poorly specified liquid mixture. The g^{E}-model UNIQUAC is chosen as the base model to model the specified subsystem comprised of lactose and water (cf. Chapter 3.2.2, Table 2, system V). The influence of the unknown part on the thermodynamic properties of the specified components is covered by the perturbation scheme.

Step II.

We did not use a commercial process simulation software here, but we set up the process simulation in Matlab [78]. The process simulation in Matlab comprises calculating the SLE of lactose in the crystallizer and calculating the resulting mass flows of the single components in stream 2 and stream 3. The SLE of lactose, i.e. the solubility of lactose, is calculated using Eq. (51). The activity of lactose is calculated using the perturbation scheme (cf. Eq. (7)). The UNIQUAC model is used as the base model for the specified subsystem comprised of water and lactose. The influence of the unknown part is covered by the the perturbation terms x^{p} (cf. Eq. (8)) and γ_k^{p} (cf. Eq. (36)). These two terms affect the calculation of the activity only if an unknown part is present. If no unknown part is present, Eq. (7) reduces to the original equation for calculating the activity. The required mass flow of lactose in stream 3 is obtained from the SLE calculation combined with the mass balance for lactose. The mass flows of water, and the unknown part u in stream 2 is obtained from the respective mass balances.

Step III.

The model parameters of the base model UNIQUAC and the perturbation scheme are required for the process simulation. The numerical values of the parameters are already given in Appendix A and Chapter 3.2.2. The UNIQUAC model parameters are taken from the literature, and the model parameters of the perturbation scheme are obtained by fitting to experimental data from Machado et al. [70]. The exact procedure of fitting the parameters is described in Chapter 3.2.2. The used experimental data points are obtained from the literature on dedicated SLE experiments. However, these data could also be obtained by process analytics in a real plant. Assuming that a poorly specified mixture with a high mass fraction of the unknown part is available, the solubility of lactose could be measured by adding lactose till saturation is reached. By adding the specified component water, the mass fraction of the unknown part could be varied, and the solubility of lactose could be measured again. Two data points describing the solubility of lactose in mixtures with different mass fractions are already sufficient since only two interaction parameters ($A_{\mathrm{lactose,u}}$ and $A_{\mathrm{water,u}}$) must be fitted. The two experimental data points used for the fit and the result for the solubility of lactose obtained from the perturbation scheme are already shown in Figure 9.

Step IV.

In the final step, the process simulation of the crystallization process (cf. Figure 16) can be run. The mass flow of the feed (stream 1) is set to the constant value $\dot{m}^{(1)} = 1$ kg/h. The mass flow of lactose in the feed is set to $\dot{m}^{(1)}_{\mathrm{lactose}} = 0.4$ kg/h. In the first study, the mass flows of water and the unknown part in the feed is varied, and the temperature T^{C1} of the crystallizer C1 is set to constant temperature 313.15 K. Figure 17 shows how

the mass flow $\dot{m}^{(2)}_{\text{lactose}}$ of lactose in stream 2 changes depending on the mass flow $\dot{m}^{(1)}_{\text{u}}$ of the unknown part in the feed (stream 1). Since the assumption is made that the crystallizer C1 always reaches equilibrium, a comparison with experimental data for the SLE of lactose in the poorly specified mixture is possible.

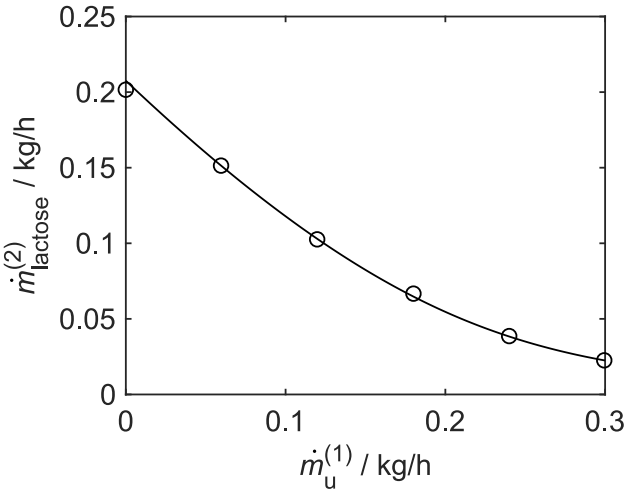

Figure 17: Crystallization of lactose at 313.15 K. Change of the mass flow $\dot{m}^{(2)}_{\text{lactose}}$ of lactose in stream 2 (cf. Figure 16) depending on the mass flow $\dot{m}^{(1)}_{\text{u}}$ of the unknown part in the feed (stream 1). Solid line: result of the perturbation scheme; Symbols: experimental data [70].

The mass flow of lactose in stream 2 decreases with increasing mass flow of the unknown part in the feed (stream 1). Hence, more lactose precipitates in the crystallizer when the mass fraction of the unknown part in the liquid mixture is higher. Furthermore, the agreement of the experimental data with the simulation with the perturbation scheme is very good. The experimental data shown in Figure 17 and used for fitting are no real process data. The experimental data shown here are obtained from corresponding SLE measurements given in the literature [70].

In the second study, the composition of the feed (stream 1) is kept constant ($\dot{m}^{(1)}_{\text{lactose}}$ = 0.40 kg/h, $\dot{m}^{(1)}_{\text{water}}$ = 0.42 kg/h, $\dot{m}^{(1)}_{\text{u}}$ = 0.18 kg/h), but the temperature in the crystallizer C1 is varied. Figure 18 shows how the mass flow $\dot{m}^{(2)}_{\text{lactose}}$ of lactose in stream 2 changes depending on the temperature T^{C1} of the crystallizer C1.

As shown in Figure 18, the mass flow $\dot{m}^{(2)}_{\text{lactose}}$ of lactose in stream 2 increases with increasing temperature. The solubility of lactose also increases with increasing temperature, so less lactose precipitates at higher temperatures. The agreement of the experimental data and the result of the perturbation scheme is again very good, although the

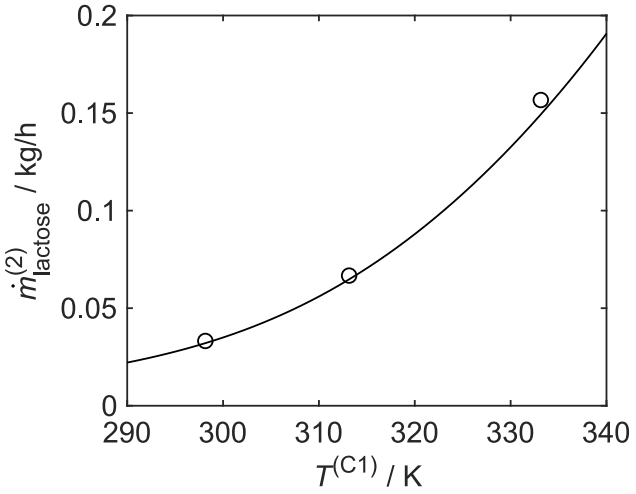

Figure 18: Crystallization of lactose with constant composition of the feed (stream 1) ($\dot{m}^{(1)}_{\text{lactose}}$ = 0.40 kg/h, $\dot{m}^{(1)}_{\text{water}}$ = 0.42 kg/h, $\dot{m}^{(1)}_{\text{u}}$ = 0.18 kg/h). Change of the mass flow $\dot{m}^{(2)}_{\text{lactose}}$ of lactose in stream 2 depending on the temperature T^{C1} of the crystallizer C1. Solid line: result of the perturbation scheme; Symbols: experimental data [70].

model parameters of the perturbation scheme were solely fitted to experimental data at 313.15 K.

4.3.2 Residue Curve of Acetone and Methanol

In the second example process, the evaporation of the two specified components, acetone and methanol, is studied in an open still at 101.3 kPa. Figure 19 schematically shows the evaporation in an open still.

The poorly specified liquid mixture that comprises the two specified components, acetone and methanol, and the unknown part (cf. Chapter 3.2.2, Table 2, system VI) is put in the open still S1 and evaporates (stream 1). It is assumed that the unknown part is non-volatile and does not evaporate. For example, it could contain electrolytes. Due to evaporation, the composition of the poorly specified liquid phase changes. As shown in Figure 10 (cf. Chapter 3.2.2), the specified binary subsystem (acetone + methanol) is azeotropic. However, the unknown part clearly influences the VLE of the specified subsystem. Therefore, the composition of the azeotrope is shifted towards pure acetone by adding the unknown part. The proposed workflow of Figure 15 is used to set up the process simulation to obtain the residue curve of the studied system:

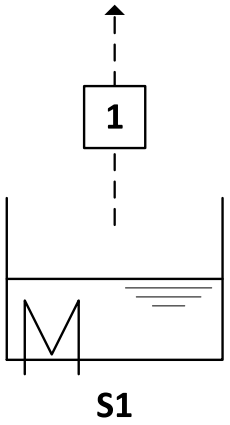

Figure 19: Process scheme for the evaporation of acetone and methanol in an open still.

Step I.

Analog to the example process before the perturbation scheme is used to model the thermodynamic properties of the poorly specified liquid mixture. For the base model of the specified subsystem comprised of acetone and methanol, the g^{E}-model NRTL is chosen (cf. Chapter 3.2.2, Table 2, system VI). The perturbation scheme covers the influence of the unknown part on the thermodynamic properties of the specified components.

Step II.

The process simulation of the open still is set up in Matlab [78]. The Rayleigh equation is used to calculate the residue curve, while the VLE of the poorly specified liquid mixture is calculated using the extended Raoult's law (cf. Eq. (52)) combined with the perturbation scheme (cf. Eq. (7)) to cover the influence of the unknown part on the specified components. The perturbation terms x^{p} (cf. Eq. (8)) and γ_k^{p} (cf. Eq. (36)) cover the influence of the unknown part on the specified components and affect the calculation of the activities only if the unknown part is present.

Step III.

Model parameters for the base model NRTL and the perturbation scheme are required. The numerical values for this system are given in Appendix A and Chapter 3.2.2. The model parameters for the base model NRTL are obtained from the literature, and the model parameters of the perturbation scheme are determined by fitting to experimental data from Li et al. [71]. The exact procedure of fitting the model parameters is described in Chapter 3.2.2. Again, the experimental data used for fitting were taken from the literature. However, the data could also be obtained for a real problem in the same manner as described in the example process before. Assuming that a poorly specified mixture with a high mass fraction of the unknown part is available, the mass fractions

of the two specified components in the liquid and vapor phase at equilibrium could be measured. Adding one of the specified components changes the composition of the specified subsystem and the mass fraction of the unknown part in the liquid phase. Again the mass fractions of the two specified components in the liquid and vapor phase at equilibrium could be measured. Consequently, the activities of the two specified components, methanol and acetone, in two mixtures with different compositions can be calculated from the experimental data. These four data points are sufficient to fit the model parameters of the perturbation scheme ($A_{\text{acetone,u}}$, $A_{\text{methanol,u}}$, and $\bar{M}_{\text{u}}$). The experimental data of the two mixtures used for the fit are already shown in Figure 10. The result for the VLE of acetone and methanol obtained from the perturbation scheme is shown in Figure 11.

Step IV.
In the final step, the residue curve of the evaporation in the open still (cf. Figure 19) can be calculated. For demonstration, two process simulations are done with the process simulation derived above: *a*) The evaporation of the fully specified binary mixture (0.9 g/g acetone + 0.1 g/g methanol) in an open still. *b*) Identical to case *a*, but the initial composition of the mixture is diluted with the unknown part so that the mass fraction of the unknown part is 0.05 g/g.

Figure 20 shows the liquid mass fraction of acetone in the subsystem acetone + methanol in the residue when evaporating the two mixtures (case *a* and case *b*) in an open still, the solid line excluding the unknown component, the dashed line including the unknown component. In the specified subsystem (acetone + methanol), the initial composition is chosen on the acetone-rich side of the azeotrope. Consequently, methanol depletes in the liquid phase faster than acetone upon evaporation when no unknown part is present. As described before, the unknown part strongly influences in the liquid phase and shifts the azeotropic point or even makes it disappear. At the selected mass fraction of the unknown component, the azeotropic point is shifted so far that the initial composition is now on the methanol-rich side of the azeotrope. Methanol is now heavy-boiling, and thus acetone is depleting faster. This simple example shows that the perturbation scheme can capture such important phenomena as the shift or disappearance of an azeotropic point and that it can be used in process simulations. Therein it gives good results, even if the unknown components have a tremendous influence on the thermodynamic properties.

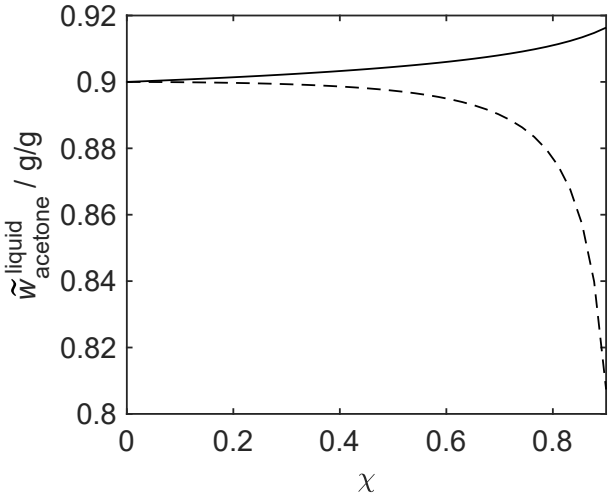

Figure 20: Liquid mass fraction $\tilde{w}^{\text{liquid}}_{\text{acetone}}$ of acetone on an unknown-free basis within the specified subsystem (acetone + methanol) in the residue during evaporation in an open still. χ gives the mass fraction of the initial mixture that is already evaporated. Full line: initial binary mixture (case *a*). Dashed line: initial mixture is poorly specified with 0.05 g/g unknown part (case *b*).

4.3.3 Recovery of Furfural and Acetic Acid from Wood Hydrolysates

In the last example process, furfural and acetic acid recovery from wood hydrolysates are studied. The importance of processes for the production of chemicals from biomass increases strongly [79]. One possible process to obtain ethanol from biomass is the fermentation of hydrolysates of lignocellulosic biomass [80–82]. However, lignocellulosic hydrolysate can not be used for fermentation directly. On the one hand, the sugar concentration is to low, and on the other hand, the hydrolysate contains numerous inhibitors, which are toxic for microorganisms [83, 84]. Galeotti et al. [85] proposed a process to combine the recovery of the valuable inhibitors acetic acid and furfural with the increase of the sugar concentration. Galeotti et al. [85] used a model quaternary mixture comprised of water, xylose, acetic acid, and furfural to represent the hydrolysate in the process. We assume that the sugar xylose is not known in the following. Thus, we model water, acetic acid, and furfural as the specified subsystem and add a perturbation term to cover the influence of the sugar. This approach is practical, as there is usually a mixture of different sugars and other unknown substances in the (real) hydrolysate. Defining the sugar part of the hydrolysate as a whole as the unknown part in the thermodynamic model makes it unnecessary to analyze the composition in detail. Figure 21 shows the process scheme proposed by Galeotti et al. [85].

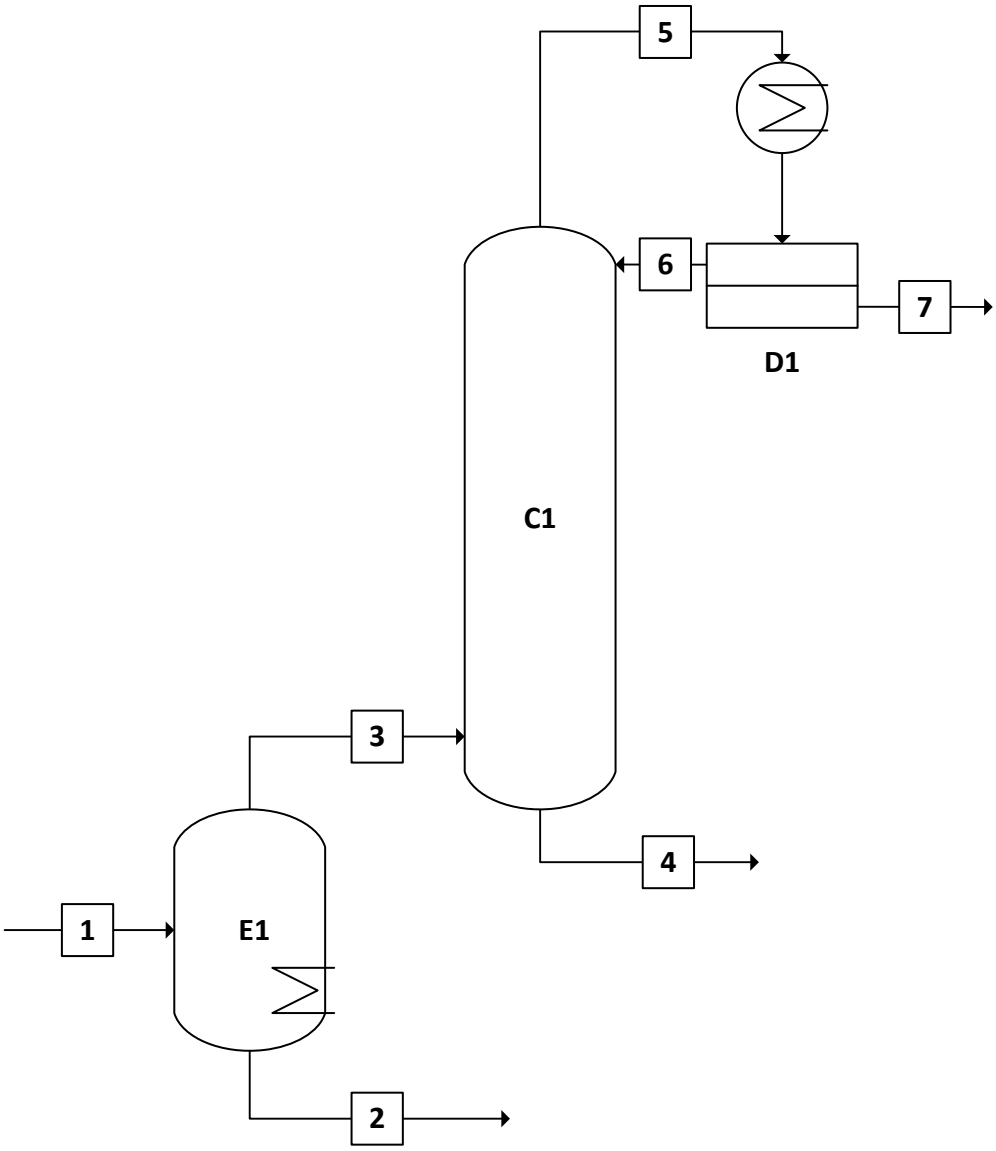

Figure 21: Process scheme for furfural and acetic acid recovery and increasing the sugar concentration.

The feed (stream 1) is the hydrolysate. The sugar concentration is increased in the evaporator E1 that operates at 20.0 kPa to avoid thermal degradation of the sugar. The sugar-rich liquid stream is separated by stream 2. The gas stream (stream 3) is directly fed to the bottom of the rectifying column C1 to recover acetic acid and furfural by heteroazeotropic distillation. The column C1 also works at 20.0 kPa to avoid gas compression. The heteroazeotrope in the system water and furfural is almost reached at the top of column C1 (stream 5). Stream 5 is condensed in the decanter D1. The water-rich phase is the reflux of column C1 (stream 6), the furfural-rich phase is the product (stream 7). The liquid phase at the bottom of the column C1 is a diluted

aqueous mixture of acetic acid (stream 4).

In the following, the proposed workflow of the present work is used again to run the process simulation of the wood hydrolysate process (cf. Figure 15):

Step I.
The g^{E}-model NRTL [9] is used as the base model for the specified subsystem comprised of water, furfural, and acetic acid. The perturbation scheme covers the influence of the unknown part on the specified components. The required values for the NRTL model parameters are obtained from Galeotti et al. [86] and are given in Appendix B.

Step II.
The column C1 and the decander D1 (cf. Figure 21) were set up in the simulator Aspen Plus [87]. To implement the perturbation scheme the calculation of the activity in the evaporator E1 must be adjusted. Since we did not have the possibility to adjust the calculation in Aspen Plus, we had to use a workaround. We set up the evaporator E1 - the part of the process simulation that includes the poorly specified mixture - in Matlab [78]. So the VLE in the evaporator E1 and the respective mass flows of stream 2 and stream 3 were calculated in Matlab. The obtained results were then transferred to Aspen Plus using a COM (Component Object Model) server and the *actxserver* function of Matlab. The VLE of the poorly specified wood hydrolysate comprised of water, furfural, acetic acid, and the unknown part in the evaporator E1 is schematically shown in Figure 22.

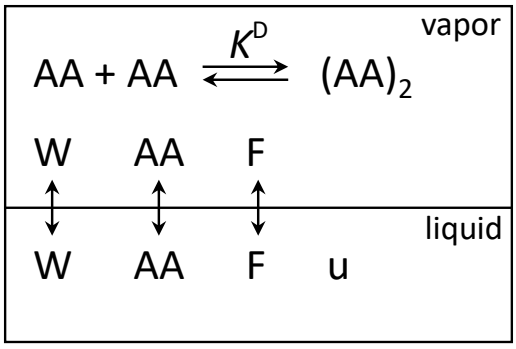

Figure 22: Scheme of the VLE of the system water (W), furfural (F), acetic acid (AA), and the unknown part (u). The dimerization of acetic acid is considered only in the vapor phase.

Analogous to the work of Galeotti et al. [88], it is assumed that acetic acid forms dimers only in the vapor phase and that the dimerization reaction is an equilibrium reaction

with the thermodynamic equilibrium constant K^{D} [89]. The dimerization of acetic acid in the vapor phase is described by the chemical theory [90, 91]. Detailed information on the chemical theory is given in Appendix B. The extended Raoult's law (cf. Eq. (52)) is used to calculate the VLE (Assumption: Poynting correction is negligible).

$$a_k = \frac{y_k p}{p_k^{\mathrm{s}}} \qquad k = \{\text{water, acetic acid, furfural}\} \tag{58}$$

Where a_k is the activity of the specified component k in the liquid phase, y_k is the mole fraction in the vapor phase, p is the pressure, and p_k^{s} is the vapor pressure. The pressure p is here 20.0 kPa. The vapor pressure p_k^{s} is calculated using the Antoine equation. The vapor pressure of acetic acid has to modified because of the chemical theory, cf. Appendix B. The Antoine equation and the corresponding parameters are given in Appendix B. The perturbation scheme (cf. Eq. (7)) is used to model the activities a_k of the specified components. The unknown part remains solely in the liquid phase of the evaporator E1, so only mixtures comprised of specified components are passed to Aspen Plus to calculate the column C1 and the decanter D1.

To validate the results obtained from the process simulation with the perturbation scheme, the complete process using the fully specified mixture with the NRTL parameters obtained from Galeotti et al. [85] was simulated in Aspen Plus. Twice the number of NRTL model parameters is required to model the quaternary model mixture representing the wood hydrolysate with the fully specified NRTL model, compared to the NRTL model parameters required by the perturbation scheme for the same system.

Step III.

Here, three interaction parameters of the perturbation term are required ($A_{\mathrm{water,u}}$, $A_{\mathrm{furfural,u}}$, $A_{\mathrm{acetic\ acid,u}}$). The average molar mass of the unknown part $\bar{M}_{\mathrm{u}}$ is set to the fixed value 50 g/mol since the specified subsystem is an aqueous system. Since only very few experimental data are available for the complete system water, furfural, acetic acid, and the unknown part, the experimental phase equilibrium data of two subsystems are studied. First, experimental data of the VLE of the system water, acetic acid, and the unknown part u (here: xylose) from Galeotti et al. [88] are used to determine the two interaction parameters $A_{\mathrm{water,u}}$ and $A_{\mathrm{acetic\ acid,u}}$. The experimental data points give the vapor-liquid partition coefficients $P_{k,\mathrm{u-free}}$ of the specified components acetic acid and water. The vapor-liquid partition coefficients $K_{k,\mathrm{u-free}}$ are defined as:

$$P_{k,\mathrm{u-free}} = \frac{w_k^{\mathrm{vapor}}}{w_{k,\mathrm{u-free}}} \qquad k = \{\text{water, acetic acid}\}\,. \tag{59}$$

Where w_k^{vapor} is the mass fraction of the specified component k in the vapor phase

and $w_{k,\text{u-free}}$ is the mass fraction of the specified component k in the u-free liquid phase. Figure 23 shows the experimental data points obtained from Galeotti et al. [88], the two data points used to fit the two interaction parameters (indicated by the filled symbols), and the results obtained from the perturbation scheme for the VLE of water, acetic acid, and the unknown part.

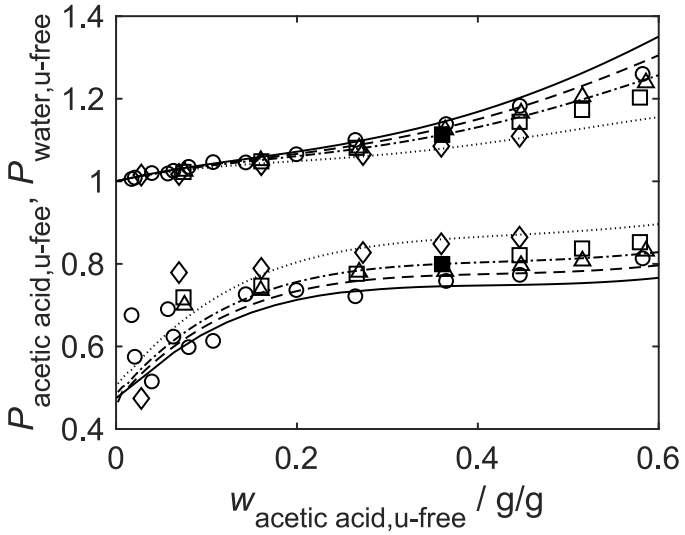

Figure 23: Vapor-liquid partition coefficients of acetic acid and water in the VLE acetic acid, water, and the unknown part with different mass fractions of the unknown part: w_u = 0 g/g (—○—), w_u = 0.05 g/g (- -△- -), w_u = 0.10 g/g (-·□-·,-·■-·), w_u = 0.20 g/g (·◊·). Symbols: Experimental data points [88]; Filled symbols: Used for fit; Lines: Perturbation scheme with $A_{\text{acetic acid,u}}$ = 24.46 kJ/mol and $A_{\text{water,u}}$ = 18.06 kJ/mol.

When comparing the results obtained from the perturbation scheme shown in Figure 23 with the results obtained from the NRTL model of the fully specified mixture (unknown part u = xylose) from Galeotti et al. [88] shown in Figure 24, a clear difference between the two models can be observed.

The perturbation scheme describes the experimental data points very well, especially when the mass fraction of acetic acid is higher than 0.2 g/g. Whereas, for high mass fractions of the unknown part, deviations between the experimental data points and the NRTL model of the fully specified mixture can be observed. When using the NRTL model for the fully specified mixture two interaction parameters are required for the interactions between acetic acid + water, acetic acid + xylose, and water + xylose, respectively. Galeotti et al. [88] used binary experimental data (acetic acid + water) to fit the two NRTL interaction parameters for acetic acid + water. Further, Galeotti et al. [88] set the NRTL interaction parameters for acetic acid + xylose to zero since the

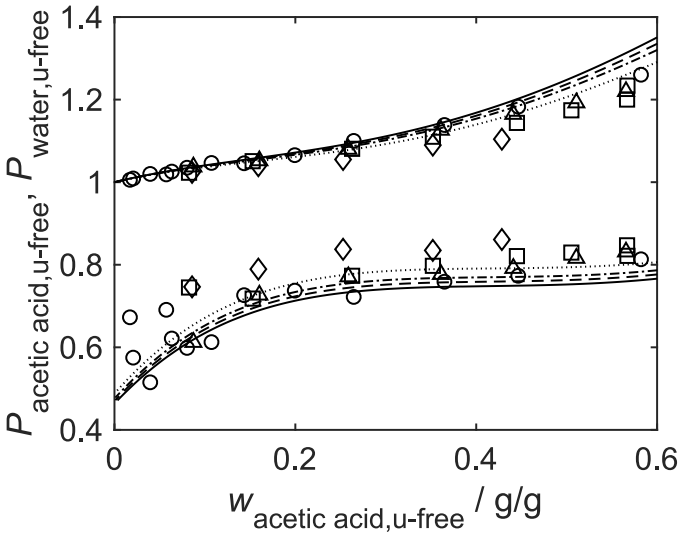

Figure 24: Vapor-liquid partition coefficients of acetic acid and water in the VLE acetic acid, water, and the unknown part with different mass fractions of the unknown part: $w_\mathrm{u} = 0$ g/g (—○—), $w_\mathrm{u} = 0.05$ g/g (- -△- -), $w_\mathrm{u} = 0.10$ g/g (-·□-·,-·■-·), $w_\mathrm{u} = 0.20$ g/g (·◊·). Symbols: Experimental data points [88]; Lines: NRTL model of the fully specified mixture.

activity coefficient of water in the binary systems with sugars are assumed to be close to unity. The two NRTL interaction parameters for acetic acid + xylose was fitted to the shown ternary experimental data. It seems that these two model parameters can not influence the result of the model in the same way as the interaction parameters of the perturbation scheme. Further, the restriction that no interaction between water and the unknown part occurs is not made for the perturbation scheme.

Secondly, experimental data of the liquid-liquid equilibrium (LLE) of the system water, furfural, and the unknown part obtained from Galeotti et al. [86] are used to determine the remaining interaction parameter $A_\mathrm{furfural,u}$. To calculate the LLE the isoactivity criteria must be fulfilled:

$$a'_k = a''_k = x'_k \gamma'_k = x''_k \gamma''_k, \tag{60}$$

where a'_k is the activity of the specified component k in the liquid phase $'$ and a''_k is the activity of the specified component k in the liquid phase $''$. Figure 25 shows experimental data points obtained from Galeotti et al. [86] and the results obtained from the perturbation scheme for the LLE of furfural, water, and unknown part.

The solid lines link the experimental data points obtained from Galeotti et al. [86] indicated by symbols. The dashed lines link the symbols obtained from the perturbation scheme. Only experimental data points, which where measured at 298.15 K and were no

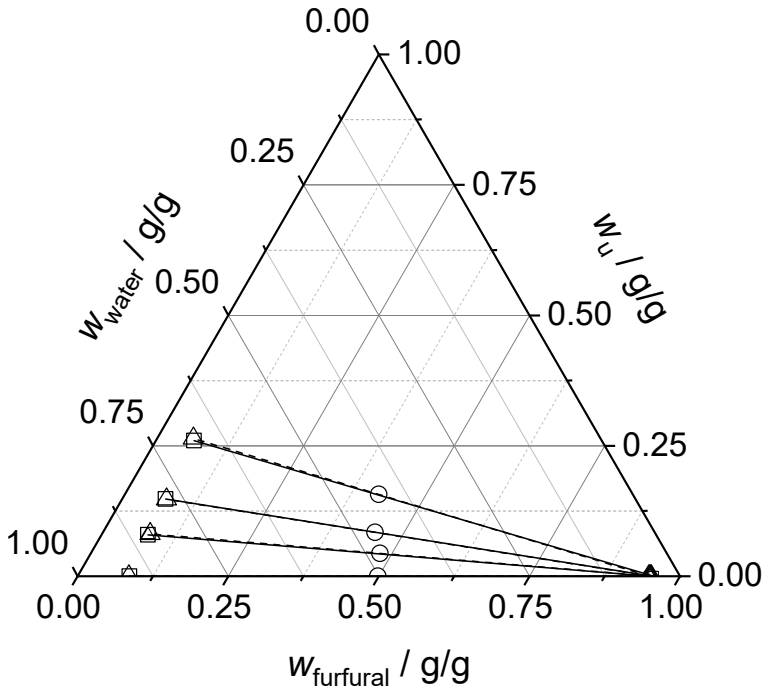

Figure 25: LLE of furfural, water, and unknown part. ○: Initial composition for experimental data points [86]; □—□: Experimental data points LLE [86]; △−−△: Perturbation scheme with $A_{\mathrm{water,u}}$ = 18.06 kJ/mol and $A_{\mathrm{furfural,u}}$ = 28.88 kJ/mol.

unknown part was present in the furfural-rich liquid phase, were used. All shown data points were used to fit the remaining interaction parameter $A_{\mathrm{furfural,u}}$. The numerical value for the interaction parameter $A_{\mathrm{water,u}}$ was used from the fit before. For the LLE, the perturbation scheme and the NRTL model of the fully specified mixture (cf. Galeotti et al. [86]) agree very well with the experimental data points.

Step IV.

In the final step, the process simulation of the wood hydrolysate process was run. In the following, the mass fraction of the unknown part u in the feed (stream 1) was varied. However, the composition of the specified subsystem comprised of water, acetic acid, and furfural was kept constant. Figure 26 shows how the mass flows of the specified components water, acetic acid, and furfural and the mass flow of the unknown part u in the feed (stream 1) of the evaporator E1 change. The mass flow of the complete feed (stream 1) is always $\dot{m}^{(1)}$ = 2000 kg/h.

Figure 27 shows the result for the process simulation using the perturbation scheme and using the fully specified system for the four streams 2, 3, 4, and 7. The simulations using the perturbation scheme and the fully specified system only differ in the calculation of

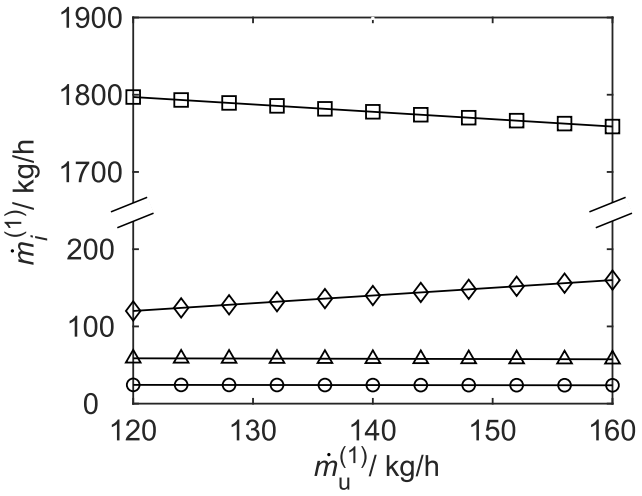

Figure 26: Variation of the mass flows $\dot{m}_i{}^{(1)}$ of the specified components (i = water, acetic acid, and furfural) and the unknown part $\dot{m}_u{}^{(1)}$ in the feed (stream 1) of the evaporator. —□— : water; —△— : furfural; —○— : acetic acid; —◇— : unknown part.

evaporator E1 since no unknown part is in stream 3 leading to the column C1. Hence, no unknown part is in stream 4 and stream 7.

The result obtained from the simulation with the perturbation scheme and the simulation with the fully specified system is very similar for the components acetic acid, furfural, and the unknown part. However, solely for the component water, a difference between the two simulations occurs in the streams 2, 3, and 4. The difference result from the different calculations of the vapor-liquid phase equilibrium in the evaporator E1. This difference is not surprising. The model parameters of both approaches - perturbation scheme and fully specified NRTL model [85] - for calculating the VLE in the evaporator were fitted to experimental data of the VLE acetic acid, water, and the unknown part [88] and the LLE data of water, furfural, and the unknown part [86]. Comparing the results of the fits already shows different agreement of the experimental data with the models.

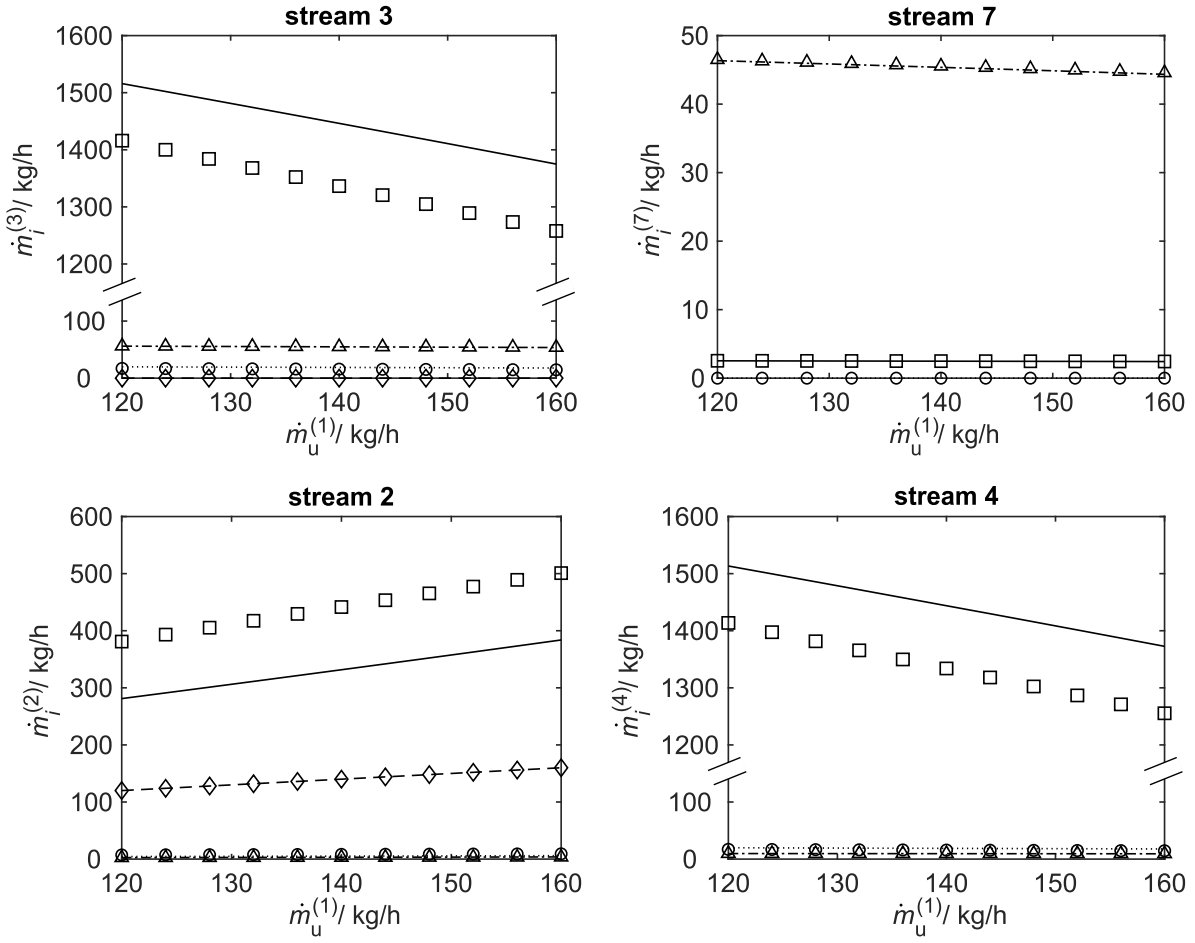

Figure 27: Mass flows of the specified components (i = water, acetic acid, and furfural) and the unknown part (u) in the different streams 2, 3, 4, and 7 (cf. Figure 21). Symbols: Perturbation scheme (□ : water; △ : furfural; ○ : acetic acid; ◊ : unknown part); Lines: fully specified NRTL model [85] (—— : water; – · –· : furfural; ··· : acetic acid; – – – : unknown part).

4.4 Conclusion

A general workflow is presented how to handle poorly specified mixtures in process simulations. The workflow is combined with the perturbation scheme of the present work and is applied to three example processes. The process simulations obtained at the end of the workflow worked well for all studied problems.

The studied crystallization process of lactose shows that only a few easy-to-measure experimental data points are required to apply the perturbation scheme to the process simulation. Furthermore, it is shown that an extrapolation of the process simulation with the perturbation scheme regarding the temperature is possible here. Also, a variation of the mass flow of the unknown part is unproblematic for the process simulation. The simulation of the residue curve of acetone and methanol in a poorly specified mixture shows that the perturbation scheme can capture the shift or disappearance of an azeotropic point caused by unknown components in process simulation. Moreover, the studied wood hydrolysate process shows that it is even possible to fit the model parameters of the perturbation scheme to subsystems that are not comprised of all specified components of the poorly specified mixture. This indicates that the perturbation scheme can also cover a variation of the composition of the specified components. So it is possible that the composition of the specified components of the experimental data used to fit the model parameters of the perturbation scheme is the same as used in the process simulation.

All in all, the proposed workflow combined with the perturbation scheme does have the advantage that only a simple modification in the calculation of the thermodynamic properties of the specified components of an existing process simulation would be necessary to cover the influence of the unknown part of a poorly specified mixture. The modification only affects the calculation of the specified components if an unknown part is present. Further advantages are that only a small number of easy-to-measure experimental data are needed to determine the required model parameters. However, the obtained process simulations only provide information regarding the specified components of the poorly specified mixture. Simulation and modeling of parameters where detailed data of all components are required (e.g. heat demand) can consequently not be calculated with the process simulations shown here.

5 Measurement and Modeling of the Solubility of α-Lactose

5.1 Introduction

Aqueous sugar solutions that contain additional organic components, electrolytes, or even both frequently appear in the food, chemical, and pharmaceutical industries [70, 92]. These additional components can have a crucial influence on the thermodynamic behavior of the solutions, e.g. the sugar solubility, and can thus have a significant impact on processes. Furthermore, reliable experimental data and thermodynamic models are necessary for process design or optimization.

There are already several publications for general solubility data of sugars in water or mixed water-alcohol solvents, e.g. [93–97], several publications for the solubility of sugars in aqueous electrolyte or ionic liquids solutions, e.g. [98–100], and a few for the solubility of sugars in mixed organic-electrolyte solvents, e.g. [101]. α-lactose - the sugar of main interest in the present chapter - appears within systems containing alcohols [70] and electrolytes [92] in the food and pharmaceutical industries. For subsystems, some experimental data on the solubility of α-lactose are available in the literature. Hudson [102] reports the solubility of α-lactose in pure water in the temperature range 0 °C to 89 °C. The solubility of α-lactose in binary mixtures of water and the anti-solvent ethanol or other alcohols is reported by Machado et al. [70] and by Majd and Nickerson [103]. The solubility of α-lactose in other aqueous mixtures, in whole milk or aqueous sucrose solutions, is reported by Hunziker and Nissen [104]. Regarding the solubility of α-lactose in aqueous electrolyte solutions, Bhargava and Jelen [105] report values for the solubility of α-lactose in different aqueous salt solutions (K_2HPO_4, $CaCl_2$, Ca lactate, $MgSO_4$, and LiCl) and whey ultrafiltration permeate solutions at 30 °C. Choscz et al. [92] measured the α-lactose solubility in different single salt solutions and, additionally, in a milk-salt model and a whey permeate model, which comprise several different electrolytes, respectively, at temperatures from 20 °C to 50 °C. Herrington [106] measured the solubility of lactose in $CaCl_2$ and $Ca(NO_2)_2$ salt solutions at 32 °C.

Jensen et al. [107] report the solubility of lactose in several salt solutions, mainly sodium, calcium, and magnesium salts at 35 °C. Smart and Smith [108] also measured the solubility of lactose in phosphate and sulfate salt solutions, in solutions with two salts, as well as in solutions with lactic acid and lactate at 35 °C. In the present work, the data basis is extended, and solubility data of α-lactose are reported for solutions of water-ethanol-NaCl and water-ethanol-$CaCl_2$ at 298.15 K. To our knowledge there are, so far, no experimental data on the solubility of α-lactose in solutions of water-ethanol-NaCl and water-ethanol-$CaCl_2$ in the literature.

Thermodynamic models used to describe or predict the solubility of sugars in aqueous solvents or mixed organic solvents are either g^{E}-models, e.g. NRTL [9] or UNIQUAC [10], or equations of state, e.g. PC-SAFT [73, 98, 109, 110]. If the solvent comprises electrolytes, then modifications of these thermodynamic base models, i.e. the non-electrolyte models, are necessary. Common approaches for mixed organic-electrolyte solutions are e.g. electrolyte NRTL [111, 112], UNIQUAC extended with a Debye-Hückel term (UNIQUAC-DH)[65] or ePC-SAFT [92, 113].

Here, the solubility data are correlated in two ways. On the one hand, the UNIQUAC-DH model proposed by Sander et al. [65] is used. The required model and interaction parameters for the subsystems water-ethanol-NaCl/$CaCl_2$ are already available in the literature. Nevertheless, the model still has many unknown interaction parameters when lactose is added to the system. These parameters were fitted to the experimental data of the present work. On the other hand, the usual non-electrolyte UNIQUAC model is combined with the general perturbation scheme of the present work, called UNIQUAC-PS, in the following. Actually, this perturbation scheme was developed for modeling poorly specified mixtures [114], but it can also be applied to fully specified mixtures. The idea of the perturbation scheme is to use an already well-known thermodynamic model for a specified subsystem as described in the chapters before. Here, the specified subsystem comprises all components except the electrolytes. The perturbation term covers the influence of the remaining part of the mixture (here: the electrolytes) on the thermodynamic behavior of the components of the specified subsystem. The idea of adding a perturbation term to a thermodynamic model is not new and has led to a large number of models, including the UNIQUAC-DH mentioned before. The UNIQUAC-PS approach is interesting because the applied perturbation term is general and can be applied to any type of thermodynamic model of the liquid phase [114]. Further, it has a small number of parameters.

Here, it is shown that both UNIQUAC-DH and UNIQUAC-PS can be successfully used to model the solubility of α-lactose in mixed organic-electrolyte solvents. The advantages

and disadvantages of both approaches are discussed at the end of this chapter.

5.2 Experimental Work

5.2.1 Chemicals

α-lactose monohydrate Ph.Eur. ($C_{12}H_{22}O_{11} \cdot H_2O$, lactose) was acquired from Carl Roth and ethanol ≥ 99.2 vol% (C_2H_5OH, ethanol) from ChemSolute. Sodium chloride ≥ 99.5 wt% (NaCl) and calcium chloride dihydrate ≥ 99.0 wt% ($CaCl_2 \cdot 2H_2O$) were purchased from Merck. Table 7 gives an overview of the chemicals used in the present work. Ultra-pure water was produced with an ELGA PURELAB Classic apparatus.

Table 7: Overview of the chemicals, the respective suppliers and purities of the chemicals used in this work.

Chemical name	Supplier	Purity[a]
α-lactose monohydrate ($C_{12}H_{22}O_{11} \cdot H_2O$)	Carl Roth	99.0 wt%
ethanol (C_2H_5OH)	ChemSolute	99.2 vol%
sodium chloride (NaCl)	Merck	99.5 wt%
calcium chloride dihydrate ($CaCl_2 \cdot 2H_2O$)	Merck	99.0 wt%

[a] Supplier specification

5.2.2 Apparatus and Procedure

The solubility of lactose was measured in water-ethanol, water-ethanol-NaCl, and water-ethanol-$CaCl_2$ mixtures. For the water-ethanol system, five mixtures with different water/ethanol mass ratios were prepared in 100 ml Erlenmeyer flasks using an analytical balance (Sartorius ENTRIS244I-1S). The volume of the mixtures in the Erlenmeyer flask was always about 20 ml. For both the water-ethanol-NaCl and the water-ethanol-$CaCl_2$ system, three stock solutions comprising water and the respective salt in three different concentrations were prepared first. Afterwards, all six stock solutions were mixed in six dilution series with ethanol analogous to the procedure for the system water-ethanol. Each dilution series was carried out three times. A total of 105 flasks were obtained by this procedure for the 35 data points (cf. Table 12). To each flask, lactose was added in excess to yield a suspension. Added amounts are quantified in more detail in Appendix C. The flasks were placed in a tempered water bath at 298.15 K at atmospheric pressure for equilibration for at least three days. Prior tests showed

that three days are sufficient to reach equilibrium. The lactose concentration in the liquid phase was measured over several days and did not significantly change anymore after two days. This is in line with an equilibration time of two days reported by Machado et al. [70] in water-ethanol sytems. The temperature was measured with a calibrated Pt100 thermometer connected to a digital multimeter (Keithley DAQ6510). Each suspension was constantly stirred during the whole equilibration using a multi-position magnetic stirrer. During the sample preparation and during equilibration, the flasks were sealed tightly to avoid evaporation of water or ethanol. Figure 28 shows a schematic representation of the experimental apparatus.

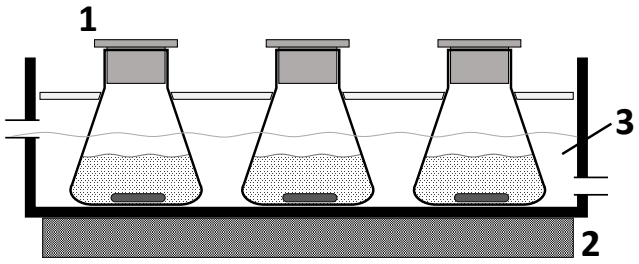

Figure 28: Schematic figure of the experimental apparatus. 1 - Erlenmeyer flask / equilibrium cell; 2 - Multi-position magnetic stirrer; 3 - water at constant temperature.

After equilibration, a sample was taken from the suspension in each flask with a syringe. The samples in the syringe were immediately filtrated using a disposal syringe filter (Macherey-Nagel CHROMAFIL® Xtra RC-10/25). Prior to use, the syringes and syringe filters were thermostatted to 298.15 K. The samples were gravimetrically diluted (dilution factor approximately 5) with ultra-pure water using the analytical balance and analyzed by High Performance Liquid Chromatography (HPLC; Detector: Refractive Index Detector Shimadzu RID-10A, Column: Phenomenex Rezex ROA-Organic Acid H+ (8%) 300 x 7.8 nm, Eluent: 0.245 g/L sulphuric acid Supra-quality 95% (H_2SO_4) Carl Roth) for lactose. The analysis was calibrated and tested using samples of known composition. The relative standard uncertainty $u_r(w_{\text{lactose}})$ of the analysis is estimated to be less than 0.019 in the studied concentration range. The solubilities were determined as the mean of three samples. The standard deviation s of the solubility of lactose is calculated with:

$$s = \sqrt{\frac{\sum_{n=1}^{3}(w_{\text{lactose},n} - \bar{w}_{\text{lactose}})^2}{2}}, \tag{61}$$

where $\bar{w}_{\text{lactose}}$ is the mean lactose solubility. The ratio of the standard deviation and

the mean was always less than 2.07 %. The mass fractions of water, ethanol and the salts were determined as the mean of the three samples from the weight measured at the preparation of the stock solutions. The weight of water includes the water from the dissolved lactose, as lactose monohydrate was dissolved. The ratio of the standard deviation and the mean of the mass fractions was here always less than 0.62 %.

Hydrates were used for sample preparation. Upon solution, these hydrates release water, which has been considered explicitly in the calibration of the HPLC and the compositions of the stock solutions containing $CaCl_2$. In the liquid phase at equilibrium, lactose is likely to be present in several forms depending on temperature and solvent composition, e.g, some of the α-lactose might have converted into β-lactose [70]. We do not differentiate between these forms and report the overall, effective solubility. The solid phase was not analyzed.

5.3 Modeling

5.3.1 Phase Equilibrium and Activity Coefficient

Here, activity-based models are used to describe the solubility of lactose. The activity a_k of a non-electrolyte component k is normalized with respect to the pure liquid according to Raoult (cf. Eq. (2)). Following Machado et al. [70] and Held et al. [73], we assumed that the solid in the solid-liquid equilibrium is pure lactose. The difference of the heat capacities of lactose in the solid and liquid state was neglected, leading to the following phase equilibrium condition (see [72] for the derivation).

$$\ln(x_{\text{lactose}}\gamma_{\text{lactose}}) = -\frac{\Delta h^{\text{f}}_{\text{lactose}}}{RT^{\text{f}}_{\text{lactose}}}\left(\frac{T^{\text{f}}_{\text{lactose}}}{T} - 1\right) \tag{62}$$

Therein, $\Delta h^{\text{f}}_{\text{lactose}}$ is the enthalpy of fusion of lactose and $T^{\text{f}}_{\text{lactose}}$ is the melting temperature of lactose. The values used for $\Delta h^{\text{f}}_{\text{lactose}}$ = 66416.39 J/mol and $T^{\text{f}}_{\text{lactose}}$ = 498.027 K were obtained from Held et al. [73] who have fitted former on to experimental solubility data of lactose at 298.15 K in water. While other sources, e.g. Machado et al. [70], are available, we chose the values from Held et al. [73] since they gave the best modeling results.

The concentrations of the salts were chosen well below their respective solubility in the water-ethanol system. Thus, we assumed that the salts neither precipitate not form peritectic compounds with the lactose.

To calculate the activity coefficient of lactose needed in Eq. (62) different models can be used. Here, the activity models are based on the UNIQUAC model proposed by Abrams and Prausnitz [10]. There, the equation to calculate the activity coefficient γ_k of a component k consists of a combinatorial term γ_k^{C} and a residual term γ_k^{R} (cf. Section 2.3). The UNIQUAC model is designed for organic or aqueous-organic mixtures. To cope with electrolytes, the UNIQUAC model must be modified. In the following, two approaches (UNIQUAC-DH and UNIQUAC-PS) for extending the UNIQUAC model to aqueous-organic-electrolyte mixtures are described. Later, both approaches are used for modeling the experimental data of the present, which also reveals the advantages and disadvantages of the two approaches.

5.3.2 UNIQUAC-Debye-Hückel (DH) Model

In the UNIQUAC-DH model proposed by Sander et al. [65] for organic-electrolyte mixtures, two main modifications are made to the UNIQUAC model. First, Eq. (46) for the residual term γ_k^{R} is modified as follows:

$$\begin{aligned} \ln \gamma_k^{\mathrm{R}} = q_k \left(1 - \ln\left(\sum_n \theta_n \Psi_{nk}\right) - \sum_l \frac{\theta_l \Psi_{kl}}{\sum_n \theta_n \Psi_{nl}}\right) \\ -\frac{2q_k}{T} \sum_i \sum_m \theta_i^2 \theta_m \sum_{j \neq i} \delta_{ij,m} \theta_j \cdot \left(\frac{\Psi_{mi}}{\sum_n \theta_n \Psi_{ni}} + \frac{\Psi_{im}}{\sum_n \theta_n \Psi_{nm}}\right). \end{aligned} \tag{63}$$

For the interaction parameters u_{im} between the ion i and the solvent m, an addition concentration dependency is introduced:

$$u_{im} = u_{im}^* + \theta_i \sum_{j \neq i} \delta_{ij,m} \theta_j \tag{64}$$

and

$$u_{mi} = u_{mi}^* + \theta_i \sum_{j \neq i} \delta_{ij,m} \theta_j, \tag{65}$$

where u_{im}^* and u_{mi}^* are reference interaction parameters. The parameter $\delta_{ij,m}$ is an additional parameter that describes interactions between the ions i and j and the solvent m. It is assumed that $\delta_{ij,m} = \delta_{ji,m}$. The summation is over all ionic species, except i.

Second, an additional Debye-Hückel term γ_k^{DH} is added to Eq. (42):

$$\ln \gamma_k = \ln \gamma_k^{\mathrm{C}} + \ln \gamma_k^{\mathrm{R}} + \ln \gamma_k^{\mathrm{DH}}. \tag{66}$$

The Debye-Hückel term is as follows:

$$\ln \gamma_i^{\mathrm{DH}} = \frac{M_i}{B_0} \frac{2A_m}{{b_m}^3} \left(1 + b_m \sqrt{I_m} - \frac{1}{1 + b_m \sqrt{I_m}} - 2 \ln \left(1 + b_m \sqrt{I_m} \right) \right) \tag{67}$$

where M_i is the molar mass of ion i. The parameters A and b are set to the fixed values A_m = 2.0 and b_m = 1.5 as suggested by Sander et al. [65]. The ionic strength I_m is calculated by

$$I_m = \frac{1}{2} \sum_i \frac{b_i}{b_0} z_i^2, \tag{68}$$

where b_i is the molality of the ion i and z_i is the charge number of the ion i. The constants b_0 and B_0 are defined as 1 mol kg^{-1} and 1 kg mol^{-1}, respectively. For salt-free mixture the Debye-Hückel term disappears and the model proposed by Sander et al. [65] reduces to the usual UNIQUAC equation proposed by Abrams and Prausnitz [10].

5.3.3 UNIQUAC-Perturbation Scheme (PS) Model

The second model used here to calculate the solubility of lactose is based on the perturbation scheme where a poorly specified mixture is hypothetically divided into two parts as described in Chapter 2: the *specified subsystem*, comprised of all specified and known components, and the remaining *unknown part* of the mixture. Here, this idea is transfered to the studied systems of this chapter. Although there are no truly unknown components in the studied systems, the mixtures can be regarded as consisting of two parts: water, ethanol and lactose comprise the *specified subsystem*, and the electrolyte (either NaCl or $CaCl_2$) is regarded as the *unknown part*. Separating the components in these two categories allows to treat the specified subsystem with the standard UNIQUAC model, while describing the influence of the electrolyte via the perturbation scheme (PS). Hence, in this way, the perturbation scheme constitutes a simple possibility for extending UNIQUAC to electrolytes. The activity coefficients and mole fractions in the specified subsystem are perturbed to cover the influence of the electrolyte part and to yield their respective counterpart in the complete mixture. The structure and the terms of the perturbation scheme are the same as described in Chapter 2. All symbols which refer to properties of the conceptually isolated specified subsystem are denoted with a tilde (~) over the symbol in the following. For the mole fraction of the component k of the specified subsystem, it holds

$$x_k = \tilde{x}_k \cdot x_k^{\mathrm{p}} = \tilde{x}_k \cdot (1 - x_{\mathrm{e}}), \tag{69}$$

where x_k^{p} is the colligative perturbation term of the mole fraction of component k, x_{e} is the cumulative mole fraction of all electrolyte components of the complete mixture.

The activity coefficient is perturbed in similar way. For a non-electrolyte component k of the specified subsystem the equation for the activity coefficient γ_k is (cf. Eq. (7)):

$$\gamma_k = \tilde{\gamma}_k \cdot \gamma_k^{\mathrm{p}}. \tag{70}$$

The activity coefficient $\tilde{\gamma}_k$ for the non-electrolyte component k of the specified subsystem is obtained directly from the usual UNIQUAC model using the mole fractions within the subsystem $\tilde{\mathbf{x}}$. The perturbation term γ_k^{p} has to capture the molecular interactions introduced by the electrolyte components. We use the term derived in Chapter 2.2:

$$\ln \gamma_k^{\mathrm{p}} = \ln \tilde{\gamma}_k \left(\frac{(1-x_{\mathrm{e}})^2 (1-x_k)}{1-x_{\mathrm{e}}-x_k} - 1 \right) + \frac{x_{\mathrm{e}}}{RT} \left(A_{k\mathrm{e}} - \sum_{i=1}^{N_s} A_{i\mathrm{e}} x_i \right), \tag{71}$$

where $A_{k\mathrm{e}}$ is the binary interaction parameter of the non-electrolyte component k with the electrolyte part e. There is one interaction parameter for every component of the specified subsystem. These interaction parameters are fitted to experimental data of the complete mixture. The term $\ln \gamma_k^{\mathrm{p}}$ disappears for negligible mole fractions of the electrolyte part, i.e. $\gamma_k^{\mathrm{p}} \to 1$ for $x_{\mathrm{e}} \to 0$.

5.3.4 Parameter Estimation

The geometric parameters for the volume r_k and the surface-area q_k are the same for both models of the non-electrolyte components. For the UNIQUAC-DH model, geometric parameters for all components are needed, whereas for the UNIQUAC-PS model no additional geometric parameters for the electrolyte components are needed. As Achard et al. [115] report, solvation effects might lead to non-constant geometric parameters for aqueous electrolyte systems. However, we opted to keep the model simple with constant geometric parameters that can be adopted from the literature. Possible deviations caused by solvation effects are effectively captured by the interaction parameters in the fitting procedure. The numerical values of all geometric parameters were taken from the literature [65, 70] and are given in Table 8.

Also the binary interaction parameters u_{kl} of the UNIQUAC model or reference interaction parameters u_{im}^* of UNIQUAC-DH model are needed. Table 9 gives the numerical values of all interaction parameters used here. The numerical values were partly taken from the literature and partly determined by fitting to experimental data of the present

Table 8: Surface-area parameter q_k and volume parameter r_k parameters of the UNIQUAC model for the components lactose, water, ethanol, Na^+, Ca^{2+}, and Cl^-. The gray marked parameters are used in both models, the remaining parameters only in the UNIQUAC-DH model.

Component k	q_k	r_k	Ref.
lactose	12.2280	12.5265	[70]
water	1.400	0.9200	[65]
ethanol	1.9720	2.1055	[65]
Na^+	3.0	3.0	[65]
Ca^{2+}	1.0	1.0	[65]
Cl^-	0.9917	0.9861	[65]

Table 9: Binary interaction parameters u_{kl} / K and binary reference interaction parameter u^*_{im} / K of the UNIQUAC-DH model and the UNIQUAC-PS model. The gray marked parameters are used in both models, the remaining parameters only in the UNIQUAC-DH model.

	Component l					
Component k	lactose	water	ethanol	Na^+	Ca^{2+}	Cl^-
lactose	0	–319.111[a]	2433.249[a]	–314.501[a]	–1428.630[a]	–639.282[a]
water	493.914[a]	0	162.4[b]	330.6[b]	–956.9[b]	–190.2[b]
ethanol	101.936[a]	–14.5[b]	0	116.9[b]	–386.8[b]	374.8[b]
Na^+	378.022[a]	–209.4[b]	86.0[b]	0	–	76.2[b]
Ca^{2+}	–583.336[a]	–593.7[b]	735.9[b]	–	0	0[b]
Cl^-	–24.811[a]	–524.9[b]	901.2[b]	–11.2[b]	0[b]	0

Ref.: a: present work, b: [65]

work (cf. Table 12) and from the literature [65].

The interaction parameters for the non-electrolyte components are the same for the UNIQUAC-DH and the UNIQUAC-PS model and are marked gray. The remaining interaction parameters for the electrolyte components are needed only in the UNIQUAC-DH model. The interaction parameters for lactose were not available in the literature and were thus fitted to experimental data from the literature and to experimental data of the present work. First, the interaction parameters $u_{\text{water,lactose}}$ and $u_{\text{lactose,water}}$ were determined by using experimental literature data and own experimental data of the solubility of lactose in pure water at several temperatures [70, 102]. The data points used for the fit are shown in Appendix C. Second, the interaction parameters $u_{\text{ethanol,lactose}}$

and $u_{\text{lactose,ethanol}}$ were determined using own experimental data of the solubility of lactose in mixed water-ethanol solvents. The data points used for this fit are also shown in Appendix C. In the fits, the solvent's composition and the temperature were specified while the estimated parameters were varied to minimize the sum of least square deviations in the experimental vs. calculated solubilities. Figure 30 and Figure 31 in Appendix C show that the results from the UNIQUAC model agree very well with the experimental data for the solubility of lactose in pure water at different temperatures and in mixed water-ethanol solvents [70, 102]. Lastly, the six reference interaction parameters of lactose and the three ions Na^+, Ca^{2+}, and Cl^- that are necessary for the UNIQUAC-DH model, were determined by using the experimental data for the solubility of lactose in mixed organic-electrolyte solvents of the present work (cf. Table 12). In all cases, the deviation between the experimental solubility of lactose and the one obtained from the model was minimized with a nonlinear least-square solver.

UNIQUAC-DH additionally requires the parameters $\delta_{ij,m}$. The parameters were taken from Sander et al. for water, ethanol, and the electrolytes Na^+, Ca^{2+}, and Cl^- [65]. The respective parameters $\delta_{ij,\text{lactose}}$ for lactose were assumed to be 0. Table 10 gives the numerical values of the parameters $\delta_{ij,m}$.

Table 10: Parameter $\delta_{ij,m}$ / K ($\delta_{ij,m} = \delta_{ji,m}$) of the UNIQUAC-DH model [65].

	m: water	m: ethanol
i	j: Cl^-	j: Cl^-
Na^+	185	63557
Ca^{2+}	10946	1163

For the UNIQUAC-PS model, the additional interaction parameters A_{ke} were determined by using the experimental data for the solubility of lactose in mixed organic-electrolyte solvents of the present work (cf. Table 12). The numerical values of all interaction parameters A_{ke} are given in Table 11.

Table 11: Interaction parameters A_{ke} of the UNIQUAC-PS model.

k	$A_{k\text{NaCl}}$ / kJ mol^{-1}	$A_{k\text{CaCl}_2}$ / kJ mol^{-1}
lactose	−190.147	−206.803
water	−191.070	−205.809
ethanol	22.880	−35.557

5.4 Results and Discussion

The experimental results of the lactose solubility are given in Table 12. Therein, the mass fractions of ethanol and the salts are given in a reduced form, i.e. if all other components but water are removed:

$$\hat{w}_i = \frac{w_i}{w_i + w_{\text{water}}}, \tag{72}$$

wherein w_i denotes the mass fraction of component i in the liquid phase. Since lactose monohydrate was used in the preparation of the experiments, the reported composition of the liquid phase includes the mass of water stemming from the dissolved monohydrate. It cannot be ruled out that the excess solid also loses water into the liquid solution. However, even in the worst case assuming all water is released from the solid excess, the reported values of $\hat{w}_{\text{ethanol}}$ and $\hat{w}_{\text{salt}}$ in Table 12 would never change by more than 0.85% (relative to the reported value).

As shown in Appendix C, the solubility data of lactose in water-ethanol mixtures obtained in the present work agree well with literature data [70, 102]. The solubility of lactose decreases with an increase of the ethanol mass fraction in all cases.

Figure 29 shows the experimental results as well as the results from the UNIQUAC-DH model and the UNIQUAC-PS model. In the top panel the mixed organic-electrolyte solvent comprises water, ethanol, and NaCl. In the bottom panel the solvent comprises water, ethanol, and $CaCl_2$. Because the differences in the experimental points are barely discernible when plotted on an absolute scale, the solubility of lactose obtained from the models is plotted normalized to the solubility of lactose in the respective electrolyte-free subsystem (water-ethanol) as calculated by the UNIQUAC model. The experimental data points are also normalized to the respective data point in the salt-free water-ethanol system. The dotted lines indicate the results obtained from the UNIQUAC-DH model. The dashed lines indicate the results obtained from the UNIQUAC-PS model. The use of the normalized solubility emphasizes the influence of the salts on the solubility of lactose in the water-ethanol-salt mixtures. Both NaCl and $CaCl_2$ affect the solubility of lactose. For low ethanol contents, the solubility of lactose decreases when salt is added. By contrast, for high ethanol contents, the solubility of lactose increases when salt is added. This effect is stronger in the system with NaCl compared to the system with $CaCl_2$. The reduction of solubility at low ethanol contents (or in pure water) can be explained as follows: the water needed for the solvation of ions is no longer available for the solvation of lactose. We have no simple explanation for the increase of solubility at high ethanol contents. The cause might be a complex interplay of different types

Table 12: Experimental data of α-lactose solubility in water-ethanol, water-ethanol-NaCl and water-ethanol-$CaCl_2$ mixtures at 298.15 K and 101.3 kPa [a]. w_{lactose} is the mass fraction of lactose in the liquid and s the standard deviation. $\hat{w}_i = w_i/(w_i + w_{\text{water}})$.

100 $\hat{w}_{\text{ethanol}}$ / g g^{-1}	100 $\hat{w}_{\text{NaCl}}$ / g g^{-1}	100 $\hat{w}_{\text{CaCl}_2}$ / g g^{-1}	100 w_{lactose} / g g^{-1}	100 s / g g^{-1}
0.00			18.00	0.012
9.81			13.22	0.046
19.00			8.76	0.071
29.89			5.32	0.103
39.76			3.18	0.041
0.00	2.44		17.18	0.058
9.91	2.45		12.89	0.151
19.45	2.45		8.82	0.061
29.91	2.46		5.70	0.063
39.74	2.46		3.58	0.031
0.00	4.80		16.82	0.033
10.02	4.81		12.99	0.125
19.36	4.82		9.38	0.054
29.84	4.83		6.26	0.070
39.82	4.84		4.07	0.039
0.00	9.30		16.21	0.059
10.10	9.31		13.35	0.138
19.60	9.33		10.30	0.054
30.41	9.34		7.40	0.028
40.24	9.35		5.08	0.050
0.00		2.45	17.02	0.103
9.96		2.45	12.60	0.055
19.13		2.46	8.64	0.082
29.90		2.46	5.36	0.061
39.65		2.47	3.33	0.040
0.00		4.83	16.81	0.060
9.96		4.84	12.57	0.060
19.25		4.85	8.79	0.041
30.00		4.86	5.63	0.038
39.80		4.86	3.57	0.047
0.00		9.39	16.39	0.170
10.18		9.41	12.76	0.120
19.68		9.42	9.26	0.053
30.52		9.44	6.15	0.064
40.69		9.45	3.97	0.082

[a] Standard uncertainties u are $u(T) = 0.20$ K, and $u(p) = 2$ kPa and the relative standard uncertainties u_r are $u_r(w_{\text{lactose}}) = 0.019$, $u_r(\hat{w}_{\text{ethanol}}) = 0.011$, $u_r(\hat{w}_{\text{NaCl}}) = 0.011$, and $u_r(\hat{w}_{\text{CaCl}_2}) = 0.019$. The uncertainties are derived in detail in Appendix C.

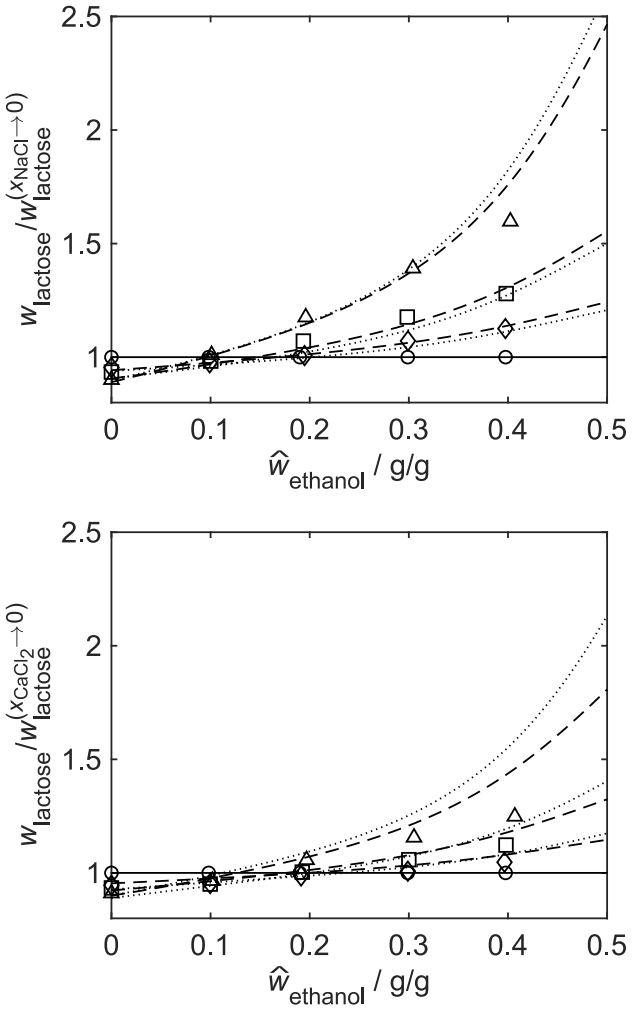

Figure 29: Experimental solubility data (symbols) and results of the models (lines) for lactose at 298.15 K. The solubility w_{lactose} of lactose obtained from the experiments and from the models is normalized to its respective value $w_{\text{lactose}}^{(x_{\text{salt}}\to 0)}$ in the electrolyte-free system and is plotted over the mass fraction of ethanol $\hat{w}_{\text{ethanol}}$ in the mixture if all other components but water are removed (top panel: NaCl; bottom panel: $CaCl_2$). The different types of symbols indicate different mass fractions of the salts, the dotted lines indicate the respective result from the UNIQUAC-DH model, and the dashed lines the respective result from the UNIQUAC-PS model (top panel: $\hat{w}_{\text{NaCl}}$ = 0.00 g/g (∘, —), $\hat{w}_{\text{NaCl}}$ = 0.0245 g/g (◊, −−, ⋯), $\hat{w}_{\text{NaCl}}$ = 0.0482 g/g (□, −−, ⋯), $\hat{w}_{\text{NaCl}}$ = 0.0933 g/g (△, −−, ⋯); bottom panel: $\hat{w}_{\text{CaCl}_2}$ = 0.00 g/g (∘, —), $\hat{w}_{\text{CaCl}_2}$ = 0.0246 g/g (◊, −−, ⋯), $\hat{w}_{\text{CaCl}_2}$ = 0.0485 g/g (□, −−, ⋯), $\hat{w}_{\text{CaCl}_2}$ = 0.0943 g/g (△, −−, ⋯)).

of molecular interactions. Molecular simulations could provide a means to explore this behavior in detail and possibly provide an explanation.

In both cases, the UNIQUAC-DH and the UNIQUAC-PS model describe the deviation in the solubility of lactose caused by the respective salt well. However, for high ethanol amounts in the mixtures with salts the deviation between the experimental data and the results from both models increase. This effect is very similar for the UNIQUAC-PS and UNIQUAC-DH model for the system with NaCl and slightly stronger in the UNIQUAC-DH model for the system with $CaCl_2$. The deviation between the experimental data and the results from both models for high ethanol amounts is not too surprising since the agreement between the experimental data and the results from the usual UNIQUAC model for the solubility of lactose in the water-ethanol-lactose system is also low for hight ethanol amounts (cf. Appendix C).

To model the solubility of lactose in a water-ethanol-NaCl mixture, 33 (10 geometric / 20 interaction / 3 DH) model parameters are necessary for the UNIQUAC-DH model. If the salt NaCl is replaced by the salt $CaCl_2$ in this system, 13 (2 geometric / 8 interaction / 3 DH) model parameters must be replaced. To model the solubility of lactose in a water-ethanol-NaCl mixture with the UNIQUAC-PS model, only 15 (6 geometric / 6 interaction / 3 PS) parameters are necessary and only 3 (0 geometric / 0 interaction / 3 PS) model parameters must be replaced if the salt is $CaCl_2$ instead.

This demonstrates the significantly smaller effort to set up the perturbation model (UNIQUAC-PS). This is possible because of the empirical way the electrolytes are treated: they are treated as non-specific components and not divided into ions. Using such an approach it is also straightforward to model unknown electrolytes, unknown organic components or even unknown mixture parts consisting of several components.

The drawback of the approach is its limited extrapolation capability. This is discussed in more detail using the following example: the vapor-liquid equilibrium in the systems water-ethanol-NaCl/$CaCl_2$ can also be described using the UNIQUAC-DH or UNIQUAC-PS models. That the UNIQUAC-DH model describes the vapor-liquid equilibrium very well was already shown by Sander et al. [65]. The good agreement of the UNIQUAC model with experimental data in the mentioned systems is not surprising since these experimental data were used to determine the respective model parameters. By contrast, the predictability by the UNIQUAC-PS model is poor. This is also not surprising since no information of the vapor-liquid equilibrium is used to determine the interaction parameters A_{ke}.

Both models can be used in practice for the description of precipitation processes of lactose and a corresponding process design and simulation. While the UNIQUAC-

DH model is expected to have a better extrapolation behavior to other types of data beyond the solubility (e.g., for evaporation of such mixtures), the UNIQUAC-PS model is slightly more accurate and can be readjusted more easily, if more data become available.

5.5 Conclusion

Reliable experimental data and viable thermodynamic models that can predict the properties of sugar solutions play an important role in the industry. This work provides experimental data of the solubility of α-lactose in solutions of water-ethanol-NaCl and water-ethanol-$CaCl_2$ at 298.15 K. For low ethanol contents, the salts decrease lactose solubility, whereas the salts increase lactose solubility for high ethanol contents. This effect is stronger for NaCl compared to $CaCl_2$. Two different models (UNIQUAC extended by a Debye-Hückel term (DH) and UNIQUAC extended by a perturbation scheme (PS)) are successfully used to correlate the experimental data. On the one hand, the UNIQAC-DH model has a larger number of model parameters, so it needs many data for parametrization and has some extrapolation abilities. On the other hand, the UNIQUAC-PS model is a simpler model with significantly fewer parameters. It has its strength when only a small number of experimental data is available, or parts of the mixture are unknown.

6 Conclusion

Poorly specified liquid mixtures containing one or more specified components besides many unknown components, and liquid mixtures with complex composition regularly appear in the process industry. Modeling and predicting the thermodynamic properties of the components of main interest in such liquid mixtures is often challenging. However, reliable thermodynamic models are a prerequisite for process design or optimization. In the present work, several poorly specified liquid mixtures and mixtures with a complex composition were studied, and a novel approach for modeling the activity of the specified components of main interest was developed. The idea of this novel approach - called perturbation scheme - is to divide a poorly specified mixture hypothetically into two parts: the *specified subsystem*, comprised of all specified and known components, and the remaining *unknown part* of the mixture. The specified subsystem can be modeled using well-known models. The perturbation terms cover the influence of the unknown part on the specified components. The idea of the perturbation scheme can also be transferred to fully specified liquid mixtures with complex composition, e.g. liquid mixtures comprised of organic and electrolyte components can be divided into two parts: a) all organic components, b) all electrolyte components. Separating the components in these two categories allows treating the part with all organic components with a standard activity model while describing the influence of the electrolyte via the perturbation scheme.

One general aspect of the perturbation scheme that should be kept in mind is that the applicability relies on the prerequisite that the composition and constitution (e.g. state of complexation, degree of dissociation) of the unknown part does not change during application. This prerequisite involves that the unknown part remains as a whole in the one liquid phase of interest. Most likely, this leads to significant limitations when liquid-liquid equilibria or vapor-liquid equilibria with volatile unknown components are studied. When studying solid-liquid equilibria, e.g. in crystallization or precipitation of a specified component, these constraints on the unknown part might, however, be well met.

However, under this restriction, the perturbation scheme shows very promising results. The perturbation scheme takes good thermodynamic models of the subsystem of specified components, which are often available, and applies a perturbation term to consider

the impact of the unknown part of the mixture on the specified components. The perturbation scheme can be combined with different thermodynamic models. Thus it has high flexibility. This flexibility was shown by combining it with different g^{E}-models for non-electrolyte and aqueous-electrolyte systems. However, the suggested perturbation terms can also be combined with equations of state. The perturbation scheme has only a few parameters that must be fitted to experimental data. The parameters are the average molar mass of the unknown part and one interaction parameter for each specified component with the unknown part. However, the results of the present work show that the average molar mass of the unknown part is not system-specific for aqueous systems. The value 50 g/mol showed promising results for all considered aqueous example systems. The interaction parameters must be fitted to few experimental data for the specified components' activities in the poorly specified mixture. No analysis of the unknown part is necessary. The approach was successfully applied to several examples based on pseudo-experimental and real experimental data. Poorly specified organic mixtures, aqueous-organic mixtures as well as aqueous-electrolyte mixtures were studied. When using the perturbation scheme, one obtains a model of the activities of all specified components within a poorly specified mixture. As long as the composition and constitution of the unknown part remain unchanged, this model can predict the activities well, even if the composition of the specified components changes or the unknown components have a tremendous influence on the thermodynamic properties of the mixture, such as the disappearance of azeotropes. The results further indicate that the approach can predict the behavior of poorly specified mixtures that result from mixing two different poorly specified mixtures for which perturbation models are available.

In addition to modeling thermodynamic properties, the perturbation scheme can also be used in process simulation. A general workflow is presented to handle poorly specified liquid mixtures in process simulations. The workflow is combined with the perturbation scheme and applied to three example processes. Promising results were obtained with these process simulations. The example processes show that extrapolation to other conditions, e.g. change in temperature, pressure, or composition of the specified components, can be possible. Further, the chosen example processes show that the workflow combined with the perturbation scheme can be applied to different processes or, rather, phase equilibria. A crystallization process (solid-liquid equilibrium) and two evaporation processes (vapor-liquid equilibrium) were studied.

Besides modeling poorly specified mixtures, the perturbation scheme can also be used to model liquid mixtures with complex compositions. Therefore, the approach is used to model the solubility of lactose in aqueous-organic-electrolyte mixtures. The results obtained from the perturbation scheme are compared with the results obtained from

a common model for aqueous-organic-electrolyte mixtures. Reliable experimental data and viable thermodynamic models that allow for new experimental data of the solubility of α-lactose in solutions of water-ethanol-NaCl and water-ethanol-$CaCl_2$ at 298.15 K were measured. For low ethanol contents, the salts decrease lactose solubility, whereas the salts increase lactose solubility for high ethanol contents. This effect is stronger for NaCl compared to $CaCl_2$. Two different models are successfully used to correlate the experimental data. Both models are based on the UNIQUAC model: UNIQUAC model extended with a Debye-Hückel term (UNIQAC-DH) and UNIQUAC model extended with the perturbation scheme (UNIQAC-PS) of the present work. On the one hand, the UNIQAC-DH model has more model parameters than the UNIQUAC-PS model. Consequently, many data for parametrization are needed. However, it has some extrapolation abilities. On the other hand, the UNIQUAC-PS model is a simpler model with significantly fewer parameters. Therefore, it has its strength when only a small number of experimental data is available or parts of the mixture are unknown.

Literature

[1] C. A. Hughey, R. P. Rodgers, A. G. Marshall: Resolution of 11 000 Compositionally Distinct Components in a Single Electrospray Ionization Fourier Transform Ion Cyclotron Resonance Mass Spectrum of Crude Oil, Analytical Chemistry 74 (2002) 4145–4149.

[2] E. Forte, S. E. Taylor: Thermodynamic modelling of asphaltene precipitation and related phenomena, Advances in Colloid and Interface Science 217 (2015) 1–12.

[3] P. H. Nielsen, K. Raunkjær, N. H. Norsker, N. A. Jensen, T. Hvitved-Jacobsen: Transformation of Wastewater in Sewer Systems – A Review, Water Science and Technology 25 (1992) 17–31.

[4] A. Guellil, F. Thomas, J.-C. Block, J.-L. Bersillon, P. Ginestet: Transfer of organic matter between wastewater and activated sludge flocs, Water Research 35 (2001) 143–150.

[5] R. G. Harrison, P. Todd, S. R. Rudge, D. P. Petrides: Bioseparations science and engineering, second edition ed., Oxford University Press, Oxford, 2015.

[6] F. Jirasek, J. Burger, H. Hasse: Application of NEAT for determining the composition dependence of activity coefficients in poorly specified mixtures, Chemical Engineering Science 208 (2019) 115161.

[7] P. M. Mathias: 110th Anniversary : A Case Study on Developing Accurate and Reliable Excess Gibbs Energy Correlations for Industrial Application, Industrial & Engineering Chemistry Research 58 (2019) 12465–12477.

[8] G. M. Kontogeorgis, X. Liang, A. Arya, I. Tsivintzelis: Equations of state in three centuries. Are we closer to arriving to a single model for all applications?, Chemical Engineering Science: X 7 (2020) 100060.

[9] H. Renon, J. M. Prausnitz: Local compositions in thermodynamic excess functions for liquid mixtures, AIChE Journal 14 (1968) 135–144.

[10] D. S. Abrams, J. M. Prausnitz: Statistical thermodynamics of liquid mixtures: A new expression for the excess Gibbs energy of partly or completely miscible systems, AIChE Journal 21 (1975) 116–128.

[11] H. Haghighi, A. Chapoy, B. Tohidi: Freezing Point Depression of Electrolyte Solutions: Experimental Measurements and Modeling Using the Cubic-Plus-Association Equation of State, Industrial & Engineering Chemistry Research 47 (2008) 3983–3989.

[12] D. L. Hall, S. M. Sterner, R. J. Bodnar: Freezing point depression of NaCl-KCl-H2O solutions, Economic Geology 83 (1988) 197–202.

[13] R. W. Potter, M. A. Clynne, D. L. Brown: Freezing point depression of aqueous sodium chloride solutions, Economic Geology 73 (1978) 284–285.

[14] F. P. Chinard: Colligative properties, Journal of Chemical Education 32 (1955) 377–380.

[15] H. Gehlen: Über die Ableitung der Gesetzmässigkeiten ideal verdünnter Lösungen, Zeitschrift für Elektrochemie und angewandte physikalische Chemie 48 (1942) 110–112.

[16] A. G. Abdul Jameel, A. M. Elbaz, A.-H. Emwas, W. L. Roberts, S. M. Sarathy: Calculation of Average Molecular Parameters, Functional Groups, and a Surrogate Molecule for Heavy Fuel Oils Using 1 H and 13 C Nuclear Magnetic Resonance Spectroscopy, Energy & Fuels 30 (2016) 3894–3905.

[17] G. L. Alexander, A. L. Creagh, J. M. Prausnitz: Phase equilibriums for high-boiling fossil fuel distillates. 1. Characterization, Industrial & Engineering Chemistry Fundamentals 24 (1985) 301–310.

[18] G. L. Alexander, B. J. Schwarz, J. M. Prausnitz: Phase equilibriums for high-boiling fossil fuel distillates. 2. Correlation of equation-of-state constants with characterization data for phase equilibrium calculations, Industrial & Engineering Chemistry Fundamentals 24 (1985) 311–315.

[19] D. L. Katz, G. G. Brown: Vapor Pressure and Vaporization of Petroleum Fractions, Ind. Eng. Chem. 25 (1933) 1373–1384.

[20] B. Carreón-Calderón, V. Uribe-Vargas, E. Ramírez-Jaramillo, M. Ramírez-de Santiago: Thermodynamic Characterization of Undefined Petroleum Fractions using Group Contribution Methods, Industrial & Engineering Chemistry Research 51 (2012) 14188–14198.

[21] E. Darwish, T. Al-Sahhaf, M. Fahim: Prediciton of the Surface Tension of Petroleum Cuts Using a Modified UNIFAC Group Contribution Method, Fluid Phase Equilibria 105 (1995) 229–239.

[22] M. A. Fahim, A. S. Elkilani: Prediction of solubility of hydrogen in petroleum cuts using modified unifac, The Canadian Journal of Chemical Engineering 70 (1992) 335–340.

[23] H. Hartounian, D. T. Allen: Group contribution methods for coal-derived liquids: hydrogen solubilities using a UNIFAC approach, Fuel 67 (1988) 1609–1614.

[24] L. Sun, H. Zhao, C. McCabe: Predicting the phase equilibria of petroleum fluids with the SAFT-VR approach, AIChE Journal 53 (2007) 720–731.

[25] L.-S. Wang, J. Gmehling: Improvement of SRK equation of state for vapor-liquid equilibria of petroleum fluids, AIChE Journal 45 (1999) 1125–1134.

[26] Z. Li, A. Firoozabadi: Cubic-Plus-Association Equation of State for Asphaltene Precipitation in Live Oils, Energy & Fuels 24 (2010) 2956–2963.

[27] Z. Li, A. Firoozabadi: Modeling Asphaltene Precipitation by n-Alkanes from Heavy Oils and Bitumens Using Cubic-Plus-Association Equation of State, Energy & Fuels 24 (2010) 1106–1113.

[28] O. Sabbagh, K. Akbarzadeh, A. Badamchi-Zadeh, W. Y. Svrcek, H. W. Yarranton: Applying the PR-EoS to Asphaltene Precipitation from n-Alkane Diluted Heavy Oils and Bitumens, Energy & Fuels 20 (2006) 625–634.

[29] B. Shirani, M. Nikazar, S. A. Mousavi-Dehghani: Prediction of asphaltene phase behavior in live oil with CPA equation of state, Fuel 97 (2012) 89–96.

[30] X. Zhang, N. Pedrosa, T. Moorwood: Modeling Asphaltene Phase Behavior: Comparison of Methods for Flow Assurance Studies, Energy & Fuels 26 (2012) 2611–2620.

[31] E. Behar, P. Mougin, A. Pina: Integration of Asphaltenes Flocculation Modeling Into Athos Reservoir Simulator, Oil & Gas Science and Technology 58 (2003) 637–646.

[32] Z. Du, C. Li, W. Sun, J. Wang: A simulation of diesel hydrotreating process with real component method, Chinese Journal of Chemical Engineering 23 (2015) 780–788.

[33] E. Eckert, T. Vaněk: New approach to the characterisation of petroleum mixtures used in the modelling of separation processes, Computers & Chemical Engineering 30 (2005) 343–356.

[34] Y. Huang, J. Feng, C.-H. Liang, P. Huang, X.-W. Zhang, Q. Xie, W.-Y. Li: Co-production of Naphthenic Oil and Phenolic Compounds from Medium- and Low-Temperature Coal Tar, Industrial & Engineering Chemistry Research 60 (2021) 5890–5902.

[35] M. Cocero, E. Alonso, M. Sanz, F. Fdz-Polanco: Supercritical water oxidation process under energetically self-sufficient operation, The Journal of Supercritical Fluids 24 (2002) 37–46.

[36] E. Lavric, H. Weyten, J. De Ruyck, V. Pleşu, V. Lavric: Delocalized organic pollutant destruction through a self-sustaining supercritical water oxidation process, Energy Conversion and Management 46 (2005) 1345–1364.

[37] E. Forte, F. Jirasek, M. Bortz, J. Burger, J. Vrabec, H. Hasse: Digitalization in Thermodynamics, Chemie Ingenieur Technik 91 (2019) 201–214.

[38] F. Jirasek, J. Burger, H. Hasse: Method for Estimating Activity Coefficients of Target Components in Poorly Specified Mixtures, Industrial & Engineering Chemistry Research 57 (2018) 7310–7313.

[39] F. Jirasek, J. Burger, H. Hasse: NEAT - NMR Spectroscopy for the Estimation of Activity Coefficients of Target Components in Poorly Specified Mixtures, Industrial & Engineering Chemistry Research 58 (2019) 9155–9165.

[40] F. Jirasek, J. Burger, H. Hasse: Application of NEAT for the simulation of liquid–liquid extraction processes with poorly specified feeds, AIChE Journal 66 (2020).

[41] T. Specht, K. Münnemann, F. Jirasek, H. Hasse: Estimating activity coefficients of target components in poorly specified mixtures with NMR spectroscopy and COSMO-RS, Fluid Phase Equilibria 516 (2020) 112604.

[42] D. Constantinescu, J. Gmehling: Further Development of Modified UNIFAC (Dortmund): Revision and Extension 6, Journal of Chemical & Engineering Data 61 (2016) 2738–2748.

[43] U. Weidlich, J. Gmehling: A Modified UNIFAC Model. 1. Prediction of VLE, hE, and $\gamma\infty$, Industrial & Engineering Chemistry Research 26 (1987) 1372–1381.

[44] A. Klamt: Conductor-like Screening Model for Real Solvents: A New Approach to the Quantitative Calculation of Solvation Phenomena, The Journal of Physical Chemistry 99 (1995) 2224–2235.

[45] A. Klamt, V. Jonas, T. Bürger, J. C. W. Lohrenz: Refinement and Parametrization of COSMO-RS, The Journal of Physical Chemistry A 102 (1998) 5074–5085.

[46] H. Kehlen, M. T. Rätzsch, J. Bergmann: Continuous thermodynamics of multicomponent systems, AIChE Journal 31 (1985) 1136–1148.

[47] M. Rätzsch, H. Kehlen: Continuous thermodynamics of complex mixtures, Fluid Phase Equilibria 14 (1983) 225–234.

[48] M. T. Rätzsch, H. Kehlen: Continuous Thermodynamics of Polymer Solutions: The Effect of Polydispersity on the Liquid-Liquid Equilibrium, Journal of Macromolecular Science: Part A - Chemistry 22 (1985) 323–334.

[49] M. T. Rätzsch, H. Kehlen, D. Browarzik: Liquid-Liquid Equilibrium of Polydisperse Copolymer Solutions. Multivariate Distribution Functions in Continuous Thermodynamics, Journal of Macromolecular Science: Part A - Chemistry 22 (1985) 1679–1690.

[50] M. T. Rätzsch, C. Wohlfarth, D. Browarzik, H. Kehlen: Liquid-Liquid Equilibrium in Polydisperse Random Copolymer Blends, Journal of Macromolecular Science: Part A - Chemistry 26 (1989) 1497–1523.

[51] M. T. Rätzsch, S. Enders, L. Tschersich, H. Kehlen: Polymer Fractionation Calculations Using Refined Free Energy Relations, Journal of Macromolecular Science: Part A - Chemistry 28 (1991) 31–46.

[52] B. T. Willman, A. S. Teja: Continuous thermodynamics of phase equilibria using a multivariate distribution function and an equation of state, AIChE Journal 32 (1986) 2067–2078.

[53] A. H. Wu, J. M. Prausnitz: Fractionation of a polydisperse polymer using an antisolvent. Application of continuous thermodynamics, Journal of Applied Polymer Science 39 (1990) 629–637.

[54] A. Chamkalani, A. H. Mohammadi, A. Eslamimanesh, F. Gharagheizi, D. Richon: Diagnosis of asphaltene stability in crude oil through "two parameters" SVM model, Chemical Engineering Science 81 (2012) 202–208.

[55] A. Farasat, A. Shokrollahi, M. Arabloo, F. Gharagheizi, A. H. Mohammadi: Toward an intelligent approach for determination of saturation pressure of crude oil, Fuel Processing Technology 115 (2013) 201–214.

[56] A. Kamari, A. Khaksar-Manshad, F. Gharagheizi, A. H. Mohammadi, S. Ashoori: Robust Model for the Determination of Wax Deposition in Oil Systems, Industrial & Engineering Chemistry Research 52 (2013) 15664–15672.

[57] M. Li, X. Huang, H. Liu, B. Liu, Y. Wu, A. Xiong, T. Dong: Prediction of gas solubility in polymers by back propagation artificial neural network based on self-adaptive particle swarm optimization algorithm and chaos theory, Fluid Phase Equilibria 356 (2013) 11–17.

[58] L. C.-K. Liau, T. C.-K. Yang, M.-T. Tsai: Expert system of a crude oil distillation unit for process optimization using neural networks, Expert Systems with Applications 26 (2004) 247–255.

[59] S. Motlaghi, F. Jalali, M. N. Ahmadabadi: An expert system design for a crude oil distillation column with the neural networks model and the process optimization using genetic algorithm framework, Expert Systems with Applications 35 (2008) 1540–1545.

[60] S. Rafiee-Taghanaki, M. Arabloo, A. Chamkalani, M. Amani, M. H. Zargari, M. R. Adelzadeh: Implementation of SVM framework to estimate PVT properties of reservoir oil, Fluid Phase Equilibria 346 (2013) 25–32.

[61] J. Burger, N. Asprion, S. Blagov, M. Bortz: Simple Perturbation Scheme to Consider Uncertainty in Equations of State for the Use in Process Simulation, Journal of Chemical & Engineering Data 62 (2017) 268–274.

[62] P. M. Mathias: Sensitivity of Process Design to Phase Equilibrium - A New Perturbation Method Based Upon the Margules Equation, Journal of Chemical & Engineering Data 59 (2014) 1006–1015.

[63] P. M. Mathias: Effect of VLE uncertainties on the design of separation sequences by distillation - Study of the benzene-chloroform-acetone system, Fluid Phase Equilibria 408 (2016) 265–272.

[64] P. M. Mathias, J. P. Gilmartin: Quantitative Evaluation of the Effect of Uncertainty in Property Models on the Simulated Performance of Solvent-Based CO2-Capture, Energy Procedia 63 (2014) 1171–1185.

[65] B. Sander, A. Fredenslund, P. Rasmussen: Calculation of vapour-liquid equilibria in mixed solvent/salt systems using an extended UNIQUAC equation, Chemical Engineering Science 41 (1986) 1171–1183.

[66] M. Kohns, G. Lazarou, S. Kournopoulos, E. Forte, F. A. Perdomo, G. Jackson, C. S. Adjiman, A. Galindo: Predictive models for the phase behaviour and solution properties of weak electrolytes: nitric, sulphuric, and carbonic acids, Physical Chemistry Chemical Physics 22 (2020) 15248–15269.

[67] B. Mukhopadhyay, S. Basu, M. J. Holdaway: A discussion of Margules-type formulations for multicomponent solutions with a generalized approach, Geochimica et Cosmochimica Acta 57 (1993) 277–283.

[68] L. A. Bromley: Thermodynamic properties of strong electrolytes in aqueous solutions, AIChE Journal 19 (1973) 313–320.

[69] M. Luckas, J. Krissmann: Thermodynamik der Elektrolytlösungen: eine einheitliche Darstellung der Berechnung komplexer Gleichgewichte, Springer, Berlin, 2001.

[70] J. J. Machado, J. A. Coutinho, E. A. Macedo: Solid-liquid equilibrium of α-lactose in ethanol/water, Fluid Phase Equilibria 173 (2000) 121–134.

[71] W. Li, Y. Du, J. Li, X. Chen, S. Guo, T. Zhang: Isobaric vapor-liquid equilibrium for acetone + methanol system containing different ionic liquids at 101.3 kPa, Fluid Phase Equilibria 459 (2018) 10–17.

[72] J. M. Prausnitz, R. N. Lichtenthaler, E. Gomes de Azevedo: Molecular Thermodynamics of Fluid-Phase Equilibria, Pearson Education, 1998.

[73] C. Held, G. Sadowski, A. Carneiro, O. Rodríguez, E. A. Macedo: Modeling thermodynamic properties of aqueous single-solute and multi-solute sugar solutions with PC-SAFT, AIChE Journal 59 (2013) 4794–4805.

[74] D. C. Botía, D. C. Riveros, P. Ortiz, I. D. Gil, O. F. Sánchez: Vapor-Liquid Equilibrium in Extractive Distillation of the Acetone/Methanol System Using Water as Entrainer and Pressure Reduction, Ind. Eng. Chem. Res. 49 (2010) 6176–6183.

[75] S. P. Pinho, E. A. Macedo: Representation of salt solubility in mixed solvents: A comparison of thermodynamic models, Fluid Phase Equilibria 116 (1996) 209–216.

[76] S. P. Pinho, E. A. Macedo: Solubility of NaCl, NaBr, and KCl in Water, Methanol, Ethanol, and Their Mixed Solvents, Journal of Chemical & Engineering Data 50 (2005) 29–32.

[77] M. A. Clynne, R. W. Potter, J. L. Haas: Solubility of sodium chloride in aqueous electrolyte solutions from 10 to 100 °C, Journal of Chemical & Engineering Data 26 (1981) 396–398.

[78] M. R2017b: The MathWorks Inc., Technical Report, The MathWorks Inc., Natick, Massachusetts, 2017.

[79] J. Burger, E. Ströfer, H. Hasse: Process Design in World 3.0 - Challenges and Strategies to Master the Raw Material Change, Chemical Engineering & Technology 39 (2016) 219–224.

[80] M. Valdivia, J. L. Galan, J. Laffarga, J.-L. Ramos: Biofuels 2020: Biorefineries based on lignocellulosic materials, Microbial Biotechnology 9 (2016) 585–594.

[81] A. Limayem, S. C. Ricke: Lignocellulosic biomass for bioethanol production: Current perspectives, potential issues and future prospects, Progress in Energy and Combustion Science 38 (2012) 449–467.

[82] L. Olsson, B. Hahn-Hägerdal: Fermentation of lignocellulosic hydrolysates for ethanol production, Enzyme and Microbial Technology 18 (1996) 312–331.

[83] L. J. Jönsson, B. Alriksson, N.-O. Nilvebrant: Bioconversion of lignocellulose: inhibitors and detoxification, Biotechnology for Biofuels 6 (2013) 16.

[84] E. Palmqvist, B. Hahn-Hägerdal: Fermentation of lignocellulosic hydrolysates. I: inhibition and detoxification, Bioresource Technology 74 (2000) 17–24.

[85] N. Galeotti, F. Jirasek, J. Burger, H. Hasse: Recovery of Furfural and Acetic Acid from Wood Hydrolysates in Biotechnological Downstream Processing, Chemical Engineering & Technology 41 (2018) 2331–2336.

[86] N. Galeotti, J. Burger, H. Hasse: Measurement and Modeling of Phase Equilibria in Systems Containing Water, Xylose, Furfural, and Acetic Acid, Journal of Chemical & Engineering Data 64 (2019) 2634–2640.

[87] A. P. V. (34.0.0.110): USA: Aspen Technology, Inc., Technical Report, Aspen Technology, Inc., 2005.

[88] N. Galeotti, J. Burger, H. Hasse: Vapor-liquid equilibrium in the ternary systems acetic acid + water + (xylose or glucose), Fluid Phase Equilibria 473 (2018) 323–329.

[89] R. Büttner, G. Maurer: Dimerisierung einiger organischer Säuren in der Gasphase, Berichte der Bunsengesellschaft für physikalische Chemie 87 (1983) 877–882.

[90] J. Marek, G. Standart: Vapor-liquid equilibria in mixtures containing an associating substance. I. Equilibrium relationships for systems with an associating component, Collection of Czechoslovak Chemical Communications 19 (1954) 1074–1084.

[91] J. Marek: Vapor-liquid equilibria in mixtures containing an associating substance. II. Binary mixtures of acetic acid at atmospheric pressure, Collection of Czechoslovak Chemical Communications 20 (1955) 1490–1502.

[92] C. Choscz, C. Held, C. Eder, G. Sadowski, H. Briesen: Measurement and Modeling of Lactose Solubility in Aqueous Electrolyte Solutions, Industrial & Engineering Chemistry Research 58 (2019) 20797–20805.

[93] S. Ó. Jónsdóttir, S. A. Cooke, E. A. Macedo: Modeling and measurements of solid–liquid and vapor–liquid equilibria of polyols and carbohydrates in aqueous solution, Carbohydrate Research 337 (2002) 1563–1571.

[94] G. L. Bockstanz, M. Buffa, C. T. Lira: Solubilities of .alpha.-anhydrous glucose in ethanol-water mixtures, Journal of Chemical & Engineering Data 34 (1989) 426–429.

[95] N. Gabas, T. Carillon, N. Hiquily: Solubilities of D-xylose and D-mannose in water-enthanol mixtures at 25.degree.C, Journal of Chemical & Engineering Data 33 (1988) 128–130.

[96] E. A. Macedo, A. M. Peres: Thermodynamics of Ternary Mixtures Containing Sugars. SLE of D-Fructose in Pure and Mixed Solvents. Comparison between Modified UNIQUAC and Modified UNIFAC, Industrial & Engineering Chemistry Research 40 (2001) 4633–4640.

[97] A. M. Peres, E. A. Macedo: Phase equilibria of d-glucose and sucrose in mixed solvent mixtures: Comparison of UNIQUAC 1-based models, Carbohydrate Research 303 (1997) 135–151.

[98] A. P. Carneiro, C. Held, O. Rodríguez, G. Sadowski, E. A. Macedo: Solubility of Sugars and Sugar Alcohols in Ionic Liquids: Measurement and PC-SAFT Modeling, The Journal of Physical Chemistry B 117 (2013) 9980–9995.

[99] L. J. A. Conceiçao, E. Bogel-Łukasik, R. Bogel-Łukasik: A new outlook on solubility of carbohydrates and sugar alcohols in ionic liquids, RSC Advances 2 (2012) 1846.

[100] A. A. Rosatella, L. C. Branco, C. A. M. Afonso: Studies on dissolution of carbohydrates in ionic liquids and extraction from aqueous phase, Green Chemistry 11 (2009) 1406.

[101] J. H. Chang, H. N. Chang: Effects of solvents and salts on the separation of fructose from a glucose-fructose mixture, Korean Journal of Food Science and Technology 16 (1983) 70–76.

[102] C. S. Hudson: Further Studies on the Forms of Milk-Sugar, Journal of the American Chemical Society 30 (1908) 1767–1783.

[103] F. Majd, T. Nickerson: Effect of Alcohols on Lactose Solubility, Journal of Dairy Science 59 (1976) 1025–1032.

[104] O. Hunziker, B. Nissen: Lactose Solubility and Lactose Crystal Formation, Journal of Dairy Science 9 (1926) 517–537.

[105] A. Bhargava, P. Jelen: Lactose Solubility and Crystal Growth as Affected by Mineral Impurities, Journal of Food Science 61 (1996) 180–184.

[106] B. Herrington: Some Physico–Chemical Properties of Lactose, Journal of Dairy Science 17 (1934) 805–814.

[107] O. Jensen, Z. Hanford, G. Supplee: Equilibrium solutions of certain lactose-salt mixtures, Journal of Dairy Science 23 (1940) 745–753.

[108] J. B. Smart, J. M. Smith: Effect of selected compounds on the rate of α-lactose monohydrate crystallization, crystal yield and quality, International Dairy Journal 2 (1992) 41–53.

[109] J. Gross, G. Sadowski: Perturbed-Chain SAFT: An Equation of State Based on a Perturbation Theory for Chain Molecules, Industrial & Engineering Chemistry Research 40 (2001) 1244–1260.

[110] J. Gross, G. Sadowski: Application of the Perturbed-Chain SAFT Equation of State to Associating Systems, Industrial & Engineering Chemistry Research 41 (2002) 5510–5515.

[111] C.-C. Chen, H. I. Britt, J. F. Boston, L. B. Evans: Local composition model for excess Gibbs energy of electrolyte systems. Part I: Single solvent, single completely dissociated electrolyte systems, AIChE Journal 28 (1982) 588–596.

[112] C.-C. Chen, L. B. Evans: A local composition model for the excess Gibbs energy of aqueous electrolyte systems, AIChE Journal 32 (1986) 444–454.

[113] L. F. Cameretti, G. Sadowski, J. M. Mollerup: Modeling of Aqueous Electrolyte Solutions with Perturbed-Chain Statistical Association Fluid Theory, Industrial & Engineering Chemistry Research 44 (2005) 8944–8944.

[114] E. Baumeister, J. Burger: General Perturbation Scheme to Model Activities in Poorly Specified Liquid Mixtures, Industrial & Engineering Chemistry Research 59 (2020) 413–422.

[115] C. Achard, C.-G. Dussap, J.-B. Gros: Prediction of pH in complex aqueous mixtures using a group-contribution method, AIChE Journal 40 (1994) 1210–1222.

A Thermodynamic Modeling - Model Parameters

A.1 NRTL Parameters

Table 13 gives all binary interaction parameters of the NRTL model that are used for the pseudo experiments or as the base model for the specified subsystem in the case study of the system IV and the vapor-liquid equilibrium of methanol and acetone (system VI). All parameters were taken from the database provided by Aspen Plus V8.8 [87].

Table 13: Binary interaction parameters of the NRTL model, $\tau_{ij} = a_{ij} + b_{ij}/T$ [87].

Component i	Component j	a_{ij}	a_{ji}	b_{ij} / K	b_{ji} / K	α_{ij}
methanol	ethanol	4.7119	−2.3127	−1162.2949	483.8436	0.3
methanol	butanol	2.22	−1.5165	−337.7124	242.6243	0.3
methanol	dodecanol	0	0	718.6667	−251.344	0.3
methanol	hexane	−1.1544	−3.6511	734.5144	1507.1545	0.2
methanol	dodecane	−0.924624	−2.88168	1420.03	1566.64	0.368718
methanol	water	−0.693	2.7322	172.9871	−617.2687	0.3
methanol	acetone	0	0	114.135	101.886	0.3
ethanol	butanol	0	0	−85.2188	128.5015	0.3
ethanol	water	−0.8009	3.4578	246.18	−586.0809	0.3
butanol	water	−2.0405	13.1102	763.8692	−3338.9536	0.33
dodecanol	hexane	0	0	−86.6008	698.42768	0.45
dodecanol	dodecane	0	0	−179.3964	638.6587	0.3
dodecanol	water	−0.9927	2.2353	389.1094	2215.7415	0.2
hexane	cyclohexane	−0.9898	1.2637	167.9446	−202.3037	0.3
hexane	benzene	0.4066	−1.554	−213.7349	797.572	0.3
hexane	dodecane	0	0	129.7698	−138.3886	0.3
hexane	diethyl ether	0	0	−223.2187	429.7714	0.3
hexane	acetone	0	0	279.4613	319.3188	0.3
hexane	acetonitrile	0	0	455.4867	587.9445	0.2
hexane	water	0	0	1512	3040	0.2
cyclohexane	benzene	0	0	−43.3406	182.7545	0.3
cyclohexane	diethyl ether	0	0	85.0007	19.3546	0.3
cyclohexane	acetone	−3.5142	−0.1061	1485.3369	359.6793	0.47
cyclohexane	acetonitrile	0	0	612.5075	464.6301	0.3
benzene	diethyl ether	−0.4759	0.0576	27.468	94.4718	0.3
benzene	acetone	0.4224	−0.1015	−239.9009	306.0663	0.3
benzene	acetonitrile	0	0	220.003	128.2503	0.3
diethyl ether	acetonitrile	0	0	43.8872	292.9133	0.2982
acetone	diethyl ether	0	0	28.8811	198.3507	0.3
acetone	acetonitrile	0	0	−53.4595	53.2853	0.3

A.2 UNIQUAC Parameters

Table 14 and Table 15 give all geometric and binary interaction parameters of the UNIQUAC model that are used as base models for the specified subsystems in the case studies of the systems II and III. All parameters were taken from the database provided by Aspen Plus V8.8 [87].

Table 14: Surface-area parameter q_k and volume parameter r_k of the UNIQUAC model.

Component k	q_k	r_k	Ref.
methanol	1.432	1.43111	[87]
ethanol	1.972	2.10547	[87]
butanol	3.048	3.45419	[87]
dodecanol	7.372	8.84641	[87]

Table 15: Binary interaction parameters of the UNIQUAC model, $u_{kl} = -(a_{kl}T + b_{kl})$.

Component k	Component l	a_{kl}	a_{lk}	b_{kl} / K	b_{lk} / K	Ref.
methanol	ethanol	−2.6509	1.2891	651.4882	−273.6917	[87]
methanol	butanol	−0.3136	0.2267	82.6364	−125.2875	[87]
methanol	dodecanol	0	0	−3.6515	−254.1765	[87]
ethanol	butanol	0	0	87.2629	−132.5787	[87]

The UNIQUAC model parameters for the specified subsystem of system V were partly taken from the literature and partly fitted to experimental data (cf. Chapter 5 for more details). Table 16 and Table 17 give the numerical values of the geometric and binary interaction parameters of lactose and water.

Table 16: Surface-area parameter q_k and volume parameter r_k of the UNIQUAC model.

Component k	q_k	r_k	Ref.
lactose	12.2280	12.5265	[70]
water	1.400	0.9200	[65]

Table 17: Binary interaction parameters u_{kl} of the UNIQUAC model (cf. Chapter 5).

Component k	Component l	u_{kl}	u_{lk}
lactose	water	−319.111	493.914

A.3 Antoine Equation and Parameters

To calculate the vapor pressures p_k^s of the pure components k depending on the temperature T the following Antoine equation is used here [74]:

$$\ln\left(p_k^s/\mathrm{kPa}\right) = A_k - \frac{B_k}{T/\mathrm{K} + C_k}. \tag{73}$$

The numerical values for the parameters were taken from Botía et al. [74]. Table 18 gives the numerical values for the components acetone and methanol.

Table 18: Parameters for the Antoine equation for the components acetone and methanol.

Component k	A_k	B_k	C_k	Ref.
acetone	6.3565	1277.0	−35.920	[74]
methanol	7.0224	1474.1	−44.020	[74]

A.4 Bromley Parameters and Equilibrium Constants

Bromley Parameters

Table 19 gives all B_{ca} parameters of the Bromley equation that is used as the base model for the specified subsystems in the case studies of the systems E-I - E-IV. All parameters were taken from Luckas and Krissmann [69].

Table 19: Parameter B_{ca} of the Bromley equation. The parameter B_{ca} is assumed constant in the temperature range considered in the present work.

Salt	B_{ca} / kg mol^{-1}	Ref.
NaCl	0.0574	[69]
KCl	0.0240	[69]
NaBr	0.0749	[69]

Equilibrium Constants

The equilibrium constants K_k of the salts potassium chloride (KCl) and sodium bromide (NaBr) are calculated with (Eq. (54)) and (Eq. (55)). The required values for the molalities of the ions at saturation were obtained from the experimental data of the solubility in pure water at 298.15 K (KCl: Pinho and Macedo [75], NaBr: Pinho and Macedo [76]). The values for the respective activity coefficients were obtained from Eq. (48). The procedure for the equilibrium constants for sodium chloride (NaCl) was analogous, except for the fact that several measurement data at different temperatures were used [76]. The results were fitted to the general function $\ln K_{\mathrm{NaCl}} = C_1 - \frac{C_2}{(T/\mathrm{K})}$ to get a temperature dependent function for the equilibrium constant of NaCl.

B Wood Hydrolysates Process

B.1 Chemical Theory

Analog to Galeotti et al. [88], the VLE with acetic acid (AA) is described using the chemical theory [90, 91]. The chemical theory considers the dimerization of acetic acid in the vapor phase.

$$\mathrm{AA} + \mathrm{AA} \rightleftharpoons (\mathrm{AA})_2$$

Hence, the overall and true concentrations in the gas phase must be distinguished. The overall mole fraction in the gas phase is denoted by y_k, the true mole fraction by y_k^*. The correlation between these two mole fractions is:

$$y_{\mathrm{AA}} = \frac{y_{\mathrm{AA}}^* + 2y_{(\mathrm{AA})_2}^*}{1 + y_{(\mathrm{AA})_2}^*}, \tag{74}$$

$$y_{\mathrm{W}} = \frac{y_{\mathrm{W}}^*}{1 + y_{(\mathrm{AA})_2}^*}. \tag{75}$$

Furthermore, the chemical equilibrium constant K^{D} of the dimerization of acetic acid in the gas phase is required to calculate the true mole fraction. The chemical equilibrium constant K^{D} is taken from Büttner and Maurer [89].

$$K^{\mathrm{D}} = \frac{p^0 y_{(\mathrm{AA})_2}^*}{p {y_{\mathrm{AA}}^*}^2} = \exp\left(-19.1001 + \frac{7928.7}{T/\mathrm{K}}\right) \tag{76}$$

Where $p^0 = 1$ bar. Also, the calculation of the pure component vapor pressure of acetic acid that is required in the extended Raoult's law must be adjusted:

$$p_{\mathrm{AA}}^{\mathrm{s}*} = \frac{\sqrt{1 + 4K^{\mathrm{D}} p_{\mathrm{AA}}^{\mathrm{s}}} - 1}{2K^{\mathrm{D}}}. \tag{77}$$

B.2 Antoine Equation and Parameters

To calculate the vapor pressures p_k^s of the pure components k depending on the temperature T the following Antoine equation is used here:

$$\ln\left(p_k^s/\mathrm{kPa}\right) = A_k + \frac{B_k}{T/\mathrm{K}} + C_k \ln\left(T/\mathrm{K}\right) + D_k \left(T/\mathrm{K}\right)^{E_k} . \tag{78}$$

The numerical values for the parameters were taken from the database provided by Aspen Plus V8.8 [87]. Table 20 gives the numerical values for the components acetic acid, furfural, and water.

Table 20: Parameters for the Antoine equation [87].

Component k	A_k	B_k	C_k	D_k	E_k
acetic acid	46.36224	−6304.5	−4.2985	0.88865E−17	6
furfural	87.6622	−8372.1	−11.13	0.008815	1
water	66.7412	−7258.2	−7.3037	0.41653E−05	2

B.3 Model Parameters

Table 21 gives the binary NRTL model parameters for the components acetic acid, water, and furfural. The numerical values for the parameters were taken from Galeotti et al. [86].

Table 21: Parameters of the NRTL model for the components acetic acid, water, and furfural [86].

Component k + l	a_{kl}	a_{lk}	b_{kl} / K	b_{lk} / K	$\alpha_{kl} = \alpha_{lk}$
water + acetic acid	−11.37710	7.29431	4318.650	−2532.240	0.47
water + furfural	3.75496	−3.21520	−55.438	1221.700	0.30
acetic acid + furfural	0.67716	0.00045	0.000	0.000	0.47

Table 22 gives the interaction parameters of the perturbation scheme that are obtained by step-wise fitting to the experimental data as described in Chapter 4.

Table 22: Interaction parameters $A_{k\mathrm{u}}$ of the perturbation scheme.

Component k	$A_{k\mathrm{u}}$ / kJ mol^{-1}
acetic acid	24.460
water	18.060
furfural	28.880

C Solubility of α-Lactose

C.1 Subsystems Modeled with the UNIQUAC Model

Figure 30 shows that the results from the UNIQUAC model for the solubility of lactose in pure water at different temperatures agree well with experimental data (Machado et al. [70], Hudson [102], and experimental data of the present work). Furthermore, the agreement of the results from the UNIQUAC model for the solubility of lactose in mixed solvents comprised of water and ethanol with experimental data of the present work) is also very good, as shown in Figure 31.

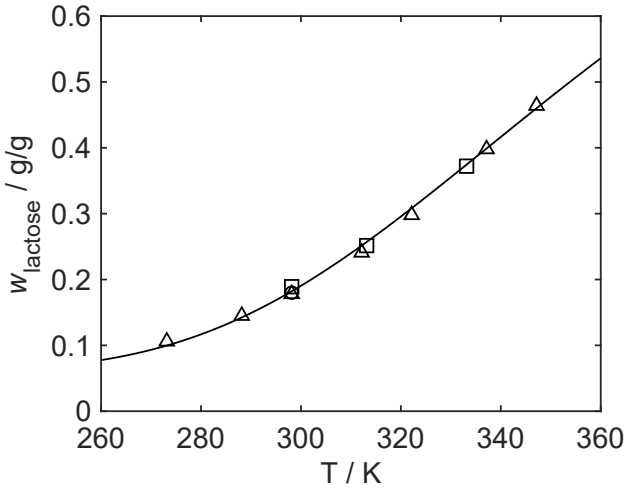

Figure 30: Experimental data (△ [102], □ [70], ○ own experimental data of the present work) and results from the UNIQUAC model (solid line) for the solubility of lactose in pure water in the temperature range 270 - 360 K.

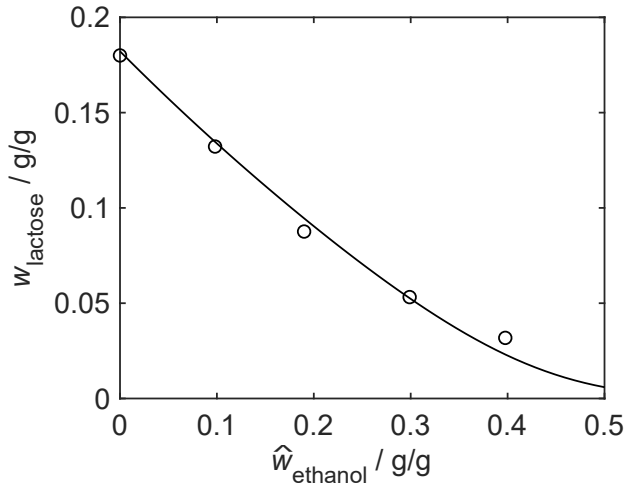

Figure 31: Experimental data of the present work (○) and results from the UNIQUAC model (solid line) for the solubility of lactose in solvents comprised of water and ethanol with different mass fractions of ethanol.

C.2 Literature Comparison of Solubility Data of Lactose

In Figure 32 the good agreement of the experimental data of the present work with data from the literature (Machado et al. [70] and Hudson [102]) for the solubility of lactose in water-ethanol mixtures is shown.

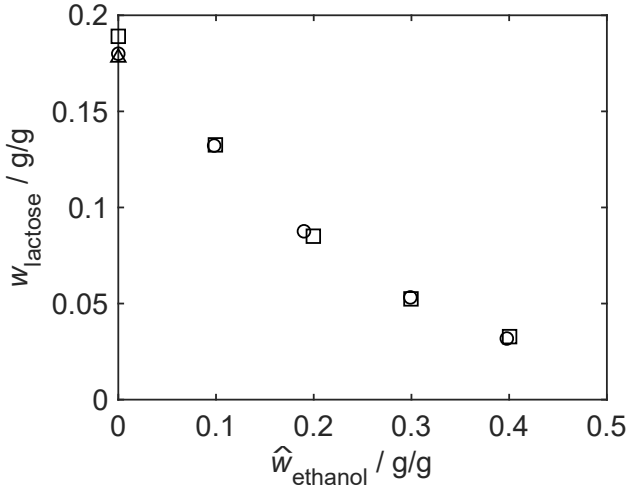

Figure 32: Comparison of the experimental data of the present work (○) and experimental data from the literature (△ [102], □ [70]) for the solubility of lactose in solvents comprised of water and ethanol with different mass fractions of ethanol.

C.3 Deviations between Experimental and Modeled Solubilities of Lactose

The following tables (cf. Table 23 - 25) give the numerical values of the solubility of lactose obtained from the experiments and the two models (UNIQUAC-DH and UNIQUAC-PS). Additionally, the relative deviations between the solubility of lactose obtained from the experiments and the two models are given.

$$f = \frac{w_{\text{lactose}}^{\text{exp}} - w_{\text{lactose}}^{\text{model}}}{w_{\text{lactose}}^{\text{exp}}} \tag{79}$$

Table 23: Solubility of **lactose in water-ethanol** mixtures obtained from the experiments and the UNIQUAC model studied in Chapter 5 and relative deviation between the experimental and modeled solubilities of lactose.

Experimental		UNIQUAC	
100 $\hat{w}_{\text{ethanol}}$ / g g^{-1}	100 w_{lactose} / g g^{-1}	100 w_{lactose} / g g^{-1}	f
0.00	18.00	18.22	0.012
9.81	13.22	13.47	0.019
19.00	8.76	9.45	0.079
29.89	5.32	5.26	0.011
39.76	3.18	2.31	0.274

Table 24: Solubility of **lactose in water-ethanol-NaCl** mixtures obtained from the experiments and the models studied in Chapter 5 (UNIQUAC-DH and UNIQUAC-PS) and relative deviation between the experimental and modeled solubilities of lactose.

Experimental			UNIQUAC-DH		UNIQUAC-PS	
100 $\hat{w}_{\text{ethanol}}$ / g g^{-1}	100 $\hat{w}_{\text{NaCl}}$ / g g^{-1}	100 w_{lactose} / g g^{-1}	100 w_{lactose} / g g^{-1}	f	100 w_{lactose} / g g^{-1}	f
0.00	2.44	17.18	17.11	0.004	17.17	0.001
9.91	2.45	12.89	12.87	0.001	12.99	0.008
19.45	2.45	8.82	9.09	0.031	9.22	0.046
29.91	2.46	5.70	5.31	0.068	5.41	0.050
39.74	2.46	3.58	2.43	0.322	2.48	0.306
0.00	4.80	16.82	16.52	0.018	16.51	0.019
10.02	4.81	12.99	12.66	0.025	12.79	0.016
19.36	4.82	9.38	9.22	0.017	9.38	0.000
29.84	4.83	6.26	5.56	0.111	5.69	0.091
39.82	4.84	4.07	2.62	0.357	2.69	0.339
0.00	9.30	16.21	16.36	0.009	16.21	0.000
10.10	9.31	13.35	13.19	0.012	13.15	0.015
19.60	9.33	10.30	10.07	0.022	10.03	0.026
30.41	9.34	7.40	6.44	0.130	6.33	0.145
40.24	9.35	5.08	3.36	0.339	3.21	0.368

Table 25: Solubility of **lactose in water-ethanol-$CaCl_2$** mixtures obtained from the experiments and the models studied in Chapter 5 (UNIQUAC-DH and UNIQUAC-PS) and relative deviation between the experimental and modeled solubilities of lactose.

Experimental			UNIQUAC-DH		UNIQUAC-PS	
100 $\hat{w}_{\text{ethanol}}$ / g g^{-1}	100 $\hat{w}_{\text{CaCl}_2}$ / g g^{-1}	100 w_{lactose} / g g^{-1}	100 w_{lactose} / g g^{-1}	f	100 w_{lactose} / g g^{-1}	f
0.00	2.45	17.02	16.89	0.008	17.38	0.021
9.96	2.45	12.60	12.74	0.011	12.97	0.030
19.13	2.46	8.64	9.12	0.055	9.23	0.069
29.90	2.46	5.36	5.22	0.027	5.26	0.019
39.65	2.47	3.33	2.38	0.286	2.37	0.287
0.00	4.83	16.81	16.21	0.036	16.81	0.000
9.96	4.84	12.57	12.46	0.008	12.74	0.013
19.25	4.85	8.79	9.02	0.026	9.14	0.040
30.00	4.86	5.63	5.27	0.064	5.29	0.060
39.80	4.86	3.57	2.46	0.312	2.41	0.325
0.00	9.39	16.39	16.39	0.000	16.39	0.000
10.18	9.41	12.76	12.85	0.007	12.69	0.005
19.68	9.42	9.26	9.46	0.021	9.25	0.001
30.52	9.44	6.15	5.69	0.074	5.45	0.114
40.69	9.45	3.97	2.69	0.321	2.44	0.386

C.4 On the Hygroscopy of $CaCl_2 \cdot 2H_2O$

$CaCl_2 \cdot 2H_2O$ is a hygroscopic salt, since the stable hydrate form of $CaCl_2$ at ambient conditions is the hexahydrate ($CaCl_2 \cdot 6H_2O$). The hygroscopy is a potential error for the gravimetric preparation of the stock solutions containing $CaCl_2$. When weighing the salt for the stock solutions, no drift of the scale was observed. To ensure that the weighed solid was the dihydrate ($CaCl_2 \cdot 2H_2O$), a verification experiment was done as follows.

13.1733 g of the $CaCl_2 \cdot xH_2O$ salt (from the same jar that was used in the solubility measurement) were dissolved in 86.5534 g of ultra-pure water. The ratio of salt and water is similar to the one in the stock solutions used for the solubility measurement.

The mass fraction of chloride in the solution was determined using ion cromatography (IC) analysis (Metrohm 930 Compact IC Flex, Metrosep A Supp 5 250/4.0 with an aqueous solution of 3.2 mmol/L sodium carbonate and 1.0 mmol/L sodium hydrogen carbonate as eluent). The IC was calibrated using independent chloride standard solutions. The analysis of the $CaCl_2$ solution was done twice and yielded 0.06607 and 0.06637 (g chloride)/(g solution), respectively. The avarage of 0.06622 (g chloride)/(g solution) with a relative uncertainty of 1 % was used for the further calculation. Using the material balance from the preparation of the solution, the hydrate number x of the $CaCl_2 \cdot xH_2O$ was determined to 2.031 ± 0.083. The dihydrate from ($CaCl_2 \cdot 2H_2O$) was confirmed. The uncertainty of the hydrate number results into a relative uncertainty of 1.4 % in the amount of $CaCl_2$ added to the solutions.

C.5 Excess Solid in the Experiments and Calculation of Uncertainties

This section derives the uncertainties given in Table 12. They are derived using Gauss'ian error propation. The mass fraction w_{lactose} of lactose in the liquid phase is measured directly by HPLC analysis. Its relative uncertainty comes from the relative analyis uncertainty (0.016; checked by analyzing gravimetrically prepared test solutions) and the impurity of the used chemical material (relative uncertainty 0.01). The resulting relative uncertainty of w_{lactose} is:

$$\frac{u(w_{\mathrm{lactose}})}{w_{\mathrm{lactose}}} = \sqrt{0.016^2 + 0.01^2} = 0.019. \tag{80}$$

The uncertainties of the $\hat{w}_{\text{ethanol}}$, $\hat{w}_{\text{NaCl}}$, and $\hat{w}_{\text{CaCl2}}$ were determined at every single experimental point as follows.

$$\hat{w}_i = \frac{m_i}{m_i + m_{\text{water}}} \tag{81}$$

$$\frac{\partial \hat{w}_i}{\partial m_i} = \frac{m_{\text{water}}}{(m_i + m_{\text{water}})^2} \tag{82}$$

$$\frac{\partial \hat{w}_i}{\partial m_{\text{water}}} = \frac{-m_i}{(m_i + m_{\text{water}})^2} \tag{83}$$

$$u(\hat{w}_i) = \sqrt{\left(\frac{\partial \hat{w}_i}{\partial m_i} u(m_i)\right)^2 + \left(\frac{\partial \hat{w}_i}{\partial m_{\text{water}}} u(m_{\text{water}})\right)^2} \tag{84}$$

The uncertainty of the masses of ethanol, NaCl, and $CaCl_2$ result from the weighing uncertainty and the impurity of the used raw material. The weighing uncertainty of $CaCl_2$ is higher due to potential hygroscopy (cf. Section C.4).

$$u(m_{\text{ethanol}}) = \sqrt{(0.001\ \text{g})^2 + (m_{\text{ethanol}} \cdot 0.008)^2} \tag{85}$$

$$u(m_{\text{NaCl}}) = \sqrt{(0.001\ \text{g})^2 + (m_{\text{NaCl}} \cdot 0.005)^2} \tag{86}$$

$$u(m_{\text{CaCl2}}) = m_{\text{CaCl2}} \sqrt{0.014^2 + 0.01^2} \tag{87}$$

The uncertainty of the mass m_{water} of water stems from the weighing uncertainty when adding ultra-pure water and the uncertainty of water freed by dehydratization the excess solid (lactose monohydrate) in the equilbrium cell. The mass $m_{\text{solid}}^{\text{excess}}$ of excess solid is calculated by substracting the the mass of lactose monohydrate that has dissolved according to the anlalyzed mass fraction of lactose in the liquid phase from the initially added mass of lactose monohydrate .

$$u(m_{\text{water}}) = \sqrt{(0.001\ \text{g})^2 + (m_{\text{water}}^{\text{excess}})^2} \tag{88}$$

$$m_{\text{water}}^{\text{excess}} = m_{\text{solid}}^{\text{excess}} \cdot 18.015/360.3 \tag{89}$$

The Tables 26 - 32 give the results of these calculations for all experimental points. They also quantify the initially added solid lactose monohydrate and the amount of excess solid (assuming it is lactose monohydrate) in equilibrium. The solid was not analyzed.

The resulting uncertainties of $\hat{w}_{\text{ethanol}}$, $\hat{w}_{\text{NaCl}}$, and $\hat{w}_{\text{CaCl2}}$ are roughly constant on a relative scale for all measurement points and do not exceed the following values.

$$u_{\mathrm{r}}(\hat{w}_{\mathrm{ethanol}}) = \frac{u(\hat{w}_{\mathrm{ethanol}})}{\hat{w}_{\mathrm{ethanol}}} = 0.011 \tag{90}$$

$$u_{\mathrm{r}}(\hat{w}_{\mathrm{NaCl}}) = \frac{u(\hat{w}_{\mathrm{NaCl}})}{\hat{w}_{\mathrm{NaCl}}} = 0.011 \tag{91}$$

$$u_{\mathrm{r}}(\hat{w}_{\mathrm{CaCl2}}) = \frac{u(\hat{w}_{\mathrm{CaCl2}})}{\hat{w}_{\mathrm{CaCl2}}} = 0.019 \tag{92}$$

Table 26: Measured values and uncertainties for experiments in the system **lactose, water, ethanol without salt**. Column meanings: A: mass $m_{\text{lactose monohydrate}}$ / g of lactose monohydrate in cell; B: mass m_{water} / g of water in cell; C: mass m_{salt} / g of salt in cell; D: mass m_{ethanol} / g of ethanol in cell; E: measured mass fraction w_{lactose} / g g^{-1} of lactose in the liquid phase; F: mass $m_{\mathrm{solid}}^{\mathrm{excess}}$ / g of excess solid; G: 100 $u_{\mathrm{r}}(\hat{w}_{\mathrm{salt}})$; H: 100 $u_{\mathrm{r}}(\hat{w}_{\mathrm{ethanol}})$.

A	B	C	D	E	F	G	H
5.6618	19.8972	0	0	18.0	1.02		0
7.3075	19.8827	0	0	18.0	2.67		0
5.1112	19.8988	0	0	18.0	0.478		0
4.1519	17.9065	0	1.9668	13.2	0.963		0.76
3.9641	17.8895	0	1.9493	13.2	0.761		0.75
4.4081	17.8452	0	1.9595	13.3	1.21		0.78
3.3006	15.8795	0	3.7131	8.84	1.30		0.73
3.3058	15.8928	0	3.7137	8.74	1.33		0.73
3.4485	15.8380	0	3.8049	8.70	1.47		0.75
2.6225	13.8854	0	5.9874	5.25	1.46		0.67
2.7613	13.8779	0	5.9082	5.43	1.56		0.69
2.3469	13.8797	0	5.9227	5.27	1.19		0.64
1.5824	11.8956	0	7.9403	3.14	0.906		0.53
1.8070	11.9281	0	7.8641	3.22	1.11		0.56
2.2243	11.9152	0	7.8482	3.19	1.54		0.62

Table 27: Measured values and uncertainties for experiments in the system **lactose, water, ethanol, NaCl** with $\hat{w}_{\mathrm{NaCl}} \approx 0.093\,\mathrm{g\,g^{-1}}$. Column meanings: A: mass $m_{\mathrm{lactose\ monohydrate}}$ / g of lactose monohydrate in cell; B: mass m_{water} / g of water in cell; C: mass m_{NaCl} / g of NaCl in cell; D: mass m_{ethanol} / g of ethanol in cell; E: measured mass fraction w_{lactose} / $\mathrm{g\,g^{-1}}$ of lactose in the liquid phase; F: mass $m_{\mathrm{solid}}^{\mathrm{excess}}$ / g of excess solid; G: $100\,u_{\mathrm{r}}(\hat{w}_{\mathrm{NaCl}})$; H: $100\,u_{\mathrm{r}}(\hat{w}_{\mathrm{ethanol}})$.

A	B	C	D	E	F	G	H
5.4279	19.3147	2.0018	0	16.2	1.07	0.52	
5.5108	19.2669	1.9969	0	16.3	1.13	0.52	
5.7330	19.2499	1.9951	0	16.2	1.38	0.56	
5.0859	17.2843	1.7914	1.9905	13.2	1.70	0.63	0.84
4.9857	17.3108	1.7941	1.9396	13.5	1.52	0.60	0.82
4.3151	17.2947	1.7925	1.9556	13.4	0.876	0.51	0.75
4.3027	15.3330	1.5892	3.7693	10.2	1.81	0.70	0.80
4.6351	15.3540	1.5913	3.7713	10.3	2.12	0.77	0.85
4.2634	15.3277	1.5886	3.7614	10.3	1.74	0.68	0.79
2.4840	13.4176	1.3907	5.9434	7.37	0.744	0.52	0.59
2.8461	13.4078	1.3896	5.8635	7.41	1.10	0.59	0.63
2.3496	13.3311	1.3817	5.8518	7.42	0.612	0.50	0.58
2.4556	11.5323	1.1953	7.8675	5.04	1.30	0.68	0.58
2.7210	11.5603	1.1981	7.8024	5.06	1.57	0.76	0.63
3.3133	11.5242	1.1944	7.7496	5.14	2.15	0.95	0.73

Table 28: Measured values and uncertainties for experiments in the system **lactose, water, ethanol, NaCl** with $\hat{w}_{\mathrm{NaCl}} \approx 0.048\,\mathrm{g\,g^{-1}}$. Column meanings: A: mass $m_{\mathrm{lactose\ monohydrate}}$ / g of lactose monohydrate in cell; B: mass m_{water} / g of water in cell; C: mass m_{NaCl} / g of NaCl in cell; D: mass m_{ethanol} / g of ethanol in cell; E: measured mass fraction w_{lactose} / $\mathrm{g\,g^{-1}}$ of lactose in the liquid phase; F: mass $m_{\mathrm{solid}}^{\mathrm{excess}}$ / g of excess solid; G: $100\,u_{\mathrm{r}}(\hat{w}_{\mathrm{NaCl}})$; H: $100\,u_{\mathrm{r}}(\hat{w}_{\mathrm{ethanol}})$.

A	B	C	D	E	F	G	H
5.6925	19.6856	1.0043	0	16.8	1.25	0.56	
6.9082	19.6198	1.0009	0	16.8	2.50	0.77	
6.3427	19.6065	1.0003	0	16.8	1.92	0.66	
5.0904	17.6405	0.9000	1.9842	13.0	1.85	0.69	0.86
4.9457	17.6373	0.8998	1.9705	13.1	1.67	0.65	0.84
5.1422	17.6276	0.8993	1.9896	12.9	1.94	0.70	0.87
2.9517	15.6957	0.8008	3.7914	9.41	0.728	0.52	0.67
3.2053	15.6717	0.7995	3.7882	9.41	0.98	0.56	0.69
3.0522	15.6917	0.8005	3.7924	9.32	0.85	0.54	0.68
3.6000	13.7000	0.6989	5.8018	6.31	2.17	0.89	0.79
3.5324	13.7054	0.6992	5.9348	6.18	2.12	0.87	0.78
2.7997	13.7033	0.6991	5.8377	6.29	1.37	0.67	0.66
3.4650	11.7494	0.5994	7.8806	4.02	2.57	1.14	0.81
1.9760	11.7901	0.6015	7.7922	4.09	1.07	0.64	0.55
2.5093	11.7869	0.6013	7.7843	4.08	1.61	0.80	0.63

Table 29: Measured values and uncertainties for experiments in the system **lactose, water, ethanol, NaCl** with $\hat{w}_{\mathrm{NaCl}} \approx 0.024\,\mathrm{g\,g^{-1}}$. Column meanings: A: mass $m_{\text{lactose monohydrate}}$ / g of lactose monohydrate in cell; B: mass m_{water} / g of water in cell; C: mass m_{NaCl} / g of NaCl in cell; D: mass m_{ethanol} / g of ethanol in cell; E: measured mass fraction w_{lactose} / $\mathrm{g\,g^{-1}}$ of lactose in the liquid phase; F: mass $m_{\mathrm{solid}}^{\mathrm{excess}}$ / g of excess solid; G: $100\,u_{\mathrm{r}}(\hat{w}_{\mathrm{NaCl}})$; H: $100\,u_{\mathrm{r}}(\hat{w}_{\mathrm{ethanol}})$.

A	B	C	D	E	F	G	H
5.5999	19.8162	0.5014	0	17.2	1.11	0.56	
6.6210	19.7663	0.5002	0	17.2	2.16	0.72	
6.3384	19.7573	0.4999	0	17.1	1.90	0.67	
5.2129	17.7619	0.4495	1.9932	12.9	2.05	0.74	0.89
4.4714	17.7572	0.4493	1.9604	13.0	1.27	0.60	0.79
4.7947	17.7787	0.4499	1.9558	12.7	1.68	0.67	0.84
3.3871	15.7469	0.3985	3.7801	8.88	1.34	0.64	0.73
3.1347	15.7692	0.3990	3.8830	8.76	1.10	0.59	0.70
3.0937	15.7439	0.3984	3.8184	8.82	1.06	0.59	0.70
2.9909	13.7907	0.3490	5.9853	5.63	1.73	0.78	0.71
2.8560	13.8000	0.3492	5.8877	5.71	1.58	0.74	0.69
2.4590	13.7452	0.3478	5.8421	5.75	1.18	0.64	0.64
1.9761	11.7873	0.2983	7.8316	3.56	1.20	0.70	0.57
1.8835	11.8085	0.2988	7.8318	3.57	1.11	0.67	0.56
2.0080	11.8413	0.2996	7.7772	3.61	1.22	0.70	0.57

Table 30: Measured values and uncertainties for experiments in the system **lactose, water, ethanol, $\mathrm{CaCl_2}$** with $\hat{w}_{\mathrm{CaCl_2}} \approx 0.094\,\mathrm{g\,g^{-1}}$. Column meanings: A: mass $m_{\text{lactose monohydrate}}$ / g of lactose monohydrate in cell; B: mass m_{water} / g of water in cell; C: mass $m_{\mathrm{CaCl_2}}$ / g of $\mathrm{CaCl_2}$ in cell; D: mass m_{ethanol} / g of ethanol in cell; E: measured mass fraction w_{lactose} / $\mathrm{g\,g^{-1}}$ of lactose in the liquid phase; F: mass $m_{\mathrm{solid}}^{\mathrm{excess}}$ / g of excess solid; G: $100\,u_{\mathrm{r}}(\hat{w}_{\mathrm{CaCl_2}})$; H: $100\,u_{\mathrm{r}}(\hat{w}_{\mathrm{ethanol}})$.

A	B	C	D	E	F	G	H
6.7869	19.2619	2.0180	0	16.5	2.34	1.65	
5.9394	19.2484	2.0166	0	16.5	1.48	1.60	
6.3657	19.2334	2.0150	0	16.2	2.01	1.63	
4.8939	16.9935	1.7804	1.9827	12.6	1.71	1.62	0.85
4.3836	17.2451	1.8067	1.9476	12.9	1.10	1.58	0.77
4.2018	17.2511	1.8073	1.9561	12.7	0.958	1.58	0.76
3.2095	15.3014	1.6031	3.7514	9.22	1.00	1.59	0.69
3.4866	15.2813	1.6010	3.7622	9.32	1.25	1.60	0.72
3.5758	15.2974	1.6027	3.8078	9.23	1.35	1.61	0.73
3.3806	13.3135	1.3948	5.9480	6.07	1.97	1.70	0.75
3.2255	13.3523	1.3989	5.8528	6.17	1.80	1.67	0.73
3.0148	13.3541	1.3991	5.8675	6.19	1.58	1.65	0.69
2.7396	11.4716	1.2018	7.8753	4.00	1.84	1.72	0.67
2.9010	11.4900	1.2038	7.7832	4.03	2.00	1.74	0.70
3.3439	11.1872	1.1720	7.8559	3.88	2.49	1.85	0.80

Table 31: Measured values and uncertainties for experiments in the system **lactose, water, ethanol, $CaCl_2$** with $\hat{w}_{CaCl_2} \approx 0.048\,g\,g^{-1}$. Column meanings: A: mass $m_{\text{lactose monohydrate}}$ / g of lactose monohydrate in cell; B: mass m_{water} / g of water in cell; C: mass m_{CaCl_2} / g of $CaCl_2$ in cell; D: mass $m_{ethanol}$ / g of ethanol in cell; E: measured mass fraction $w_{lactose}$ / $g\,g^{-1}$ of lactose in the liquid phase; F: mass m_{solid}^{excess} / g of excess solid; G: $100\,u_r(\hat{w}_{CaCl_2})$; H: $100\,u_r(\hat{w}_{ethanol})$.

A	B	C	D	E	F	G	H
6.8494	19.5472	1.0022	0	16.8	2.44	1.74	
5.4727	19.5173	1.0007	0	16.7	1.10	1.66	
5.5939	19.5583	1.0028	0	16.9	1.17	1.66	
4.6114	17.5604	0.9003	1.9786	12.5	1.52	1.69	0.82
4.9832	17.5239	0.8985	1.9443	12.6	1.88	1.71	0.86
4.0317	17.5290	0.8987	1.9461	12.6	0.927	1.66	0.76
3.7466	15.5616	0.7979	3.7097	8.78	1.71	1.72	0.78
3.0979	15.5727	0.7984	3.7442	8.84	1.04	1.67	0.70
4.0526	15.5660	0.7981	3.7518	8.76	2.02	1.75	0.83
2.7052	13.5923	0.6969	5.9047	5.59	1.45	1.71	0.67
2.5211	13.6427	0.6995	5.8367	5.63	1.25	1.69	0.65
2.5401	13.6137	0.6980	5.8402	5.66	1.27	1.70	0.65
2.4474	11.7033	0.6000	7.7834	3.53	1.67	1.77	0.64
2.7461	11.6996	0.5998	7.7516	3.62	1.95	1.82	0.70
2.6082	11.6878	0.5992	7.7348	3.54	1.83	1.80	0.67

Table 32: Measured values and uncertainties for experiments in the system **lactose, water, ethanol, $CaCl_2$** with $\hat{w}_{CaCl_2} \approx 0.024\,g\,g^{-1}$. Column meanings: A: mass $m_{\text{lactose monohydrate}}$ / g of lactose monohydrate in cell; B: mass m_{water} / g of water in cell; C: mass m_{CaCl_2} / g of $CaCl_2$ in cell; D: mass $m_{ethanol}$ / g of ethanol in cell; E: measured mass fraction $w_{lactose}$ / $g\,g^{-1}$ of lactose in the liquid phase; F: mass m_{solid}^{excess} / g of excess solid; G: $100\,u_r(\hat{w}_{CaCl_2})$; H: $100\,u_r(\hat{w}_{ethanol})$.

A	B	C	D	E	F	G	H
4.6970	19.7640	0.5014	0	16.9	0.325	1.68	
5.9096	19.6887	0.4995	0	17.1	1.50	1.72	
6.5941	19.6807	0.4993	0	17.1	2.19	1.76	
4.5951	17.7063	0.4492	1.9884	12.5	1.54	1.73	0.82
5.6352	17.7435	0.4502	1.9971	12.6	2.55	1.82	0.96
6.1415	17.7211	0.4496	1.9473	12.6	3.06	1.87	1.06
3.4685	15.7140	0.3987	3.7794	8.55	1.51	1.74	0.75
3.7668	15.7064	0.3985	3.6931	8.69	1.78	1.77	0.79
3.9195	15.7345	0.3992	3.7459	8.70	1.92	1.78	0.81
3.8102	13.6839	0.3472	5.9277	5.31	2.63	1.92	0.87
3.2280	13.7010	0.3476	5.8537	5.35	2.04	1.83	0.77
3.1935	13.7558	0.3490	5.8405	5.43	1.99	1.82	0.76
2.5666	11.7842	0.2990	7.7945	3.28	1.86	1.84	0.68
2.6328	11.8032	0.2995	7.7596	3.33	1.91	1.85	0.69
2.3958	11.8246	0.3000	7.7832	3.36	1.67	1.81	0.64